IS-T--960

DE82 005455

Some Reduced Ternary and Quaternary Oxides of Molybdenum Containing Strong Metal-Metal Bonds

by

Charlie Carmine Torardi

Ph.D. Thesis submitted to Iowa State University

Ames Laboratory, U.S. DOE

Iowa State University

Ames, Iowa 50011

Date Transmitted: October 1981

PREPARED FOR THE U. S. DEPARTMENT OF ENERGY

UNDER CONTRACT NO. W-7405-Eng-82.

DISCLAIMER

DISCLAIMER

Printed in the United States of America

Available from
National Technical Information Service
U.S. Department of Commerce
5265 Port Royal Road
Springfield, VA 22161

Some reduced ternary and quaternary oxides of molybdenum containing strong metal-metal bonds[1]

Charlie Carmine Torardi

Under the supervision of Robert E. McCarley
From the Department of Chemistry
Iowa State University

Several new, reduced ternary and quaternary oxides of molybdenum are reported, each containing molybdenum in an average oxidation state < 4.0. All of these compounds contain either discrete molybdenum atom clusters or infinite chains of bonded molybdenum atoms.

The compounds $ScZnMo_3O_8$, $LiZn_2Mo_3O_8$, and $Zn_3Mo_3O_8$ have been synthesized and crystal structures have been determined for the latter two. These oxides contain the same type of triangular molybdenum atom clusters found in the compound $Zn_2Mo_3O_8$ (McCarroll, W. H.; Katz, L.; Ward, J. J. Am. Chem. Soc. 1957, 79, 5410). However, each of the trimeric clusters in these new compounds has available one or two additional electrons for participation in metal-metal bonding.

Another newly prepared and characterized ternary oxide containing discrete metal atom clusters is $Ba_{1.14}Mo_8O_{16}$. The structure of this

---

[1]DOE Report IS-T-960. This work was performed under Contract W-7405-eng-82 with the Department of Energy.

compound consists of molybdenum-oxide cluster chains extended parallel with the c axis. These chains are built from clusters of the type Mo_4O_{16} sharing the oxygen atoms on the four outer edges of the planar tetrameric molybdenum atom cluster to give an Mo_4O_8 stoichiometry. Two different infinite chains, built up from $Mo_4O_8^{2-}$ and $Mo_4O_8^{0.28-}$ cluster units, respectively, are interlinked via Mo-O-Mo bridge bonding to create four-sided tunnels in which the Ba^{2+} ions reside.

The new compound $NaMo_4O_6$ contains infinite chains of bonded molybdenum atom clusters. These chains are comprised of clusters of the type Mo_6O_{12} fused at opposite edges by removal of two edge-bridging oxygen atoms, and sharing of the metal and remaining oxygen atoms between cluster units. The sodium ions occupy sites in channels formed by four molybdenum-oxide cluster chains crosslinked by strong Mo-O-Mo bonds.

Another new compound, whose structure is closely related to that of $NaMo_4O_6$, is $Ba_{0.62}Mo_4O_6$. This material also exhibits a superlattice ordering of barium ions within the channels. An analysis of this superstructure from single crystal x-ray diffraction data is discussed.

Other compounds that have been prepared and also partially characterized by chemical analyses and x-ray powder diffraction data are tentatively formulated as $K_{2+x}Mo_{12}O_{19}$, $Na_{2+x}Mo_{12}O_{19}$, and $CaMo_5O_8$.

Some reduced ternary and quaternary oxides of molybdenum containing strong metal-metal bonds

by

Charlie Carmine Torardi

An Abstract of

A Dissertation Submitted to the

Graduate Faculty in Partial Fulfillment of the

Requirements for the Degree of

DOCTOR OF PHILOSOPHY

Approved:

Robert E. McCarley
In Charge of Major Work

David K. Hoffman
For the Major Department

M. J. Ulmer
For the Graduate College

Iowa State University
Ames, Iowa
1981

Some reduced ternary and quaternary oxides of molybdenum containing strong metal-metal bonds

by

Charlie Carmine Torardi

A Dissertation Submitted to the
Graduate Faculty in Partial Fulfillment of the
Requirements for the Degree of
DOCTOR OF PHILOSOPHY

Department: Chemistry
Major: Inorganic Chemistry

Approved:

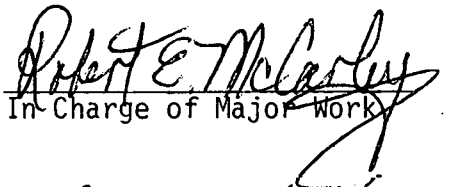
In Charge of Major Work

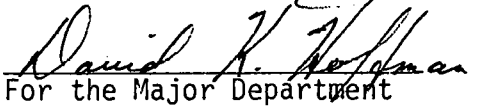
For the Major Department

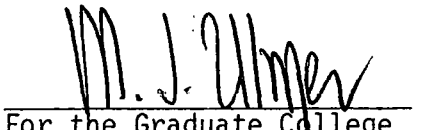
For the Graduate College

Iowa State University
Ames, Iowa

1981

TABLE OF CONTENTS

LIST OF TABLES

LIST OF FIGURES

GENERAL INTRODUCTION

Over the past decade, there has been an increasing interest in solid state compounds containing discrete transition metal atom clusters and condensed transition metal atom clusters which form chain and sheet structures. Many sulfur, selenium, tellurium, and halogen compounds containing metal atom clusters have been synthesized. One important family of compounds, known as Chevrel phases (1), incorporates the discrete Mo_6X_8 cluster unit with X = S, Se and Te (an Mo_6X_8 cluster is composed of an octahedron of bonded molybdenum atoms with X atoms bridging the eight faces of the octahedron). Members of this family have the same basic solid state structure and many have interesting superconducting properties. In halide compounds, examples of condensed cluster systems include the compounds Gd_2Cl_3 (2), Sc_5Cl_8 (3), and ZrCl (4). The first compound contains infinite chains derived from bonded metal atom clusters of type M_6X_8. The second compound is related to the first but contains infinite chains derived from bonded scandium atom clusters of type M_6X_{12} (an M_6X_{12} cluster consists of an octahedron of M atoms with X atoms bridging the twelve edges of the octahedron). The compound ZrCl is composed of sheets of bonded metal atoms and sheets of halogen atoms in a double layered arrangement (...Cl-Zr-Zr-Cl...). Structures such as these are clearly dominated by metal-metal interactions and the stability of these compounds must certainly arise from the contributions made to the lattice energy by metal-metal bonding.

In contrast, transition metal atom clusters and condensed clusters in oxide systems are relatively few in number. The most commonly

observed metal cluster geometry in these oxide compounds involves bonding between two metal atoms to form dimers. Some examples of these oxides include the rutile-related dioxides (5) of V, Nb, Mo, Tc, and W, and the compounds $Nd_4Re_2O_{11}$ (6) and $La_4Re_2O_{10}$ (7). Prior to 1970, oxide compounds which contained clusters consisting of three or more bonded metal atoms were rare. Several examples of these compounds were $A_2^{II}Mo_3O_8$ (A = Mg, Mn, Fe, Co, Ni, Zn, and Cd) (8), the perovskite-related $BaRuO_3$ (9), orthorhombic ReO_2 (10), the compound Pt_3O_4 (11), and the highly reduced compound NbO (12). These compounds contain triangular clusters of molybdenum ions, linear clusters of three ruthenium ions, infinite zig-zag chains of rhenium ions, infinite linear chains of platinum ions, and corner-sharing octahedra of niobium ions, respectively. Since that time, other oxides reported to contain clusters of three or more bonded metal atoms include the compounds $A_2^{II}Mo_{3-x}W_xO_8$ (with $0 < x \leq 3$ and A = Mg, Mn, Fe, Co, Ni, Zn, and Cd) (13), the compounds $LiRMo_3O_8$ (R = Sc, Y, In, Sm, Gd, Tb, Dy, Ho, Er, Yb) (14), and the compound $Mg_3Nb_6O_{11}$ (15). The first two groups of compounds incorporate triangular clusters such as those found in the $A_2^{II}Mo_3O_8$ compounds (mentioned above) while the latter compound contains discrete octahedra of bonded niobium atoms.

The research presented here began in an attempt to better understand the metal-metal bonding interactions in the trinuclear clusters of the compounds $A_2^{II}Mo_3O_8$. The initial experiments have led to the discovery of several other new reduced ternary and quaternary oxides of molybdenum. Some of these new compounds possess unprecedented

structures in an oxide system. One compound contains discrete planar tetrameric molybdenum atom clusters (16) (section II), while two other compounds contain infinite chains of condensed octahedral molybdenum atom clusters (17) (sections III and IV).

Explanation of Dissertation Format

This dissertation is divided into five sections. Each of the first four sections is written in a form suitable for publication as a technical paper. The research presented in this dissertation is the work of the author. While references cited in the general introduction may be found at the end of the dissertation, each section contains an independent listing of references which are cited in that section.

SECTION I. SYNTHESIS, CRYSTAL STRUCTURES, AND PROPERTIES OF $LiZn_2Mo_3O_8$ AND $Zn_3Mo_3O_8$. SYNTHESIS AND CHARACTERIZATION OF $ScZnMo_3O_8$. COMPOUNDS CONTAINING THE Mo_3O_{13} CLUSTER UNIT

INTRODUCTION

Many sulfides, selenides, tellurides and halides containing discrete metal atom clusters and condensed cluster arrangements are known. A few classic examples of these are $PbMo_6S_8$ (1), Mo_6Cl_{12} (2), Gd_2Cl_3 (3) and ZrCl (4). However, metal atom clusters and condensed clusters in oxide systems are relatively few in number. Some examples of these oxides are NbO_2 (5), $Mg_3Nb_6O_{11}$ (6), $Ba_{1.14}Mo_8O_{16}$ (7), and $NaMo_4O_6$ (8).

An interesting family of compounds incorporating the Mo_3O_{13} cluster unit includes compounds of the types $A_2^{II}Mo_3O_8$ (A = Mg, Mn, Fe, Co, Ni, Zn, Cd) (9) and $LiRMo_3O_8$ (R = Sc, Y, In, Sm, Gd, Tb, Dy, Ho, Er, Yb) (10). The crystal structure of $Zn_2Mo_3O_8$ was determined (11) and shown to consist of a distorted hexagonal close-packed arrangement of oxygen atoms (with layer stacking sequence abac) where the oxygen layers are held together by alternating zinc atom layers and molybdenum atom layers. The divalent zinc ions occupy both tetrahedral and octahedral sites in a 1:1 ratio. The tetravalent molybdenum ions occupy octahedral sites to form strongly bonded triangular clusters of molybdenum atoms in which three MoO_6 octahedra are each shared along two edges. Oxygen atoms of the Mo_3O_{13} clusters are shared with other cluster units as represented by the formulation $Mo_3O_4O_{6/2}O_{3/3}$, to give the Mo_3O_8 stoichiometry. A molecular orbital calculation (12) for the Mo_3O_{13} cluster unit explained the strong bonding, weak paramagnetism, and low electrical conductivity of the $A_2Mo_3O_8$ compounds by showing that the six electrons available for Mo-Mo bonding occupy bonding orbitals with all electron spins paired. The basic structure of the $LiRMo_3O_8$ compounds differs from the $A_2Mo_3O_8$

compounds in having a simple oxygen layering of the (abab) type with the Li^+ ions in tetrahedral sites and the R^{3+} ions in octahedral positions.

The M_3X_{13} cluster unit has also been observed in the halide compounds Nb_3X_8 (X = Cl, Br, I) (13), and Ti_7X_{16} (X = Cl, Br) (14). The first molecular example of a compound containing the M_3X_{13} cluster unit was $W_3(OCH_2C(CH_3)_3)O_3Cr_3(O_2CC(CH_3)_3)_{12}$ (15) where M = tungsten, while the first reported ionic example of an M_3X_{13} cluster was the $W_3O_4F_9^{5-}$ (16) anion. Ionic species containing the Mo_3O_{13} cluster unit have recently been prepared from aqueous solutions of molybdenum(IV). Two such examples of these ions are $[Mo_3O_4(C_2O_4)_3(H_2O)_3]^{2-}$ (17), and $[Mo_3OCl_3(O_2CCH_3)_3(H_2O)_3]^{2+}$ (18).

This section reports the preparation, crystal structures, magnetic and physical properties of the new compounds $LiZn_2Mo_3O_8$ and $Zn_3Mo_3O_8$. These phases represent two new types of reduced molybdenum oxides containing Mo_3O_{13} cluster units, $LiA_2^{II}Mo_3O_8$ and $A_3^{II}Mo_3O_8$. The triangular molybdenum atom cluster units in these new compounds have available 7 and 8 electrons, respectively, for Mo-Mo bonding. Also described in this section are the preparation, x-ray powder diffraction data, magnetic and physical properties of another reduced quaternary oxide of molybdenum, $ScZnMo_3O_8$. This phase represents the first example of an $A^{II}B^{III}Mo_3O_8$ type compound.

EXPERIMENTAL

Materials

The starting materials used were Alfa Products Li_2MoO_4 (98.5%), Fisher Certified A.C.S. ZnO, MoO_3, and KOH (85.6%), Atomergic Sc_2O_3 (99.9%), Hach Chemical CsCl (99.9%), Thermo-Electron Mo tubing (99.97%), Rembar Mo sheet (99.95%), Aldrich Mo powder (99.99%), and MoO_2. The Li_2MoO_4 and ZnO were dried at 120°C before use. Potassium molybdate, which was used as a flux, was prepared by the reaction of KOH with a slight stoichiometric excess of MoO_3 in deionized water. After the solution was filtered, its volume was reduced by heating, and the precipitate collected on a glass frit, washed with ethanol, dried at 120°C, and stored over P_4O_{10}. Cesium molybdate, also used as a flux, was prepared by passing an aqueous solution of CsCl through a column of Amberlite IRA-400 strongly basic ion exchange resin in hydroxide form and neutralizing the effluent with the stoichiometric quantity of MoO_3. The solution was slowly evaporated to dryness and the white solid dried in vacuo at 110°C for several hours, then stored over P_4O_{10}. Molybdenum dioxide was prepared by two methods; reaction of MoO_3 and Mo powder in mole ratio 2:1 in an evacuated fused quartz tube held at 700°C for 2 days, and by the hydrogen reduction of MoO_3 at 460°C for 48 hours. Each preparation of MoO_2 was washed several times with alternate portions of 3M NH_4OH, deionized water, and 3M HCl until the washings were colorless, and finally dried in vacuo at 110°C. The product of the MoO_3/Mo reaction was later found to contain higher molybdenum oxides and

its use was discontinued. The product of the H_2 reduction reaction was analyzed and found to contain 74.9% Mo *vs* the calculated 75.0% Mo for MoO_2.

Syntheses

$LiZn_2Mo_3O_8$

This crystalline compound was first discovered in a multiphase product obtained from a reaction of Li_2MoO_4, ZnO and MoO_2 (containing higher molybdenum oxide impurities) in mole ratio 1:2:5. The reactants were ground together in a mortar, pelletized under *ca.* 10,000 lb/in^2, sealed in an evacuated molybdenum tube (3 cm long x 1.9 cm diam) which, in turn, was sealed in an evacuated fused quartz protection tube, and held at 1100°C for 2 days. Other identified products were unreacted MoO_2 and a new ternary oxide of lithium and molybdenum presently under investigation. Crystals of $LiZn_2Mo_3O_8$ grew as black chunks and thin plates. The composition of this phase was determined from single crystal and powder x-ray diffraction data as well as chemical analyses (see below).

The compound $LiZn_2Mo_3O_8$ was prepared with 90% purity in powder form by reacting the stoichiometric quantities of Li_2MoO_4, ZnO, MoO_2 (99.9%) and Mo powder as a pellet in a molybdenum tube at 1100°C for 5 days. The polycrystalline product pellet was powdered in a mortar and washed several times with 3M HCl and deionized water to remove unreacted ZnO and Li_2MoO_4; the solid was then dried under vacuum at 110°C. A Guinier x-ray powder diffraction pattern of this product showed only the

strongest lines for Mo and MoO_2, and the lines that could be calculated (19) from the single crystal structure of $LiZn_2Mo_3O_8$. Samples for chemical analyses were prepared by dissolving weighed portions of product in aqua regia and diluting to 100 ml in volumetric flasks. The Li and Zn analyses were performed by atomic absorption spectroscopy and Mo was analyzed spectrophotometrically. Anal. Calcd. for $LiZn_2Mo_3O_8$: Li, 1.25; Zn, 23.6; Mo, 52.0. Found: Li, 1.1; Zn, 21.2; Mo, 54.9.

The observed percentage composition confirmed the Zn/Li ratio of 2.0. However, the observed results were low when compared to the calculated values for Li and Zn, and were high when compared to the calculated value for Mo. These results could be explained when the results of oxidation-reduction titrations for molybdenum were considered. For determination of the oxidation state of molybdenum, weighed samples were dissolved in standardized ceric sulfate - 3M H_2SO_4 solution. After complete oxidation of all molybdenum to Mo(VI), the excess Ce(IV) was titrated with standard Fe(II) solution. The results of these redox titrations showed molybdenum to be in an average oxidation state of +3.48 when based on the calculated value of 52.0% Mo, and +3.61 when the observed value of 54.9% Mo was used. An MoO_2 impurity would have raised the percent molybdenum above that calculated for $LiZn_2Mo_3O_8$ but would have resulted in an average molybdenum oxidation state greater than +3.66. An Mo metal impurity would have lowered the net oxidation state value below that calculated for $LiZn_2Mo_3O_8$ but would not have been enough to account for the high Mo analysis. The best explanation

for these results was that both MoO_2 and Mo powder remained unreacted in the product as seen in the x-ray powder diffraction pattern. The composition of the product was, therefore, calculated as containing approximately 89% $LiZn_2Mo_3O_8$, 9.5% MoO_2, and 1.5% Mo.

$ScZnMo_3O_8$

It was found that a fluxing agent such as K_2MoO_4 or Cs_2MoO_4 was necessary in the preparation of this compound. Three to five percent by weight of flux was mixed by grinding with the stoichiometric quantities of Sc_2O_3, ZnO, MoO_2 (99.9%), and Mo. The reactant mixture was pelletized, sealed in an evacuated molybdenum tube (3 cm in length x 1.3 cm diam) which, in turn, was sealed in an evacuated inconel protection tube, and fired at 1100°C for 5-7 days. The product was powdered in a mortar and washed several times with 3M HCl to remove ZnO, then rinsed with deionized water and dried. A Guinier x-ray powder diffraction pattern, taken on the washed product where K_2MoO_4 flux was used, showed lines of the desired phase, $ScZnMo_3O_8$ (see x-ray powder data below), lines of the new phase $K_2Mo_{12}O_{19}$ (20), and the strongest lines of Sc_2O_3. The powder pattern of $ScZnMo_3O_8$ is essentially the same as that for $Zn_2Mo_3O_8$ except the unit cell volume is larger for the new compound. If all of the K_2MoO_4 reacted to form $K_2Mo_{12}O_{19}$, then the resultant mixture should contain approximately 80.7% $ScZnMo_3O_8$, 17.2% $K_2Mo_{12}O_{19}$, and 2.1% Sc_2O_3. In contrast, when Cs_2MoO_4 flux was used, the lines of $ScZnMo_3O_8$, $Zn_2Mo_3O_8$, Sc_2O_3, MoO_2, and Mo were all visible in the x-ray diffraction powder pattern.

$Zn_3Mo_3O_8$

This phase was first discovered in a reaction product obtained from a mixture of K_2MoO_4, ZnO, and MoO_2 (containing higher molybdenum oxide impurities) in mole ratio 1:2:5. The reactants were ground in a mortar, pressed into a pellet, sealed in an evacuated molybdenum tube (2.5 cm long x 1.9 cm diam) which, in turn, was sealed in an evacuated fused quartz tube, and held at 1100°C for 10 days. Crystals of this new phase grew mostly as bundles of smaller irregularly shaped crystals. Electron microprobe analysis confirmed the presence of Zn and Mo as the only metallic elements in this phase. A Guinier x-ray powder diffraction pattern of these crystals was essentially identical to that of $LiZn_2Mo_3O_8$ except the unit cell volume was larger for $Zn_3Mo_3O_8$ (see x-ray powder data below). The composition and structure of $Zn_3Mo_3O_8$ was obtained from single crystal x-ray diffraction data and supported by a magnetic susceptibility measurement, infrared spectra, and physical property observations (see below). Other identified products in the above reaction were $Zn_2Mo_3O_8$ (9) and the new compound $K_2Mo_{12}O_{19}$ (20) as evidenced from a Guinier x-ray powder diffraction pattern taken on the product pellet.

It was later found that $Zn_3Mo_3O_8$ could be prepared in approximately 97% purity by mixing the stoichiometric quantities of ZnO, MoO_3, and Mo, and heating the pelletized reaction mixture in a molybdenum tube at 1100°C for 5 days (shorter reaction times were not investigated). This product was powdered in a mortar, washed several times with 2M HCl, rinsed with deionized water, and dried. A Guinier x-ray powder

diffraction pattern of this preparation showed only the lines that could be calculated from the structure of $Zn_3Mo_3O_8$ and faintly showed the strongest line for Mo metal. The average molybdenum oxidation state for this product was determined as described for $LiZn_2Mo_3O_8$. The results showed a net molybdenum oxidation state of +3.03 when based on pure $Zn_3Mo_3O_8$. This result was low when compared to the calculated value of +3.33. Based on this information, the product was calculated as containing 97% $Zn_3Mo_3O_8$ and 3% Mo metal.

$Zn_2Mo_3O_8$

This compound was prepared as described in the literature (9) by grinding together the stoichiometric quantities of ZnO and MoO_2, pressing the reaction mixture into a pellet, sealing in an evacuated fused quartz tube, and heating at 1100°C for 4 days. The product was washed with 3M HCl to remove unreacted ZnO, rinsed with deionized water, and dried.

Physical Measurements and Properties

Magnetic susceptibilities of the solid compounds $LiZn_2Mo_3O_8$, $ScZnMo_3O_8$, and $Zn_3Mo_3O_8$ were measured by the Gouy method in air at room temperature. The gram susceptibility of $ScZnMo_3O_8$ was corrected for the presence of $K_2Mo_{12}O_{19}$ (20) impurity. The correction was based on the estimated impurity level calculated above (see Syntheses) and on the observed gram susceptibility obtained for pure $K_2Mo_{12}O_{19}$ (20). Molar susceptibilities were corrected for diamagnetic contributions

from the constituent atoms. Corrected molar susceptibilities, χ_m', and effective magnetic moments, μ_{eff}, per gram molecule (formula unit) of each compound are given in Table I-1. The moments were calculated assuming that the compounds obeyed the Curie law, $\mu_{eff} = 2.84\ (\chi_m' T)^{\frac{1}{2}}$.

Table I-1. Magnetic data for oxide compounds containing the Mo_3O_{13} cluster unit

Compound	χ_m' (cgs)	μ_{eff} (B.M.)
$Zn_2Mo_3O_8$[a]	1.4×10^{-4}	0.6
$ScZnMo_3O_8$	8.7×10^{-4}	1.5
$LiZn_2Mo_3O_8$	5.5×10^{-4}	1.2
$Zn_3Mo_3O_8$	1.6×10^{-4}	0.6

[a]Reference 9.

Infrared spectra in the region 300 - 1000 cm^{-1} were taken using a Beckman IR 4250 spectrometer with Nujol mulls of the samples on CsI windows. The spectra were calibrated using polystyrene absorptions in the region 1000 - 1200 cm^{-1}. The observed absorptions for the compounds $Zn_2Mo_3O_8$, $ScZnMo_3O_8$, $LiZn_2Mo_3O_8$, $Zn_3Mo_3O_8$, and ZnO are shown in Figure I-1, and the absorptions attributed to Mo-O bonds are listed in Table I-2.

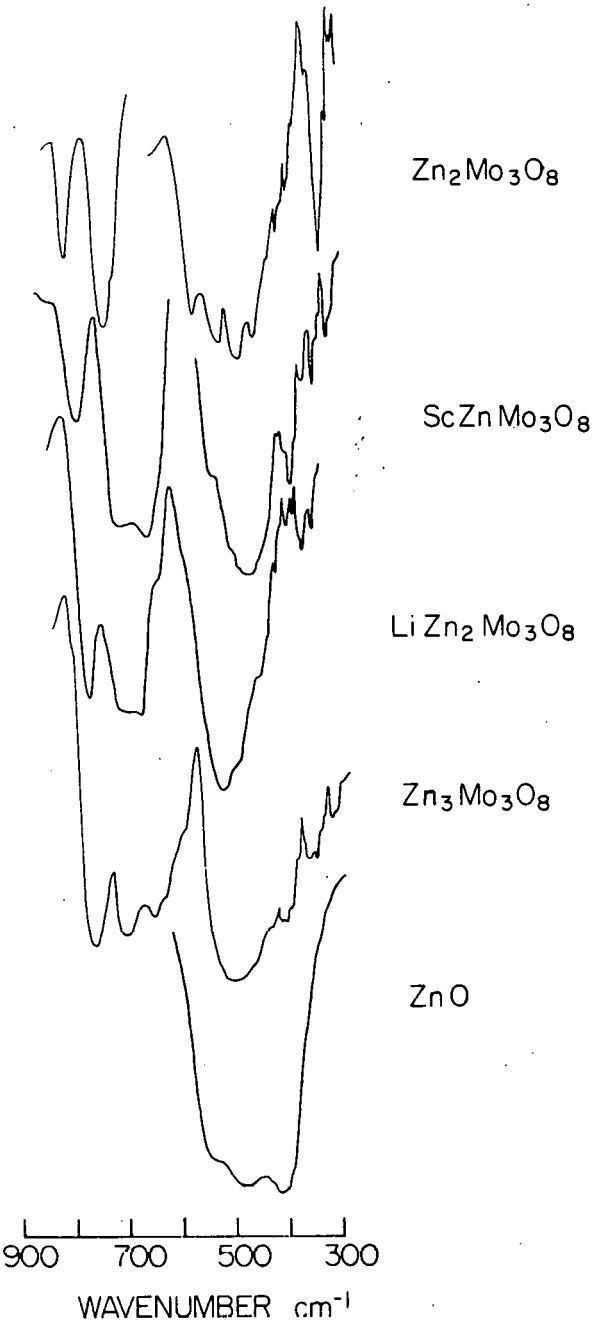

Figure I-1. Infrared absorption spectra for Mo_3O_{13} cluster-containing compounds. Mo-O absorptions are in the 600 - 900 cm^{-1} region. Zn-O absorptions are in the 300 - 600 cm^{-1} region

Table I-2. Infrared data (cm^{-1}) for Mo-O absorptions in the 600 - 900 cm^{-1} region[a]

$Zn_2Mo_3O_8$	$ScZnMo_3O_8$	$LiZn_2Mo_3O_8$	$Zn_3Mo_3O_8$
817 (m)	790 (m)	767 (s)	760 (s)
742 (s)	712 (s)	695 (s)	700 (s)
725 (m,sh)	660 (s)	670 (s)	650 (s)
		635 (m,sh)	630 (m,sh)

[a] s = strong, m = medium, sh = shoulder.

When finely powdered, $LiZn_2Mo_3O_8$ and $ScZnMo_3O_8$ were black in color while $Zn_2Mo_3O_8$ was dark green and $Zn_3Mo_3O_8$ was dark brown. All of the new compounds appeared stable towards 3M hydrochloric acid but, unlike $Zn_2Mo_3O_8$, they were rapidly decomposed in 3M HNO_3 and slowly decomposed in 1.5M HNO_3 with gas evolution.

X-Ray Powder Diffraction Data

An Enraf Nonius Delft triple focusing Guinier x-ray powder diffraction camera was used with Cu K_{α_1} radiation (λ = 1.54056 Å) to obtain unit cell data. National Bureau of Standards silicon powder was mixed with all samples as an internal standard. The lattice parameters for $ScZnMo_3O_8$, $Zn_3Mo_3O_8$ and $Zn_2Mo_3O_8$ were calculated by a least squares method and are listed in Table I-3. The compound

Table I-3. Lattice parameters for oxide compounds containing the Mo_3O_{13} cluster unit

Compound	a, Å	c, Å	V, Å^3
$LiZn_2Mo_3O_8$	5.8116(6)	31.013(8)	3(302.4)[a]
$ScZnMo_3O_8$	5.8050(7)	9.996(3)	291.7[b]
$Zn_3Mo_3O_8$	5.8617(4) 5.8503(2)	31.100(3) 31.207(3)	3(308.5)[a] 3(308.3)[b]
$Zn_2Mo_3O_8$	5.7742(3) 5.759(4)	9.920(1) 9.903(5)	286.4[b] 284.4[c]

[a]From single crystal x-ray diffraction data.

[b]From powder x-ray diffraction data.

[c]Reference 11.

$ScZnMo_3O_8$ was indexed on the basis of a hexagonal unit cell and $Zn_3Mo_3O_8$ on the basis of an R-centered hexagonal unit cell. The lattice parameters for $Zn_3Mo_3O_8$ were calculated using the strongest 13 lines, and the lattice parameters for $ScZnMo_3O_8$ were calculated using the strongest 14 lines which remained when the lines of known impurities were removed. The observed vs calculated d-spacings for these two compounds are listed in Tables I-4 and I-5. Lattice parameters for $Zn_2Mo_3O_8$ were calculated using the strongest 18 lines observed in its x-ray powder diffraction pattern.

Table I-4. X-ray powder data for $ScZnMo_3O_8$

h	k	ℓ	d_{obsd}	d_{calcd}	I_{obsd}[a]
0	0	2	4.977	4.999	s
1	0	1	4.475	4.491	m
0	1	2	3.543	3.545	vs
0	1	3	2.776	2.778	m
1	1	2	2.511	2.510	vs
2	0	1	2.438	2.438	vs
0	2	2	2.246	2.246	m
2	0	3	2.007	2.007	s
2	1	0	1.901	1.900	w
1	2	1	1.867	1.867	m
0	2	4	1.772	1.772	m
2	1	3	1.651	1.651	s
0	3	2	1.588	1.589	m
2	0	5	1.565	1.565	m
2	2	0	1.451	1.451	s
2	2	2	1.393	1.394	vw
3	0	5	1.285	1.284	vw
2	2	4	1.255	1.255	vw

[a] vs = very strong, s = strong, m = medium, w = weak, vw = very weak.

Table I-5. X-ray powder data for $Zn_3Mo_3O_8$

h	k	ℓ	d_{obsd}	d_{calcd}	I_{obsd}[a]
0	0	6	5.205	5.199	s
1	0	1	4.996	4.999	m
0	1	2	4.819	4.817	s
1	0	4	4.252	4.248	vw
0	1	5	3.928	3.932	vw
1	0	7	3.348	3.346	w
0	1	8	3.091	3.090	s
1	1	0	2.926	2.924	m
1	0	10	2.658	2.656	s
0	0	12	2.600	2.599	w
1	1	6	2.550	2.549	vs
2	0	2	2.500	2.500	vs
0	2	4	2.410	2.409	s
2	0	8	2.125	2.124	s
0	2	10	1.967	1.966	vw
1	2	5	1.830	1.830	vw
1	2	8	1.719	1.718	vw
2	0	14	1.674	1.673	w
2	1	10	1.632	1.632	w
3	0	6	1.606	1.606	m
1	2	11	1.587	1.587	vw
0	2	16	1.545	1.545	m
3	0	9	1.518	1.518	vw
2	2	0	1.463	1.462	m
1	3	10	1.281	1.281	vw
2	2	12	1.274	1.274	vw

[a] vs = very strong, s = strong, m = medium, w = weak, vw = very weak.

X-Ray Data Collection for $LiZn_2Mo_3O_8$

A single crystal of $LiZn_2Mo_3O_8$ in the form of a thin plate of dimensions 0.14 x 0.13 x 0.03 mm was mounted on the tip of a glass fiber with epoxy adhesive and used for x-ray data collection. The crystal was indexed as C-centered monoclinic on an automated four-circle diffractometer, designed and built in Ames Laboratory (21), with an automatic indexing program (22) that uses reflections taken from several ω-oscillation photographs as input. The data set was collected on the same diffractometer at ambient temperature using Mo K_α radiation (λ = 0.71034 Å) monochromatized with a graphite single crystal. All data within a sphere defined by $2\theta \leq 60°$ were collected in the HKL and $HK\bar{L}$ octants using an ω-scan mode. The peak heights of three standard reflections which were remeasured every 75 reflections did not show any significant change over the period of data collection. Final unit cell parameters and their estimated standard deviations were obtained from the same crystal by a least-squares refinement of 2θ values of 14 Friedel-related pairs of independent reflections randomly distributed in reciprocal space having $2\theta > 30°$. The results were a = 26.624(5) Å, b = 5.811(1) Å, c = 12.326(3) Å, and β = 107.95(2)°.

Structure Determination and Refinement of $LiZn_2Mo_3O_8$

Upon examination of the data, it was found that all but two very weak reflections (which were then eliminated) satisfied the condition for C-centering, h+k = 2n. The observed intensities were corrected for

Lorentz-polarization effects and their standard deviations calculated (23) to yield 868 observed independent reflections with $I > 3\sigma_I$ after averaging of equivalent reflections.

Patterson-superposition techniques (24) were used to locate the positions of all 36 molybdenum atoms in the unit cell and to determine the space group as C2/m (no. 12). A full-matrix least-squares refinement (25) on the positional parameters of the molybdenum atoms initially resulted in an unweighted residual $R = \Sigma\left||F_o|-|F_c|\right|/\Sigma|F_o|$ of 0.35, but the positions were very strongly correlated and quickly caused the refinement to diverge. At that point, a study of the structure from an electron density map (26) showed that the monoclinic cell could be transformed to a smaller monoclinic cell containing one-third the volume with a = 10.062(3), b = 5.811(1), c = 10.869(5) Å, and $\beta = 107.95°$. Transformation matrices were calculated to obtain new reflection indices and fractional coordinates for the smaller cell, and all but two very weak reflections were transformed to integer indices. Examination of this data set revealed the systematic nonextinction condition h+k = 2n, and again the space group C2/m was selected.

Least-squares refinement of molybdenum positions then proceeded smoothly with no correlation effects. Zinc and oxygen positions were located from electron density Fourier maps and subsequent refinement of positional parameters, zinc multipliers, and isotropic thermal parameters converged to give R = 0.082. The zinc atom positions were all partially occupied and resulted in a total zinc occupation number of 7.84(8) atoms/cell. Because the crystal possessed a linear

absorption coefficient of 140 cm^{-1} and a thin plate morphology, relative transmission factors were found to vary from 0.3 to 0.7. An absorption correction was made using an empirical ϕ-scan method (27) where the intensity of a selected reflection at $\chi = 90°$ was measured every 10° in ϕ on the x-ray diffractometer. Isotropic refinement of the structure then converged at R = 0.054 and R_w = 0.070 where $R_w = [\Sigma\omega(|F_o|-|F_2|)^2/\Sigma\omega|F_o|^2]^{\frac{1}{2}}$ and $\omega = \sigma_F^{-2}$. Further refinement of the scale factor, positional parameters, zinc multipliers, and anisotropic thermal parameters gave convergence at R = 0.049 and R_w = 0.064 with no significant change in zinc multipliers.

A study of the structure and symmetry led to the discovery that $LiZn_2Mo_3O_8$ could be better described in an R-centered hexagonal unit cell. Indices in the monoclinic reduced data set were all converted to the rhombohedral equivalents and redundant data averaged to yield 352 independent reflections satisfying the condition $-h+k+\ell = 3n$. The 14 reflections originally used to obtain the large monoclinic cell parameters were relabeled and a least-squares fit gave an R-hexagonal unit cell with a = 5.8116(6) Å and c = 31.013(8) Å (also listed in Table I-3). A full-matrix least-squares refinement of scale factor, positional parameters, zinc occupation numbers, and anisotropic thermal parameters in space group $R\bar{3}m$ (no. 166) gave R = 0.042 and R_w = 0.055 with a total zinc occupation number of 11.77(14) atoms/cell or 1.96(2) zinc atoms per molybdenum trimer. In both the monoclinic and rhombohedral refinements, one of the 'octahedrally' coordinated zinc atoms was found to be disordered within its site. Electron

density maxima were found along the hexagonal z direction just above and below the inversion center located at this site. (Constraining the zinc atom on this $\bar{3}$m position at 0,0,½ resulted in a very large isotropic thermal parameter for this atom and poor overall refinement with R = 0.12.) The lithium atoms could not be found from subsequent electron density difference maps and were assumed to be partially occupied in the same sites that are partially occupied by zinc atoms. These sites would, therefore, always be occupied by zinc or lithium atoms. A final difference Fourier synthesis map was flat to $\leq$ 0.5 e/Å^3.

The atomic scattering factors used were those of Hanson et al. (28) for neutral atoms, and molybdenum and zinc were corrected for the real and imaginary parts of anomalous dispersion (29).

X-Ray Data Collection for $Zn_3Mo_3O_8$

Many irregularly shaped crystals of $Zn_3Mo_3O_8$ were carefully selected and mounted in 0.2 mm Lindemann glass capillaries with a small amount of silicone grease. Each crystal was, in turn, placed on the four-circle x-ray diffractometer (21) and three or four ω-oscillation photographs were taken at various ϕ settings. The photographs showed that most of the crystals were actually multiple crystals or twinned crystals. The three best crystals, possessing relatively sharp single diffraction peaks, were indexed (22) and the reduced cells which resulted could be transformed to the desired R-centered hexagonal unit cell. Based on the quality of the oscillation photographs and an examination of several diffraction peak widths, a crystal

0.22 x 0.22 x 0.12 mm was selected for data collection. The data set was collected on the basis of a hexagonal unit cell on the same x-ray diffractometer and under the same conditions described above. All data in a sphere defined by $2\theta \leq 60°$ were collected in the HKL, $\bar{H}\bar{K}L$, and $H\bar{K}\bar{L}$ octants using an ω-scan mode. The peak heights of three standard reflections which were remeasured every 75 reflections did not show any significant change over the period of data collection. Final unit cell parameters were obtained from the same crystal by a least-squares refinement of $\pm 2\theta$ values of 21 independent reflections randomly distributed in reciprocal space having $2\theta > 24°$. The results were a = 5.8617(4) Å, c = 31.100(3) Å, and V = 925.5 $Å^3$ (also listed in Table I-3).

Structure Refinement of $Zn_3Mo_3O_8$

Examination of the data set revealed that all of the observed reflections satisfied the nonextinction condition of $h-k+\ell = 3n$. The indices were transformed to give $-h+k+\ell = 3n$ and an absorption correction (27) was made (μ = 160 cm^{-1}) using an empirical ϕ-scan method as described above for $LiZn_2Mo_3O_8$. The observed intensities were corrected for Lorentz and polarization effects and their standard deviations calculated as previously described (23) to yield 1308 reflections with $I > 3\sigma_I$. The data were finally averaged in $\bar{3}m$ symmetry to give 370 independent reflections for the final data set.

Previous x-ray powder diffraction data had shown this new compound to be isostructural with that of $LiZn_2Mo_3O_8$, see Tables I-3 and I-5.

Therefore, the atomic positions for $LiZn_2Mo_3O_8$ were used as the starting set of positions for $Zn_3Mo_3O_8$ in space group $R\bar{3}m$. The zinc atom that was found to be disordered through an inversion center within its octahedral site in $LiZn_2Mo_3O_8$ was initially constrained to that special position at 0,0,½ in this new structure, and all zinc atom multipliers were constrained to give full site occupancies. A full-matrix least-squares refinement (25) on all positional and isotropic thermal parameters resulted in an unweighted residual R of 0.150 but, as seen for $LiZn_2Mo_3O_8$, the one zinc atom had a large isotropic temperature factor of 3.5 $Å^2$. This atom was then removed from the atomic parameter list and an electron density map was generated (26) which revealed zinc electron density maxima along the hexagonal c axis just above and below the site of $\bar{3}m$ symmetry at 0,0,½ as seen in $LiZn_2Mo_3O_8$. The zinc atom was then placed at z = 0.48 and a refinement of all positional and isotropic thermal parameters as well as all zinc occupation numbers (multipliers) converged to give R = 0.076 and R_w = 0.099 with 18.0(4) Zn atoms/cell or 3.00(7) zinc atoms per molybdenum trimer. Further refinement of the scale factor, zinc multipliers, positional and anisotropic thermal parameters gave convergence at R = 0.060 and R_w = 0.080 with 2.98(5) zinc atoms per molybdenum trimer. A correlation matrix showed the multipliers of zinc atoms Zn1 and Zn4 to be correlated and multipliers of Zn2 and Zn3 also correlated with correlation values of 0.4 and 0.5, respectively. A final difference Fourier synthesis map was flat to $\leq$ 1e/$Å^3$.

The atomic scattering factors and corrections for anomalous dispersion were as described above (28,29).

RESULTS AND DISCUSSION

Crystal Structures of $LiZn_2Mo_3O_8$ and $Zn_3Mo_3O_8$

Final positional parameters for $LiZn_2Mo_3O_8$ and $Zn_3Mo_3O_8$ are listed in Tables I-6 and I-7, and thermal parameters in Tables I-8 and I-9, respectively. Important interatomic distances for both compounds are given in Table I-10, and bond angles for both compounds are listed in Table I-11. Observed and calculated structure factors are available as supplementary material.

The essential structural features of $LiZn_2Mo_3O_8$(I) and $Zn_3Mo_3O_8$(II) are the same and are related to those of $Zn_2Mo_3O_8$ (11). Both new compounds consist of a distorted cubic close packing (abc) of oxygen atoms in which the oxygen layers are held together by alternate layers of zinc and molybdenum ions. The zinc ion sites in $LiZn_2Mo_3O_8$ are fractionally occupied with roughly one-fourth of the zinc ions in approximately octahedral coordination with oxygen and three-fourths in approximately tetrahedral coordination with oxygen. When the sites are not occupied by zinc ions, they are assumed to contain the lithium ions and result in the formulation $Li^{o}_{0.56}Li^{t}_{0.48}Zn^{o}_{0.44}Zn^{t}_{1.52}Mo_3O_8$ (this assumes the x-ray scattering power of Li^{+} to be negligible and to have no affect on the zinc ion occupation numbers). The same zinc ion sites are fully occupied in $Zn_3Mo_3O_8$ with one-third of the zinc ions in approximately octahedral coordination with oxygen and two-thirds in approximately tetrahedral coordination with oxygen, thus resulting in the formulation $Zn^{o}_{1}Zn^{t}_{2}Mo_3O_8$. Within the molybdenum layers of

Table I-6. Positional parameters for $LiZn_2Mo_3O_8$

Atom	Position[a]	Multiplier	x	y	z
Mo 1	18h	0.50	0.1856(2)	0.8144	0.08395(2)
O 1	18h	0.50	0.8454(12)	0.1546	0.0479(2)
O 2	18h	0.50	0.4941(14)	0.5059	0.1247(2)
O 3	6c	0.16666	0.00	0.00	0.1174(3)
O 4	6c	0.16666	0.00	0.00	0.3704(3)
Zn 1	3a	0.037(1)	0.00	0.00	0.00
Zn 2	6c	0.097(1)	0.00	0.00	0.18033(9)
Zn 3	6c	0.156(1)	0.00	0.00	0.30803(5)
Zn 4	6c	0.037(1)	0.00	0.00	0.4873(2)

[a]Space group $R\bar{3}m$ (no. 166).

Table I-7. Positional parameters for $Zn_3Mo_3O_8$

Atom	Position[a]	Multiplier	x	y	z
Mo 1	18h	0.50	0.1866(2)	0.8134	0.08351(3)
O 1	18h	0.50	0.8469(20)	0.1531	0.0462(3)
O 2	18h	0.50	0.4955(27)	0.5045	0.1261(4)
O 3	6c	0.16666	0.00	0.00	0.1168(5)
O 4	6c	0.16666	0.00	0.00	0.3714(5)
Zn 1	3a	0.081(2)	0.00	0.00	0.00
Zn 2	6c	0.160(3)	0.00	0.00	0.17968(9)
Zn 3	6c	0.163(2)	0.00	0.00	0.30754(9)
Zn 4	6c	0.092(2)	0.00	0.00	0.4881(2)

[a]Space group $R\bar{3}m$ (no. 166).

Table I-8. Thermal parameters for $LiZn_2Mo_3O_8$[a]

Atom	B_{11}	B_{22}	B_{33}	B_{12}	B_{13}	B_{23}
Mo 1	0.54(3)	0.54	0.67(3)	0.30(2)	-0.007(7)	0.007
O 1	0.80(17)	0.80	1.27(23)	0.41(18)	-0.30(8)	0.30
O 2	0.99(20)	0.99	1.66(26)	-0.01(21)	-0.21(9)	0.21
O 3	0.66(22)	0.66	0.66(32)	0.33		
O 4	0.85(23)	0.85	0.54(31)	0.42		
Zn 1	1.22(16)	1.22	1.03(21)	0.61		
Zn 2	1.07(9)	1.07	0.64(11)	0.54		
Zn 3	0.76(5)	0.76	0.73(7)	0.38		
Zn 4	0.54(18)	0.54	0.73(25)	0.27		

[a]The general thermal parameter expression used is $\exp[-1/4(B_{11}h^2a^{*2} + B_{22}k^2b^{*2}\ldots 2B_{23}k\ell b^*c^*)]$.

Table I-9. Thermal parameters for $Zn_3Mo_3O_8$[a]

Atom	B_{11}	B_{22}	B_{33}	B_{12}	B_{13}	B_{23}
Mo 1	0.15(4)	0.15	0.64(5)	0.10(3)	-0.01(1)	0.01
O 1	0.75(29)	0.75	0.79(34)	0.61(32)	-0.13(13)	0.13
O 2	0.67(29)	0.67	2.04(45)	-0.32(32)	-0.69(18)	0.69
O 3	0.18(35)	0.18	1.12(59)	0.09		
O 4	0.31(36)	0.31	0.73(55)	0.16		
Zn 1	0.41(11)	0.41	0.60(15)	0.21		
Zn 2	0.96(9)	0.96	0.39(11)	0.48		
Zn 3	0.25(8)	0.25	0.65(11)	0.13		
Zn 4	0.06(12)	0.06	1.53(23)	0.03		

[a]The general thermal parameter expression used is $\exp[-1/4(B_{11}h^2a^{*2} + B_{22}k^2b^{*2}\ldots 2B_{23}k\ell b^*c^*)]$.

Table I-10. Interatomic distances (Å) for $LiZn_2Mo_3O_8$ and $Zn_3Mo_3O_8$

	$LiZn_2Mo_3O_8$	$Zn_3Mo_3O_8$
Mo1-Mo1	2.578(1)	2.580(2)
Mo1-Mo1	3.234(1)	3.282(2)
Mo1-O1	2.063(6)	2.100(9)
Mo1-O2	2.003(8)	2.056(13)
Mo1-O3	2.138(5)	2.160(8)
Mo1-O4	2.079(7)	2.054(11)
Zn1-O1	2.151(7)	2.115(10)
Zn2-O2	1.952(7)	1.939(13)
Zn2-O3	1.948(10)	1.955(17)
Zn3-O1	1.931(6)	1.937(10)
Zn3-O4	1.936(10)	1.986(16)
Zn4-O2	1.851(8)	1.873(13)
Zn4-O2	2.344(9)	2.318(13)

Table I-11. Bond angles (deg) in $LiZn_2Mo_3O_8$ and $Zn_3Mo_3O_8$

	$LiZn_2Mo_3O_8$	$Zn_3Mo_3O_8$
Mo1-Mo1-Mo1	60.00	60.00
Mo1-O2-Mo1	80.1(3)	77.7(4)
Mo1-O4-Mo1	76.6(3)	77.8(5)
O1-Mo1-O1	81.6(2)	79.7(3)
O1-Mo1-O2	93.8(3)	94.8(4)
O1-Mo1-O2	167.8(3)	166.6(5)
O1-Mo1-O3	78.6(2)	78.4(3)
O1-Mo1-O4	90.0(2)	90.3(3)
O2-Mo1-O2	88.5(2)	87.8(4)
O2-Mo1-O3	89.5(5)	88.6(9)
O2-Mo1-O4	101.3(3)	102.0(5)
O3-Mo1-O4	164.8(3)	165.2(5)
O4-Mo1-Mo1	51.7(2)	51.1(3)

both compounds, the ions are arranged with 3-fold symmetry to form an equilateral triangular pattern of bonded (and nonbonded) Mo atoms each in approximately octahedral coordination with oxygen with the octahedra sharing edges.

Each trimeric molybdenum atom cluster is bonded to a total of 13 oxygen atoms as shown by the ORTEP drawing in Figure I-2. The solid, black lines in this figure represent Mo-Mo bonding, the unfilled lines represent Mo-O bonding, while the atomic labels correspond to those in Tables I-10 and I-11. Each Mo atom in the cluster is bonded to two other molybdenum atoms and six oxygen atoms. The Mo_3O_{13} cluster unit contains one oxygen atom (O4) which is triply bridging to the three Mo atoms in a trigonal pyramidal fashion, and has three oxygen atoms (O2) which are each doubly bridging to two Mo atoms along the three edges of the triangle. Each molybdenum atom in the cluster is also bonded to three terminal oxygen atoms (O1 and O3). These terminally bonded oxygen atoms also connect individual clusters to six other surrounding clusters in a hexagonal-like pattern. Oxygen atoms (O1) are each shared between two triangular cluster units while oxygen atoms (O3) are each shared between three separate cluster units resulting in the connectivity formula $[Mo_3O_{1/1}O_{3/1}O_{6/2}O_{3/3}] \equiv Mo_3O_8$, as shown in Figure I-3. All atoms in the unit cells for both compounds I and II lie on mirror planes.

Within the Mo_3O_{13} clusters, the molybdenum ions are strongly bonded to one another with bond distances of 2.578(1) Å (I) and 2.580(2) Å (II), which are ca. 0.15 Å shorter than the distance between nearest

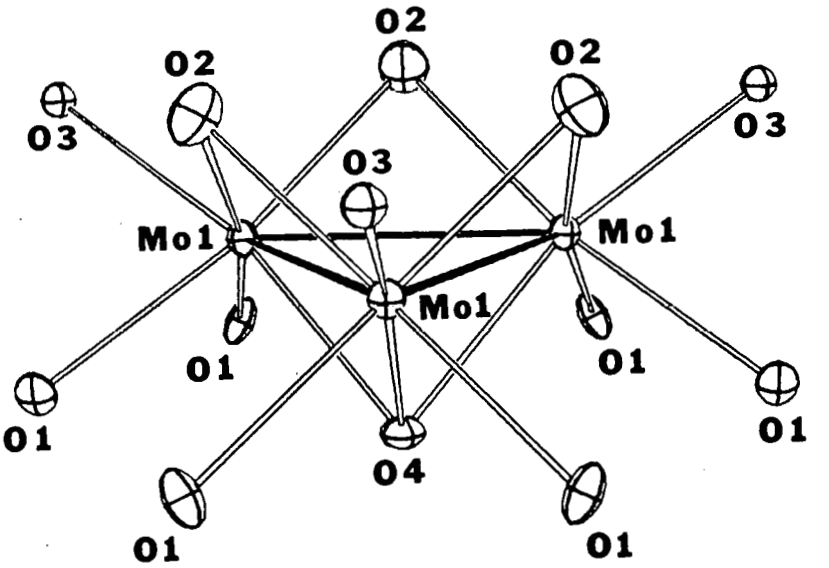

Figure I-2. The Mo_3O_{13} cluster unit as found in the compounds $LiZn_2Mo_3O_8$, $Zn_3Mo_3O_8$, and $Zn_2Mo_3O_8$. Fifty percent probability anisotropic thermal ellipsoids of $LiZn_2Mo_3O_8$ are shown

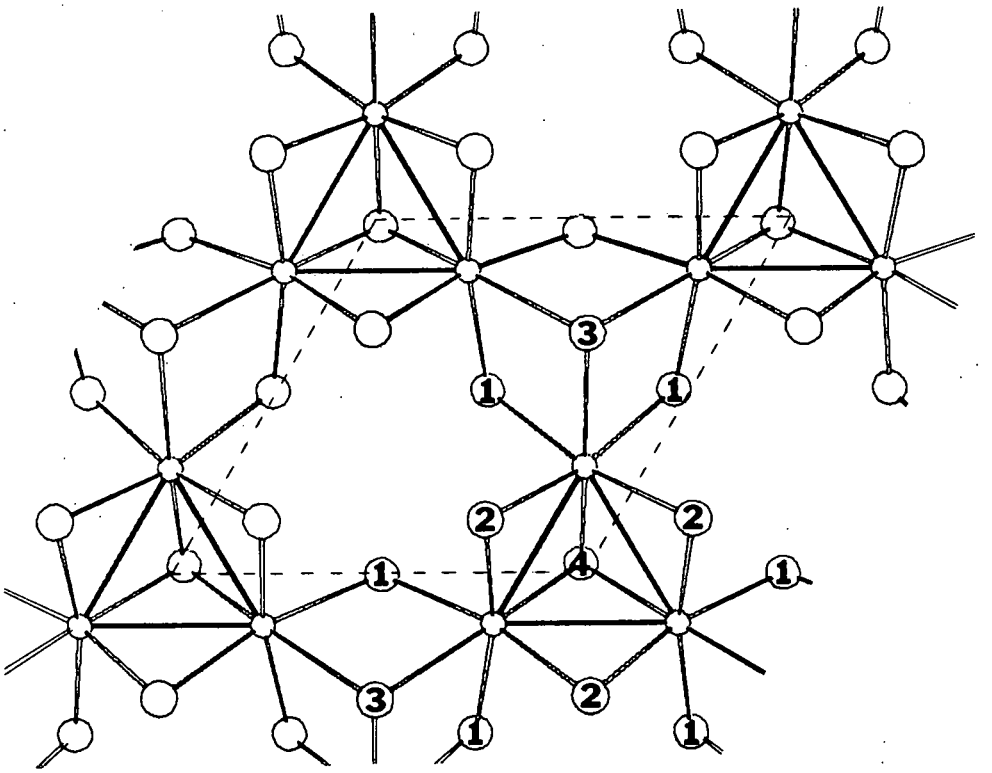

Figure I-3. A view down the c axis of $LiZn_2Mo_3O_8$ and $Zn_3Mo_3O_8$ showing an O-Mo-O section, and the connectivity between Mo_3O_{13} cluster units, $Mo_3O_{1/1}O_{3/1}O_{6/2}O_{3/3}$

neighbors in bcc molybdenum metal. The next nearest Mo-Mo interatomic distances of 3.234(1) Å (I) and 3.282(2) Å (II) indicate no metal-metal bonding interaction between trimeric cluster units. Each triply bridging oxygen atom (O4) with Mo-O distances of 2.079(7) Å (I) and 2.054(11) Å (II) is also coordinated to tetrahedral zinc (Zn3). The doubly bridging oxygen atoms (O2) are each strongly bonded to two molybdenum atoms with Mo-O distances of 2.003(8) Å (I) and 2.056(13) Å (II), and are also coordinated to tetrahedral zinc (Zn2) and octahedral zinc (Zn4). The longest Mo-O bond lengths are those involving oxygen atoms (O3); 2.138(5) Å for compound (I) and 2.160(8) Å for compound (II). These terminal oxygen atoms are also coordinated to tetrahedral zinc (Zn2). Terminal oxygen atoms (O1) are bonded to molybdenum with bond distances of 2.063(6) Å (I) and 2.100(9) Å (II), and also form octahedral interstices for zinc ions (Zn1).

The distorted octahedral coordination around Zn1 involves six O1 oxygen atoms with Zn-O bond distances of 2.151(7)(6X) Å (I) and 2.115(10)(6X) Å (II), which are representative of typical six-coordinate Zn-O distances. These oxygen atoms are arranged around Zn1 to form a trigonal antiprism with O-O distances of 2.695(11)(6X) and 3.353(13)(6X) Å (I); and 2.692(18)(6X) and 3.264(18)(6X) Å (II). The distorted octahedral interstice containing the disordered Zn4 ions is composed of six O2 oxygen atoms; three belonging to one cluster unit above and three belonging to another cluster unit below this octahedral site which lies on a center of inversion symmetry as shown in Figure I-4. The disordered zinc ion positions result in three short and

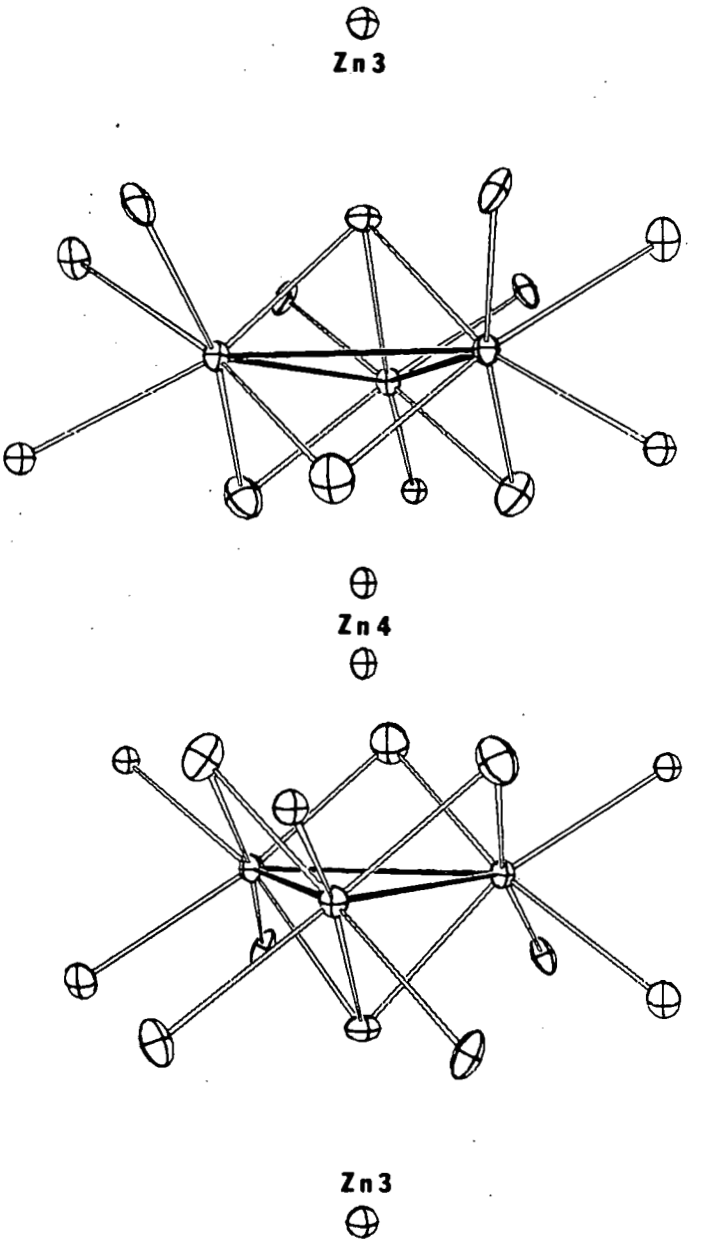

Figure I-4. A view perpendicular to the c axis of $LiZn_2Mo_3O_8$ and $Zn_3Mo_3O_8$ showing the arrangement of two Mo_3O_{13} clusters and the disordered octahedral zinc ion (Zn4) site. Fifty percent probability anisotropic thermal ellipsoids for $LiZn_2Mo_3O_8$ are shown

three long Zn-O bonds in both compounds; 1.851(8)(3X) and 2.344(9)(3X) Å for (I), and 1.873(13)(3X) and 2.318(13)(3X) Å for (II). The oxygen atoms form a trigonal antiprism around this inversion center with O-O distances of 2.795(13)(6X) and 3.066(13)(6X) Å (I); and 2.851(23)(6X) and 3.015(20)(6X) Å (II). Tetrahedral zinc ions (Zn2) are each bonded to three O2 oxygen atoms from three separate clusters and one O3 oxygen atom which bridges three separate cluster units. These distorted tetrahedral sites have Zn-O bond lengths of 1.952(7)(3X) and 1.948(10)(1X) Å (I); and 1.939(13)(3X) and 1.955(17)(1X) Å (II); with O-O distances of 3.017(13)(3X) and 3.321(11)(3X) Å (I); and 3.011(20)(3X) and 3.307(19)(3X) Å (II). Tetrahedral zinc ions (Zn3) are each bonded to three O1 oxygen atoms and one O4 oxygen atom (Figure I-4) which is triply bridging on one trimeric molybdenum atom cluster. The Zn-O bond lengths are 1.931(6)(3X) and 1.936(10)(1X) Å (I); and 1.937(10)(3X) and 1.986(16)(1X) Å (II); with O-O distances of 3.117(11)(3X) and 3.192(11)(3X) Å (I); and 3.170(18)(3X) and 3.195(16)(3X) Å (II). The tetrahedral Zn-O distances for both Zn2 and Zn3 are slightly shorter than the typical average four-coordinate value of 1.98 Å (30).

The oxygen atom layers are distorted from a closest packing arrangement in both $LiZn_2Mo_3O_8$ and $Zn_3Mo_3O_8$. The intralayer O-O distances range from 2.70 to 3.12 Å, and 2.69 to 3.17 Å for compounds (I) and (II), respectively. The average interlayer O-O spacing is shorter between O-Mo-O sections, 2.41 Å (I) and 2.47 Å (II), than between O-Zn-O sections, 2.76 Å (I) and 2.71 Å (II).

Discussion of the $LiZn_2Mo_3O_8$ and $Zn_3Mo_3O_8$ Compounds

The crystal structure refinement of $LiZn_2Mo_3O_8$ has established the Zn, Mo, and O stoichiometry, while chemical analyses have shown the Zn/Li ratio to be 2.0. Evidence for the presence of lithium in this phase also comes from x-ray powder diffraction data obtained on the chemically analyzed preparations. The only lines present in these powder patterns are the same lines that can be calculated (19) from the trigonal structure of $LiZn_2Mo_3O_8$ and the strongest lines of Mo and MoO_2. If the Li^+ ions were to reside in the partially occupied zinc ion sites when zinc was absent from these sites, then the $LiZn_2Mo_3O_8$ stoichiometry would result. This occupation scheme appears most likely for several reasons. One reason is that both zinc and lithium ions are known to occupy octahedral and tetrahedral oxygen interstices. Another reason is that the ionic radii for Zn^{2+} and Li^+ are almost identical (30) with 0.74 vs 0.76 Å for octahedral, and 0.60 vs 0.59 Å for tetrahedral Zn^{2+} and Li^+ ions, respectively. Further support for this Zn-Li occupation model comes from the crystal structure of $Zn_3Mo_3O_8$. The zinc ions in $Zn_3Mo_3O_8$ fully occupy the same octahedral and tetrahedral sites that are only partially occupied by zinc ions in $LiZn_2Mo_3O_8$ (i.e., additional zinc ions do not occupy any 'new' sites in $Zn_3Mo_3O_8$).

Magnetic susceptibility measurements for $LiZn_2Mo_3O_8$ and $Zn_3Mo_3O_8$ support the structures of these two compounds. The molybdenum ions in $LiZn_2Mo_3O_8$ are in the net oxidation state of +3.66 so there are

7 electrons available per trinuclear cluster unit for metal-metal bonding. Six of these electrons are known to reside in bonding orbitals (12) with their spins paired, therefore leaving one unpaired electron. The observed room temperature magnetic moment of 1.2 B.M. for $LiZn_2Mo_3O_8$ (Table I-1) is consistent with this assessment. The Mo ions in $Zn_3Mo_3O_8$ are in the +3.33 net oxidation state and there are 8 electrons available per molybdenum trimer for Mo-Mo bonding. Once again, six of these eight electrons reside in bonding orbitals with their spins paired, and according to a molecular orbital calculation (12), the next two electrons should occupy an a_1 orbital (C_{3v} symmetry) with their spins paired. The observed small magnetic moment of 0.6 B.M. for $Zn_3Mo_3O_8$ (Table I-1) supplies evidence for this spin-paired electron occupation scheme. The weak magnetic moment observed for this material may be due to a temperature-independent paramagnetic (TIP) contribution.

It has also been observed that the metal-metal and metal-oxygen bond distances in these trinuclear cluster compounds become longer as the oxidation state of molybdenum is lowered. Table I-12 compares the Mo-Mo and Mo-O bond lengths for the compounds $Zn_2Mo_3O_8$, $LiZn_2Mo_3O_8$, and $Zn_3Mo_3O_8$. The increase in Mo-Mo bond lengths is attributed to Mo-O pi bonding effects and is discussed below. The increase in Mo-O bond distances arises from the placement of more electron density on the molybdenum ions. This weakening of Mo-O interactions is also manifested in the interlayer oxygen spacings of the new compounds. As the Mo-O interactions become weaker, the interlayer oxygen distance in

Table I-12. Comparison of Mo-Mo and Mo-O bond distances (Å) in $Zn_2Mo_3O_8$, $LiZn_2Mo_3O_8$, and $Zn_3Mo_3O_8$

	$Zn_2Mo_3O_8$[a]	$LiZn_2Mo_3O_8$	$Zn_3Mo_3O_8$
Mo1-Mo1	2.524(2)	2.578(1)	2.580(2)
Mo1-O1	2.058(10)	2.063(6)	2.100(9)
Mo1-O2	1.928(20)	2.003(8)	2.056(13)
Mo1-O3	2.128(30)	2.138(5)	2.160(8)
Mo1-O4	2.002(30)	2.079(7)	2.054(11)
Mo1-O (ave)	2.017	2.058	2.088

[a]Reference 11.

the O-Mo-O layers becomes longer while in the O-Zn-O layers the oxygen interlayer spacing becomes shorter. As expected, the molybdenum-oxygen infrared absorption bands for these compounds shift to relatively lower energies as the triangular clusters are reduced. Figure I-1 shows the IR absorption spectra for these compounds, and Table I-2 lists the observed band energies assigned to Mo-O absorptions. The bands in the region 300 - 600 cm^{-1} are attributed to Zn-O absorptions as seen for the compound ZnO. Although ZnO contains only tetrahedrally coordinated Zn ions, octahedral Zn-O bonds would be expected to absorb radiation of lower energies. The 2% increase in unit cell volume for $Zn_3Mo_3O_8$, relative to $LiZn_2Mo_3O_8$, thus results from the increase in the molybdenum-molybdenum and molybdenum-oxygen bond distances.

Structure and Discussion of $ScZnMo_3O_8$

Based on x-ray powder diffraction data (Tables I-3 and I-4), the structure of $ScZnMo_3O_8$ is essentially identical to that of hexagonal $Zn_2Mo_3O_8$ (space group $P6_3mc$) (11). The 2% increase in unit cell volume for $ScZnMo_3O_8$ is attributed to longer Mo-Mo and Mo-O bond distances arising from a one electron reduction of the Mo_3O_{13} clusters that are present in $Zn_2Mo_3O_8$. The Sc^{3+} ions are assumed to occupy the octahedral sites while the Zn^{2+} ions occupy the tetrahedral sites. Ionic radii for trivalent scandium and divalent zinc ions in octahedral oxygen coordination are almost identical (30), 0.745 Å for Sc^{3+} and 0.74 Å for Zn^{2+}. Therefore, it is assumed that the presence of Sc^{3+} ions in the octahedral sites has negligible effect on the change in unit cell

volume when comparing $Zn_2Mo_3O_8$ and $ScZnMo_3O_8$. A comparison of the Mo-O infrared absorption energies for these two compounds (Figure I-1 and Table I-2) reflects the longer Mo-O bond lengths in $ScZnMo_3O_8$.

Magnetic susceptibility data for this new compound (Table I-1) supply evidence that the Mo_3O_{13} clusters each possess 7 electrons for metal-metal bonding. The effective magnetic moment of 1.5 B.M. confirms the presence of one unpaired electron in each trinuclear cluster unit as expected for the stoichiometry $ScZnMo_3O_8$. The much greater reactivity of this new compound towards oxidation in dilute nitric acid solutions, relative to $Zn_2Mo_3O_8$, also supports the assessment of $ScZnMo_3O_8$ as a more reduced phase.

CONCLUSIONS

The new compounds $LiZn_2Mo_3O_8$, $ScZnMo_3O_8$, and $Zn_3Mo_3O_8$ are three new important members in the family of reduced molybdenum oxides containing the Mo_3O_{13} cluster unit. The metal orbitals in these trinuclear molybdenum atom clusters are now known to accommodate 6, 7, and 8 electrons in the compounds $Zn_2Mo_3O_8$, $LiZn_2Mo_3O_8/ScZnMo_3O_8$, and $Zn_3Mo_3O_8$, respectively. The individual Mo_3O_{13} clusters in $Zn_2Mo_3O_8$, which possess 3m (C_{3v}) symmetry, were treated by an LCAO-MO method and Hückel-type calculations were carried out (12). Two d orbitals per molybdenum atom were reserved for Mo-O bonding and the three remaining d orbitals were used for metal-metal interactions. The energy level diagram which emerged from this calculation provided three bonding orbitals (a_1 and e), an approximately nonbonding level (a_1), and five antibonding orbitals (2e and a_2). This energy level scheme explained the weak paramagnetism (Table I-1), low electrical conductivity, and short Mo-Mo bond distance of 2.524(2) Å in $Zn_2Mo_3O_8$. Each molybdenum atom, with formal oxidation state of +4, would contribute two electrons to the orbitals of the cluster. These six electrons fill the strongly bonding a_1 and e molecular orbitals. According to this molecular orbital picture, a seventh electron (as in $LiZn_2Mo_3O_8$) would occupy a relatively nonbonding orbital. However, the observed Mo-Mo bond distance of 2.578(1) Å in $LiZn_2Mo_3O_8$ is 0.054 Å longer than the Mo-Mo bond distance in $Zn_2Mo_3O_8$, indicative of an antibonding effect.

The observed differences in metal-metal bond lengths can be explained when Mo-O pi bonding interactions are introduced to the molecular orbital diagram. Evidence for molybdenum-oxygen pi bonding comes from an examination of Mo-O bond lengths in the Mo_3O_{13} clusters. It has been observed that the shortest Mo-O bond distances in these compounds are those involving the doubly bridging oxygen atoms, O2 in Figure I-2 and Table I-12. These oxygen atoms in $Zn_2Mo_3O_8$ are each bonded to two Mo atoms and one Zn ion in an sp^2-like planar arrangement (the sum of the Mo-O-Mo and Mo-O-Zn bond angles around this oxygen atom is 356°). The unhybridized p orbital remaining on this oxygen atom is in excellent alignment to overlap with one d orbital on each of the adjacent Mo atoms in the trinuclear cluster. These d orbitals are the same ones that give rise to the nonbonding a_1 orbital. This pi interaction would destabilize the nonbonding a_1 orbital, making it antibonding in character. The same oxygen atoms in $LiZn_2Mo_3O_8$ and $Zn_3Mo_3O_8$ are each bonded to two Mo atoms and two Zn ions (or Li^+ ions in $LiZn_2Mo_3O_8$) in an arrangement that is halfway between an sp^2- and sp^3-like configuration. If the hybridization of this oxygen atom had remained essentially sp^2-planar, a weaker Mo-O pi interaction would have been expected due to an increase in electron density resulting from the addition of the seventh or eighth electrons to the triangular clusters. In $LiZn_2Mo_3O_8$, the pi overlap is further weakened because all of the oxygen atom's p orbitals are utilized in forming metal-oxygen bonds. The a_1 antibonding orbital is, therefore, lowered in energy but still possesses antibonding character. The seventh

electron in the $LiZn_2Mo_3O_8$ clusters thus occupies this orbital and causes an increase in the Mo-Mo bond distance. The pi interactions in the $Zn_3Mo_3O_8$ clusters are much weaker than in $LiZn_2Mo_3O_8$ for the reasons given above. This can be seen in the Mo1-O2 bond distance of 2.056 Å for $Zn_3Mo_3O_8$ which is rather long for a strong Mo-O bond. The antibonding a_1 orbital is lowered further in energy so as to become a weakly antibonding level. The seventh and eighth electrons in the $Zn_3Mo_3O_8$ clusters fill this orbital and cause essentially no change in the Mo-Mo bond length from that in $LiZn_2Mo_3O_8$.

It can be argued that the placement of zinc ion (Zn4) in a position that interacts with the otherwise nonhybridized p orbital on oxygen atom (O2) causes the weakening of Mo-O pi bonding. It can also be argued that the weakening of the Mo-O pi bonding, due to electronic charge build-up on the clusters, allows zinc ion (Zn4) to occupy this otherwise nonavailable site. The true picture probably represents a synergistic effect between these two types of interactions. The assessment of Mo-O pi vs Zn-O interactions could possibly be clarified with a crystal structure determination of $ScZnMo_3O_8$. This compound, which is isostructural with $Zn_2Mo_3O_8$, would contain the sp^2-like planar oxygen atoms (O2); therefore, the effect of another cation competing for the lone pair orbital on oxygen would be eliminated.

REFERENCES

1. Chevrel, R.; Sergent, M.; Prigent, J. J. Solid State Chem. 1971, 3, 515.
2. Schafer, H.; von Schnering, H. G.; Tillack, J.; Kuhnen, F.; Wohrle, H.; Baumann, H. Z. Anorg. Allg. Chem. 1967, 353, 281.
3. Lokken, D. A.; Corbett, J. D. Inorg. Chem. 1973, 12, 556.
4. Adolphson, D. G.; Corbett, J. D. Inorg. Chem. 1976, 15, 1820.
5. Marinder, B. O. Arkiv Kemi 1962, 19, 435.
6. Marinder, B. O. Chemica Scripta 1977, 11, 97.
7. Torardi, C. C. Ph.D. Dissertation, Iowa State University, Ames, Iowa, 1981, Section II.
8. Torardi, C. C.; McCarley, R. E. J. Am. Chem. Soc. 1979, 101, 3963.
9. McCarroll, W. H.; Katz, L.; Ward, R. J. Am. Chem. Soc. 1957, 79, 5410.
10. McCarroll, W. H. Inorg. Chem. 1977, 16, 3351.
11. Ansell, G. B.; Katz, L. Acta Crystallogr. 1966, 21, 482.
12. Cotton, F. A. Inorg. Chem. 1964, 3, 1217.
13. Simon, A.; von Schnering, H. G. J. Less-Common Metals 1966, 11, 31.
14. Schafer, H.; Laumanns, R.; Krebs, B.; Henkel, G. Angew. Chem. 1979, 91, 343.
15. Katovic, V.; Templeton, J. L.; McCarley, R. E. J. Am. Chem. Soc. 1976, 98, 5705.
16. Mattes, R.; Mennemann, K. Z. Anorg. Allg. Chem. 1977, 437, 175.
17. Bino, A.; Cotton, F. A.; Dori, Z. J. Am. Chem. Soc. 1978, 100, 5252.
18. Bino, A.; Cotton, F. A.; Dori, Z. Inorg. Chim. Acta 1979, 33, L133.

19. Clark, C. M.; Smith, D. K.; Johnson, G. J. "A Fortran IV Program for Calculating X-Ray Powder Diffraction Patterns -- Version 5", Department of Geosciences, Pennsylvania State University, September 1973.

20. Torardi, C. C. Ph.D. Dissertation, Iowa State University, Ames, Iowa, 1981, Section V.

21. Rohrbaugh, W. J.; Jacobson, R. A. Inorg. Chem. 1974, 13, 2535.

22. Jacobson, R. A. J. Appl. Crystallogr. 1976, 9, 115.

23. Lawton, S. L.; Jacobson, R. A. Inorg. Chem. 1968, 7, 2124.

24. Hubbard, C. R.; Babich, M. W.; Jacobson, R. A. "A PL/1 Program System for Generalized Patterson Superpositions", 1977, US AEC Report IS-4106.

25. Lapp, R. L.; Jacobson, R. A. "ALLS, A Generalized Crystallographic Least Squares Program", 1979, US DOE Report IS-4708.

26. Powell, D. R.; Jacobson, R. A. "FOUR: A General Crystallographic Fourier Program", 1980, US DOE Report IS-4737.

27. Karcher, B. A. Ph.D. Dissertation, Iowa State University, Ames, Iowa, 1981.

28. Hanson, H. P.; Herman, F.; Lea, J. D.; Skillman, S. Acta Crystallogr. 1964, 17, 1040.

29. Templeton, D. H. In "International Tables for X-Ray Crystallography", 1st ed.; Macgillavry, C. H. and Rieck, G. D., Eds.; Kynoch Press: Birmingham, England, 1962; Vol. III, page 215.

30. Shannon, R. D. Acta Crystallogr. 1976, A32, 751.

SECTION II. SYNTHESIS AND CRYSTAL STRUCTURE OF $Ba_{1.14}Mo_8O_{16}$. A HOLLANDITE-RELATED PHASE CONTAINING PLANAR TETRAMERIC MOLYBDENUM ATOM CLUSTERS AND A SUPERLATTICE ORDERING OF BARIUM IONS

INTRODUCTION

Tetranuclear metal atom clusters are known to exist in halide, sulfide, and selenide compounds, and in ionic and molecular solids in three different geometries. In one type, the four metal atoms bond together with tetrahedral or distorted tetrahedral symmetry as in the compounds $Mo_4S_4Br_4$ (1) and $GaMo_4S_8$ (2). A different but related geometry of metal atoms is the open tetrahedral or 'butterfly' arrangement where one edge of a tetrahedron is elongated relative to the others. This cluster type is found in the anion of the compound $(Bu_4N)_2Mo_4I_{11}$ (3). A third type of cluster has the four metal atoms in a planar diamond-shaped or edge-sharing triangular arrangement. Two of the metal atoms in this tetranuclear cluster are each bonded to three metal atoms while the two end atoms are each bonded to only two metal atoms as in the compounds MNb_4X_{11} (M = Rb, Cs; X = Cl, Br) (4), and $W_4(OEt)_8$ (5). The compounds ReS_2 (6) and $ReSe_2$ (7) also contain this planar four metal atom cluster, but these clusters are linked into infinite, one-dimensional chains by Re-Re bonds between adjacent cluster units. However, tetranuclear metal atom clusters of any type have not been found in an oxide system until recently.

This section describes the preparation and single crystal structure of the new ternary compound $Ba_{1.14}Mo_8O_{16}$. It is the first example of an oxide containing a tetranuclear metal atom cluster, and it is also the first example of a hollandite-related (8) tunnel structure containing molybdenum. The structure of $Ba_{1.14}Mo_8O_{16}$ has also been found to exhibit a superlattice ordering of barium ions within the tunnels.

EXPERIMENTAL

Materials

Barium molybdate was prepared by mixing an aqueous solution of $BaCl_2 \cdot 2H_2O$ ('Baker Analyzed' Reagent, 99.6%) with an aqueous solution containing the stoichiometric quantity of ammonium heptamolybdate tetrahydrate ('Baker Analyzed' Reagent, 83.0% as MoO_3) and ammonium hydroxide. The white precipitate was filtered, washed several times with deionized water, dried at 120°C for 20 hours, and stored over P_4O_{10}. Molybdenum dioxide was prepared by the hydrogen reduction of MoO_3 (Fisher Certified A.C.S.) at 460°C for 40 hours. The reduced material was then washed several times with alternate portions of 3M NH_4OH, deionized water, and 3M HCl until the washings were colorless, and finally dried in vacuo at 110°C. Anal. Calculated for MoO_2: Mo, 74.99. Found: Mo, 74.96. Molybdenum tubing was obtained from Thermo-Electron Corp. (99.97%), Mo sheet from Rembar Co. (99.95%), and Mo powder from Aldrich (99.99%).

Synthesis

Barium molybdate and molybdenum dioxide, in mole ratio 2:5, were ground together in a mortar and then sealed in an evacuated molybdenum reaction vessel (3 cm long x 1.3 cm diam) by electron beam welding. This molybdenum tube was then sealed in an evacuated inconel protection tube and the reaction mixture held at 1100°C for 9 days. The free-flowing contents of the tube contained some unreacted $BaMoO_4$, as well as four types of crystals; thin hexagonal-like platelets, long black

columnar crystals, thin metallic colored needles of $Ba_{0.62}Mo_4O_6$ (9), and crystals of MoO_2. The composition of the columnar crystals proved to be $Ba_{1.14}Mo_8O_{16}$ from single crystal x-ray diffraction data (see below). The composition and structure of the thin hexagonal-like platelets has not yet been determined.

An attempt was made to prepare the pure compound $BaMo_8O_{16}$ using the stoichiometric quantities of $BaMoO_4$, MoO_2, and Mo. The pelletized reaction mixture was sealed in a molybdenum tube which, in turn, was sealed in an inconel protection tube, and fired at 1100°C for 7 days. A multiphase product was again observed.

Crystal Selection

Several long columnar crystals were selected from the multiphase product mixture and mounted in 0.2 mm Lindemann glass capillaries with a small amount of silicone grease. Each crystal was mounted with the long dimension nearly collinear with the ϕ-circle axis on a four-circle x-ray diffractometer designed and built in the Ames Laboratory (10). Three or four ω-oscillation photographs were taken on each crystal at various ϕ settings. These photographs revealed that the crystals exhibited a range of imperfections, from those showing relatively discrete sharp diffraction maxima to those which produced two or more closely spaced peaks; only the three best crystals were then indexed. Several independent reflections were selected from these photographs and their coordinates input into an automatic indexing program (11). The reduced cell and reduced-cell scalars which

resulted indicated triclinic symmetry with the same lattice parameters for all three crystals. A crystal of dimensions 0.14 x 0.08 x 0.07 mm was selected for data collection based on the quality of its oscillation photographs.

X-Ray Data Collection

X-ray data were collected on the same x-ray diffractometer at ambient temperature using Mo K_α radiation (λ = 0.71034 Å) monochromatized with a graphite single crystal. An ω-scan mode was used to collect all data in the HKL, $\bar{H}\bar{K}L$, $\bar{H}K\bar{L}$ and $H\bar{K}\bar{L}$ octants with $2\theta \leq 50°$. The peak heights of three standard reflections which were remeasured every 75 reflections did not show any significant change over the period of data collection. Final cell parameters and their estimated standard deviations were obtained from the same crystal by a least-squares refinement of $\pm 2\theta$ values of 16 independent reflections randomly distributed in reciprocal space having $2\theta > 30°$. The results were a = 7.311(1) Å, b = 7.453(1) Å, c = 5.726(1) Å, α = 101.49(2)°, β = 99.60(2)°, γ = 89.31(2)°, and V = 301.4 $Å^3$.

Structure Determination and Refinement

The observed intensities were corrected for Lorentz-polarization effects and standard deviations calculated (12) to give 1316 observed reflections ($I > 3\sigma(I)$) from a possible 1368. Appropriate averaging of duplicate reflections yielded 1024 independent reflections for the final data set.

A Patterson-superposition method (13) was used to locate the positions of all 8 molybdenum atoms and 1 barium atom. Space group $P\bar{1}$ (no. 2) was selected with barium on the special position $\frac{1}{2},\frac{1}{2},0$ and a full-matrix least-squares refinement (14) on the positional parameters for Mo resulted in a residual $R = \Sigma\left||F_o|-|F_c|\right|/\Sigma|F_o|$ of 0.253. Oxygen atom positions were located from an electron density Fourier map (15) and refinement of all Mo and O positional parameters gave R = 0.205. The barium atom multiplier and isotropic thermal parameter as well as all Mo and O positional parameters were next varied and refinement converged at R = 0.127. This was then followed with a refinement of Ba atom multiplier, all heavy atom isotropic thermal parameters, and all Mo and O positional parameters to give R = 0.122. At this point, an electron density map revealed a small amount of electron density near the special position $\frac{1}{2},\frac{1}{2},\frac{1}{2}$. Oxygen was first placed at this site but refinement led to a highly negative isotropic temperature factor and a high occupation number (>1 atom/site) for this atom. Barium was then placed at this position and a refinement of barium multipliers and atomic positional and isotropic thermal parameters converged at R = 0.081 and R_w = 0.120 where $R_w = [\Sigma\omega(|F_o|-|F_c|)^2/\Sigma\omega|F_o|^2]^{\frac{1}{2}}$ and $\omega = \sigma_F^{-2}$. An absorption correction for the crystal shape was made (μ = 106 cm^{-1}) using an empirical ϕ-scan method (16) where the intensity of a selected reflection at $\chi \sim 90°$ was measured every 10° in ϕ using the x-ray diffractometer, but this correction made no improvement in the refinement. A full anisotropic refinement gave R = 0.041 and R_w = 0.059 with a total population of

1.14(1) Ba atoms/cell; however, two oxygen atoms had negative temperature factors. An examination of the structure factors showed many strong low-angle reflections to have $F_o < F_c$, which suggested a secondary extinction problem. The value for a secondary extinction factor, $g = 8 \times 10^{-7}$, was obtained from a linear regression calculation using the expression $|F_c|/|F_o| = 1 + g\ I_c$. It was also observed that the data at high and low values of $\sin \theta/\lambda$ had larger values of $\omega\left||F_o|-|F_c|\right|$. Thus, the data were reweighted in fifty overlapping groups sorted according to F_o so that $\omega\Delta^2$ was essentially constant. A final full-matrix least-squares refinement, varying the scale factor, barium multipliers, positional and anisotropic thermal parameters, converged at $R = 0.036$ and $R_w = 0.049$ with no significant change in the Ba atom multipliers. A final difference Fourier synthesis map was flat to ≤ 1.5 e/Å^3.

The atomic scattering factors used were those of Hanson et al. (17) for neutral atoms; molybdenum and barium were corrected for the real and imaginary parts of anomalous dispersion (18).

RESULTS AND DISCUSSION

Crystal Structure of $Ba_{1.14}Mo_8O_{16}$

The final positional parameters are given in Table II-1 and thermal parameters in Table II-2. Important interatomic distances and angles listed in Tables II-3 and II-4, respectively, correspond to the labels in Figures II-1 and II-2. Observed and calculated structure factors are available as supplementary material.

The structure of $Ba_{1.14}Mo_8O_{16}$ consists of molybdenum-oxide cluster chains extended parallel to the c axis. The chains are built up from clusters of the type Mo_4O_{16} sharing the oxygen atoms on the four outer edges of the planar tetrameric molybdenum atom cluster. (Conceptually, an Mo_4O_{16} cluster can be formed by adding a molybdenum atom with three attached oxygen atoms to one edge of the molybdenum triangle found in the Mo_3O_{13} cluster unit (19).) The barium ions occupy sites along the c axis in channels formed by four metal-oxide cluster chains cross-linked by molybdenum-oxygen bonds.

Figure II-1 is an ORTEP drawing of a section of one molybdenum-oxide cluster chain which shows the arrangement of molybdenum atoms within the individual clusters and also the connectivity within the chains via the sharing of oxygen atoms between cluster units. Bonds between molybdenum atoms are represented in this figure by the black solid lines and Mo-O bonds by the open unfilled lines. The individual clusters contain two types of Mo atoms; the end or apical atoms Mo1 and Mo1' which are each bonded to two other molybdenum atoms and six

Table II-1. Positional parameters for $Ba_{1.14}Mo_8O_{16}$[a]

Atom	x	y	z	Multiplier
Ba1	0.50	0.50	0.00	0.433(3)
Ba2	0.4717(6)	0.4805(6)	0.4071(8)	0.135(3)
Mo1	0.9809(1)	0.3155(1)	0.1064(1)	
Mo2	0.0083(1)	0.6562(1)	0.4410(1)	
Mo3	0.6699(1)	0.9761(1)	0.2013(1)	
Mo4	0.3498(1)	0.0122(1)	0.3506(1)	
O1	0.8045(8)	0.4563(8)	0.3266(9)	
O2	0.1458(8)	0.5450(8)	0.1612(9)	
O3	0.1451(8)	0.2004(8)	0.3309(10)	
O4	0.8675(8)	0.7850(8)	0.1666(10)	
O5	0.5302(8)	0.7991(8)	0.3529(10)	
O6	0.4658(8)	0.1570(8)	0.1398(10)	
O7	0.8087(8)	0.1294(8)	0.4875(10)	
O8	0.2034(8)	0.8717(8)	0.0120(10)	

[a]Space group $P\bar{1}$ (no. 2).

Table II-2. Thermal parameters for $Ba_{1.14}Mo_8O_{16}$[a]

Atom	B_{11}	B_{22}	B_{33}	B_{12}	B_{13}	B_{23}
Ba1	1.32(5)	0.71(5)	2.81(6)	0.45(3)	-1.08(4)	-0.71(3)
Ba2	0.74(18)	0.95(19)	1.42(17)	0.16(12)	0.17(12)	0.62(14)
Mo1	0.56(3)	0.40(3)	0.35(3)	0.18(2)	-0.04(2)	0.01(2)
Mo2	0.53(3)	0.30(3)	0.34(3)	0.07(2)	-0.09(2)	0.04(2)
Mo3	0.54(3)	0.36(3)	0.25(3)	0.11(2)	-0.05(2)	-0.05(2)
Mo4	0.54(3)	0.29(3)	0.33(3)	0.13(2)	-0.08(2)	-0.02(2)
O1	1.47(26)	0.66(23)	0.16(21)	0.41(19)	-0.03(19)	0.19(17)
O2	0.74(22)	0.43(22)	0.29(20)	0.13(16)	-0.32(17)	-0.17(17)
O3	1.10(24)	0.37(23)	0.74(22)	0.11(19)	-0.02(19)	-0.09(18)
O4	0.83(23)	0.65(23)	0.33(21)	0.18(18)	0.15(17)	0.10(17)
O5	1.20(25)	0.75(23)	0.59(22)	-0.09(19)	-0.40(19)	0.24(18)
O6	0.87(23)	0.59(23)	0.71(22)	0.21(18)	0.16(19)	-0.15(18)
O7	1.10(24)	0.33(22)	0.83(23)	-0.06(19)	0.15(19)	0.10(18)
O8	0.94(23)	0.73(23)	0.82(23)	-0.13(19)	-0.31(19)	-0.16(18)

[a]The general thermal parameter expression used is $\exp[-1/4(B_{11}h^2a^{*2} + B_{22}k^2b^{*2} + \ldots 2B_{23}k\ell b^*c^*)]$.

Table II-3. Interatomic distances (Å) in $Ba_{1.14}Mo_8O_{16}$

Mo-Mo and Mo-O Distances

Distorted Cluster		Regular Cluster	
Mo1-Mo2	2.847(1)	Mo3-Mo4	2.616(1)
Mo1-Mo2'	2.546(1)	Mo3-Mo4'	2.578(1)
Mo1-Mo2'	3.197(1)	Mo3-Mo4'	3.158(1)
Mo2-Mo2'	2.560(1)	Mo4-Mo4'	2.578(1)
Mo1-O1	2.082(6)	Mo3-O4	2.022(6)
Mo1-O2	2.046(6)	Mo3-O5	2.079(6)
Mo1-O2'	2.104(6)	Mo3-O6	2.034(6)
Mo1-O3	1.931(6)	Mo3-O6'	2.095(6)
Mo1-O4	2.079(6)	Mo3-O7	1.936(6)
Mo1-O8	1.894(6)	Mo3-O8	2.143(6)
Mo2-O1	2.051(6)	Mo4-O3	2.043(6)
Mo2-O1'	2.038(6)	Mo4-O5	2.053(6)
Mo2-O2	2.062(6)	Mo4-O5'	2.053(6)
Mo2-O3	2.003(6)	Mo4-O6	2.055(6)
Mo2-O4	2.119(6)	Mo4-O7	2.023(6)
Mo2-O7	2.030(6)	Mo4-O8	2.128(6)

Ba-O Distances

Ba1-O1	2.720(6)	Ba2-O1	2.710(7)
Ba1-O2'	2.885(6)	Ba2-O2"	2.649(7)
Ba1-O5	2.677(6)	Ba2-O5'	2.506(7)
Ba1-O6'	2.852(6)	Ba2-O6	3.329(7)
Ba2-O1'	2.549(7)	Ba2-O5	2.716(7)
Ba2-O2	3.440(/)	Ba2-O6"	2.582(7)

Table II-4. Bond angles (deg) in $Ba_{1.14}Mo_8O_{16}$

Intrachain Bond Angles

Mo1-Mo2-Mo2'	55.88(3)	Mo3-Mo4-Mo4'	59.52(3)
Mo1-Mo2'-Mo2	67.78(4)	Mo3-Mo4'-Mo4	60.96(3)
Mo2-Mo1-Mo2'	56.34(3)	Mo4-Mo3-Mo4'	59.52(3)
Mo1-O1-Mo2	87.04(23)	Mo3-O5-Mo4	78.55(21)
Mo1-O1-Mo2'	76.30(21)	Mo3-O5-Mo4'	77.22(21)
Mo2-O1-Mo2'	77.49(21)	Mo4-O5-Mo4'	77.80(21)
Mo1-O2-Mo2	87.74(22)	Mo3-O6-Mo4	79.54(20)
Mo1-O3-Mo2'	80.62(22)	Mo3-O7-Mo4'	81.25(23)
Mo1-O2'-Mo1'	103.30(24)	Mo3-O6'-Mo3'	100.05(24)
Mo1-O2'-Mo2'	100.27(24)	Mo3-O6'-Mo4'	99.08(24)
Mo1-O4-Mo2'	99.22(24)	Mo3-O8-Mo4'	95.37(24)

Interchain Bond Angles

Mo1-O3-Mo4	142.82(31)
Mo2-O3-Mo4	136.27(30)
Mo1-O4-Mo3	133.35(29)
Mo2-O4-Mo3	126.88(27)
Mo2-O7-Mo3	136.31(31)
Mo2-O7-Mo4	141.94(31)
Mo1-O8-Mo3	126.14(30)
Mo1-O8-Mo4	138.47(32)

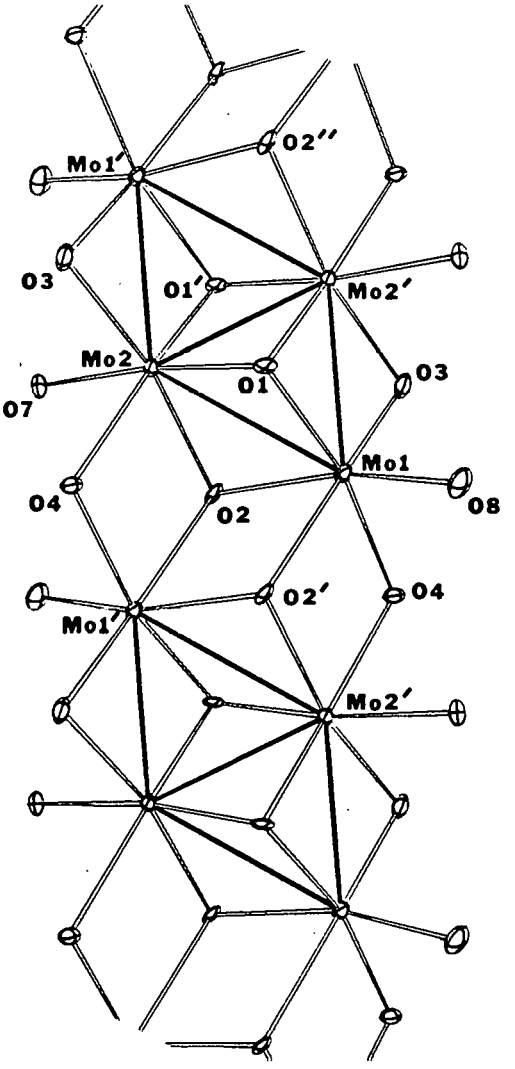

Figure II-1. A section of one metal-oxide chain containing the 'distorted' molybdenum atom clusters in $Ba_{1.14}Mo_8O_{16}$. Fifty percent probability anisotropic thermal ellipsoids are shown

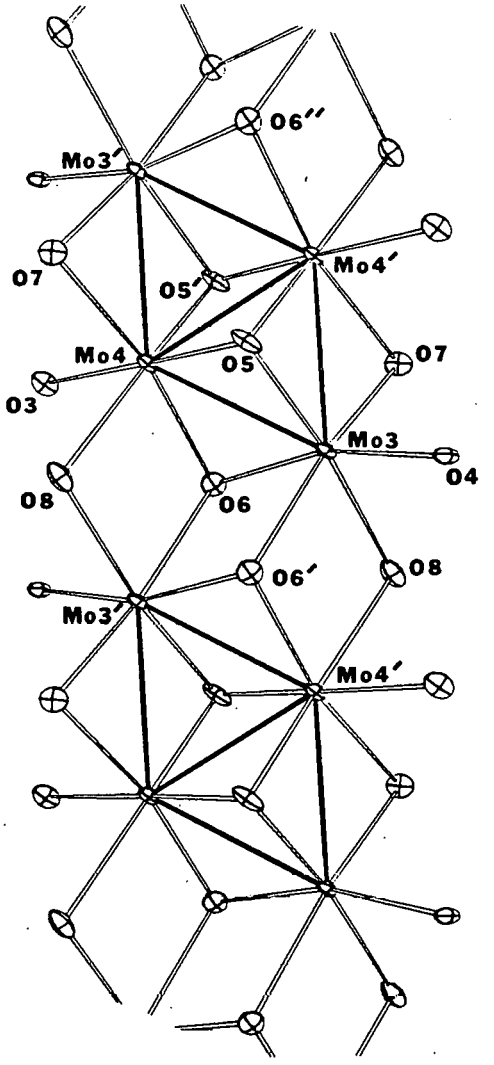

Figure II-2. A section of one metal-oxide chain containing the 'regular' molybdenum atom clusters in $Ba_{1.14}Mo_8O_{16}$. Fifty percent probability anisotropic thermal ellipsoids are shown

oxygen atoms, and the atoms Mo2 and Mo2' which are each bonded to three molybdenum and six oxygen atoms. The molybdenum atoms are all in approximately octahedral coordination with oxygen. Each metal-oxide cluster can also be viewed as a small section of a close-packed arrangement of two oxygen atom layers with the Mo atoms occupying neighboring octahedral sites between the two layers with the MoO_6 octahedra sharing edges. Molecular species, without metal-metal bonding, which have the same structural arrangement are $Ti_4(OR)_{16}$, where R = methyl (20) and ethyl (21), and $W_4O_{16}^{8-}$ as found in the compound $Ag_8W_4O_{16}$ (22) and the silver ion conductor $Ag_{26}I_{18}W_4O_{16}$ (23). Each metal-oxide cluster chain in $Ba_{1.14}Mo_8O_{16}$ contains four types of oxygen atoms which are all three-coordinate with respect to molybdenum. One type, O1 - Figure II-1, is triply bridging to three Mo atoms within an Mo_4O_{16} cluster, while a second type, O2, is doubly bridging on an edge of one cluster unit and singly bonded to an apical Mo atom in a neighboring cluster, thereby linking the individual clusters within the chain. Both types of oxygen atoms are bonded to molybdenum atoms in a trigonal-pyramidal fashion, and are also coordinated to barium (see below). A third type of oxygen, O4 - Figure II-1, connects two intrachain cluster units along one edge of the chain and also serves as an interchain link by bonding to an apical Mo atom, Mo3 - Figure II-2, in an adjacent metal-oxide cluster chain. The fourth type of oxygen atoms, O3 and O7 - Figures II-1 and II-2, respectively, which also connect individual cluster chains, are doubly bridging along an outer edge of one Mo_4O_{16} cluster unit and singly bonded to an Mo atom

in an adjacent metal-oxide cluster chain. Individual chains are, therefore, each connected to four other cluster chains via Mo-O-Mo bonds. These interchain-bridging oxygen atoms are in a trigonal planar-like coordination with molybdenum atoms as evidenced by the sum of Mo-O-Mo bond angles around each O atom, 359.5 to 360°. The interlinking of the cluster units within and between chains can be represented in the connectivity formula $Mo_4O_2O_{8/2}O_{6/3} = Mo_4O_8$.

An interesting feature of the structure is that there are two different types of infinite chains. One chain contains distorted cluster units, as shown in Figure II-1, which have three short and two long Mo-Mo bonds; 2.560(1)(1X), 2.546(1)(2X), and 2.847(1)(2X) Å. The other chain consists of regular cluster units, as shown in Figure II-2, where the five Mo-Mo bonds in the edge-shared bitriangle are nearly equal; 2.578(1)(3X) and 2.616(1)(2X) Å. Both types of cluster chains possess $\bar{1}$ symmetry within the planar tetrameric cluster units. There is also a point of inversion symmetry between individual clusters along each chain, e.g., relating O2 with O2', Mo1 with Mo1', etc.

Within the clusters of regular geometry, the Mo-Mo bonding is understood as resulting from 10 electrons in bonding σ-orbitals directed along the 5 bonded edges with each edge having a bond order of 1.0. This indicates that the Mo atoms on the shared edge of the triangles furnish 3 electrons each and are in the net oxidation state 3+, whereas the Mo atoms on the outer apices furnish 2 electrons each and are in the 4+ net oxidation state. Each regular cluster unit is then formulated as $Mo_4O_8^{2-}$. From the Mo-Mo distances in the distorted

cluster unit, it appears the three short bonds are of order 1.0 and the two elongated bonds are approximately of order 0.5. Thus, a total of ca. 8 electrons is involved in the Mo-Mo bonding and the net oxidation states are 3.5+ for the atoms on the shared edge and 4.5+ for the atoms on the outer apices. In both the distorted and regular cluster units, the shortest Mo-O distances are those around the outer apical Mo atoms; 2.02 vs 2.05 Å (ave) in the distorted clusters, and 2.05 vs 2.06 Å (ave) in the regular clusters, which supports their assessment of a higher net oxidation state. In view of these considerations, the compound may be formulated as the mixed-valence species $Ba^{2+}_{1.14}(Mo_4O_8^{2-})(Mo_4O_8^{0.28-})$.

A 3-dimensional view down the c axis of $Ba_{1.14}Mo_8O_{16}$ is given in Figure II-3 (only Ba1 is shown). In this view, there is a strong resemblance between this structure and that of $NaMo_4O_6$ (24) or $Ba_{0.62}Mo_4O_6$ (25). In each case, the molybdenum-oxide cluster chains are linked together to form tunnels in which the Na^+ or Ba^{2+} cations are located. The structure of $Ba_{1.14}Mo_8O_{16}$ is, however, more closely related to the structure of the mineral hollandite (8), $BaMn_8O_{16}$, but is reduced in symmetry through strong metal-metal bonding to form the tetranuclear cluster units.

The barium ions in $Ba_{1.14}Mo_8O_{16}$ are fractionally occupied in sites of low symmetry. The eight intrachain oxygen atoms in the coordination sphere of Ba1 form a distorted rectangular box compressed along the c axis with Ba-O distances from 2.68 to 2.89 Å. Of these, the shortest distances involve the O atoms, O1 and O5, which bridge three Mo atoms

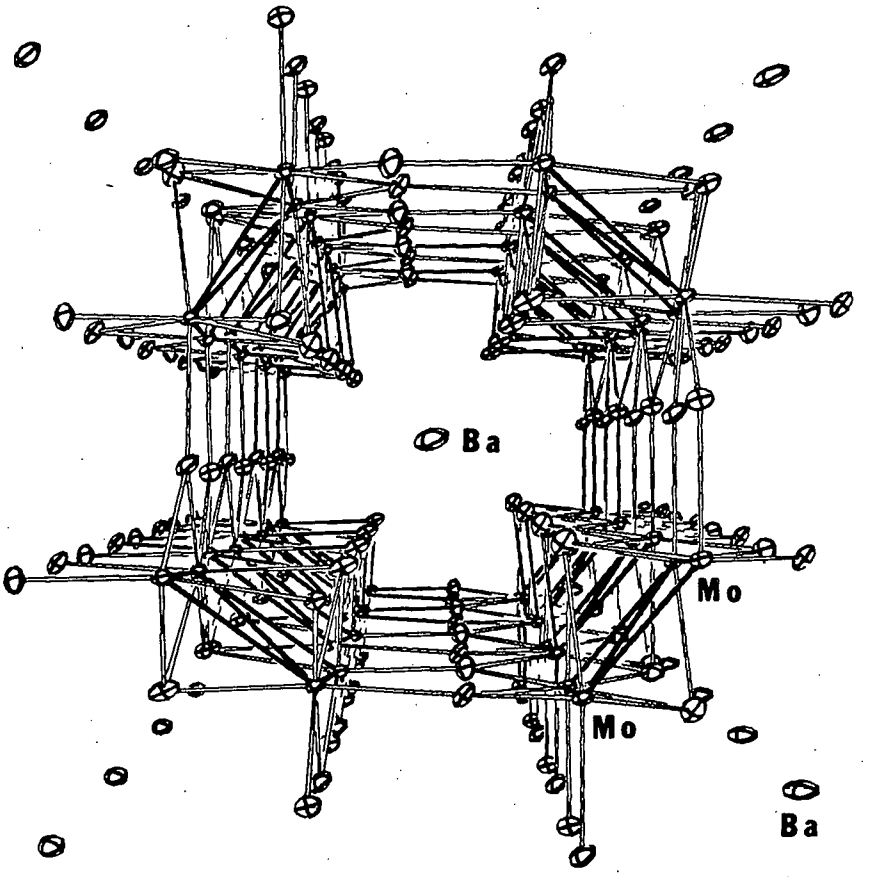

Figure II-3. A three-dimensional view down the c axis of $Ba_{1.14}Mo_8O_{16}$. Molybdenum and barium atoms are labeled. Fifty percent probability anisotropic thermal ellipsoids are shown

within an Mo_4O_{16} unit as shown in Figures II-4 and II-5. Because oxygen atoms O2 and O6 bridge two separate clusters within a chain, they are located closer to the plane of Mo atoms and, therefore, further from barium. The oxygen coordination around the Ba2 ions is depicted in Figure II-5. The partially occupied Ba2 site is disordered, consisting of two inversion-related positions within a distorted rectangular box of eight oxygen atoms. This oxygen atom arrangement is therefore similar to that of Ba1 except the cation has now been shifted upwards or downwards and to the side in the distorted rectangular box. This results in six short, 2.51 - 2.72 Å, and two long, 3.33 and 3.44 Å, Ba-O distances.

The fractional occupation numbers as well as the large B_{33} thermal parameter for barium (Ba1) suggested a superlattice ordering of Ba^{2+} ions within the channels, as frequently observed in hollandite-related phases. For example, the compounds $Ba_xMg_xTi_{8-x}O_{16}$ exhibit an incommensurate superlattice ordering (26) of Ba^{2+} ions with $0.8 \leq x \leq 1.33$ and $x \neq 1.20$. An axial oscillation photograph along the c axis of a single crystal of $Ba_{1.14}Mo_8O_{16}$ revealed layers of superlattice reflections which indicated the true unit cell dimension along the c axis was 5n (5.726) Å, where n is an integer. This, of course, also implied that the superlattice ordering was commensurate with the length of the subcell c axis. Using the fractional occupation numbers, ratio of occupation numbers, total barium content, and reciprocal lattice layer spacings obtained from the axial photograph, a value of n = 3 was calculated to best fit all of the above

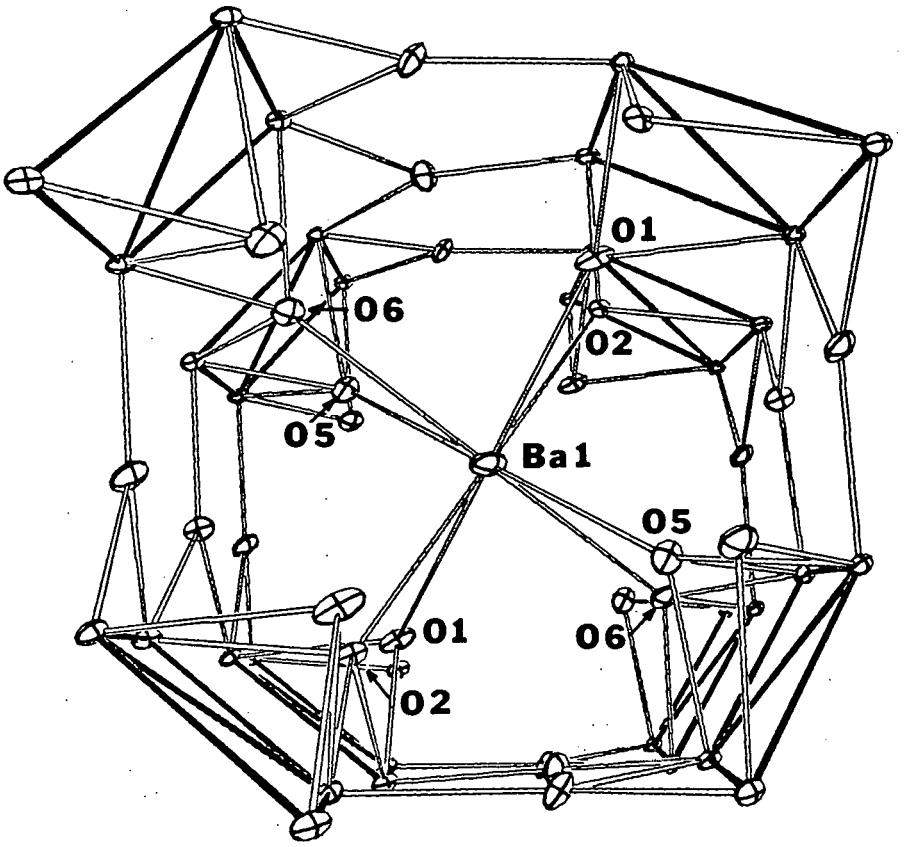

Figure II-4. A three-dimensional view down the c axis of $Ba_{1.14}Mo_8O_{16}$ showing the oxygen coordination around barium ion (Ba1). Fifty percent probability anisotropic thermal ellipsoids are shown

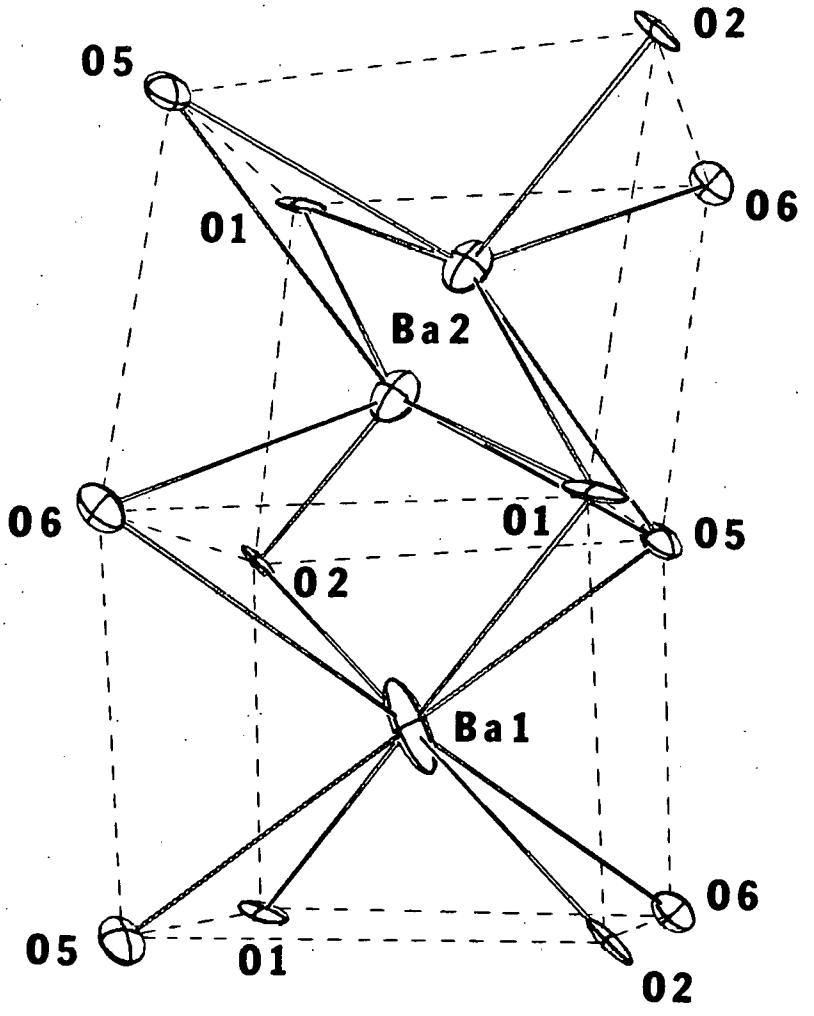

Figure II-5. A view perpendicular to the c axis of $Ba_{1.14}Mo_8O_{16}$ showing the oxygen coordination around the two barium ion sites. Fifty percent probability anisotropic thermal ellipsoids are shown

information. In this model, there would be 30 possible barium sites within each channel along the c axis of the superlattice cell; 13 barium ions would occupy sites similar to Ba1 and 4 would occupy sites similar to Ba2. However, the compound $Ba_{1.14}Mo_8O_{16}$ may actually exhibit an incommensurate superlattice ordering of barium ions with a c axis repeat unit much less than 15(5.726) Å (i.e., the superlattice repeat unit would be a nonintegral multiple of the subcell c axis).

As can be discerned from Figure II-3, the structure also includes additional oxygen-lined tunnels running parallel to the c axis. These tunnels have walls composed of the interchain, trigonal planar-like oxygen atoms (O3, O4, O7, and O8). The oxygen atoms are arranged along the c axis to form infinite chains of edge-sharing octahedra. A section of one such chain is pictured in Figure II-6. These vacant channels are the same as those found in rutile (TiO_2) and related metal dioxides.

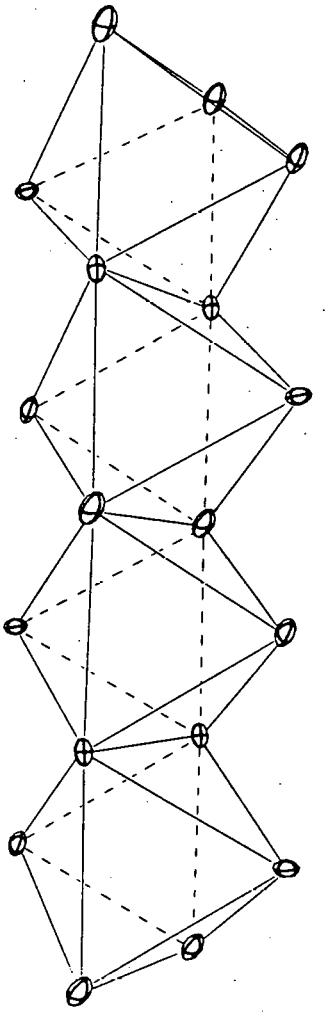

Figure II-6. A section of one of the empty channels found in $Ba_{1.14}Mo_8O_{16}$ showing the edge-sharing, octahedral oxygen atom arrangement along the c axis

CONCLUSIONS

Although the distorted Mo_4O_{16} clusters in $Ba_{1.14}Mo_8O_{16}$ have only $\bar{1}$ (C_i) symmetry, the regular clusters very closely approximate 2/m (C_{2h}) symmetry and a molecular orbital bonding picture for both cluster types can be sketched. Two metal d orbitals per Mo atom are reserved for Mo-O bonding and the three remaining metal d orbitals are used in forming Mo-Mo bonds. In the regular clusters, these 12 orbitals combine in C_{2h} symmetry to provide a set of five bonding ($2a_g + b_g + a_u + b_u$), two nonbonding ($a_g + b_u$), and five antibonding molecular orbitals ($a_g + b_g + 2a_u + b_u$) (27). Therefore, the 10 metal electrons in the regular cluster fill the five bonding levels and result in an average Mo-Mo bond order of 1.0. This molecular orbital scheme can be modified, however, by considering Mo-O pi bonding interactions. Evidence for metal-oxygen pi orbital overlap comes from a study of the molybdenum-oxygen distances in the regular Mo_4O_{16} cluster units. The shortest Mo-O distances in these clusters, 1.936(6) Å, are those involving the apical Mo atoms, Mo3, and the trigonal planar-like, interchain oxygen atoms, O7, which are edge bridging to the individual cluster units. The unhybridized p orbital on these oxygen atoms can effectively overlap with the molybdenum d orbitals that are nonbonding with respect to Mo-Mo interactions, i.e., the ($a_g + b_u$) set. This pi orbital overlap would lower the energy of these oxygen p orbitals and consequently raise the energy of the otherwise nonbonding set of molybdenum molecular orbitals to an antibonding position. The five

bonding levels would remain essentially unchanged. It may therefore be very difficult to further reduce these 10-electron Mo_4O_{16} clusters because additional electrons would have to reside in antibonding orbitals.

The distorted clusters, which possess only C_i symmetry, also exhibit this mode of pi bonding interaction between atoms Mo1 and O3 as seen in the Mo-O bond length of 1.931(6) Å. More important for the distorted clusters, however, is the interaction between this apical Mo1 atom and the terminally bonded, sp^2-like oxygen atom, O8, which results in a very short Mo-O bond distance of 1.894(6) Å. This short bond length arises, in part, from a higher net oxidation state for this Mo atom, thereby increasing the Mo-O electrostatic attraction. However, the strongest interaction between these two atoms, which gives rise to the short Mo-O bond distance, is a pi bonding interaction. The unhybridized p orbital on this oxygen atom is in a position to pi bond with the same molybdenum d orbital involved in forming the long bond between atoms Mo1-Mo2 and Mo1'-Mo2'. Because this d orbital participates in an electron-deficient Mo-Mo bond, it is more accessible to pi bonding with oxygen atom O8. This interaction raises one of the five bonding molecular orbitals to higher energy leaving four bonding MO's to hold eight electrons. It therefore seems likely that this compound could be reduced by ca. 2 electrons to give equivalent, regular cluster units in all of the molybdenum-oxide cluster chains.

However, reduction of the compound $Ba_{1.14}Mo_8O_{16}$ by the insertion of additional Ba^{2+} ions into the channels to give $Ba_2Mo_8O_{16}$ does not

appear likely for two reasons. The first reason is that the divalent barium ions would have to occupy sites that are only 2.86 Å apart making electrostatic repulsion a destabilizing effect. Secondly, the two barium ion sites within the unit cell are not equivalent, and one of the sites is apparently favored as evidenced by the occupation numbers of 0.87 for Ba1 and 0.27 for Ba2. The latter site is located in front of four surrounding molybdenum-oxide clusters while the former site is situated in between four linked pairs of molybdenum-oxide clusters that form a section of the tunnel walls. It may be possible to reduce $Ba_{1.14}Mo_8O_{16}$ by ca. one electron by substituting trivalent cations for barium ions within the channels to make, for example, $LaMo_8O_{16}$.

As mentioned previously, the structure of $Ba_{1.14}Mo_8O_{16}$ also possesses vacant tunnels consisting of edge-shared octahedra of oxygen atoms such as those found in rutile and related metal dioxides. Several of these MO_2 compounds are known to react with butyllithium at room temperature to form compounds Li_xMO_2 ($x < 2$) with varying lithium content (28). It may be possible to reduce the 'electron-deficient' clusters in $Ba_{1.14}Mo_8O_{16}$ by similar reactions that would insert hydrogen or lithium into the vacant oxygen-lined channels.

REFERENCES

1. Perrin, C.; Chevrel, R.; Sergent, M. C. R. Acad. Sci. Paris 1975, 281C, 23.

2. Vandenberg, J. M.; Brasen, D. J. Solid State Chem. 1975, 14, 203.

3. Stensvad, S.; Helland, B. J.; Babich, M. W.; Jacobson, R. A.; McCarley, R. E. J. Am. Chem. Soc. 1978, 100, 6257.

4. Broll, A.; Simon, A.; von Schnering, H. G.; Schafer, H. Z. Anorg. Allg. Chem. 1969, 367, 1.

5. Chisholm, M. H.; Huffman, J. C.; Leonelli, J. J. Chem. Soc., Chem. Commun. 1981, 6, 270.

6. Wildervanck, J. C.; Jellinek, F. J. Less-Common Metals 1971, 24, 73.

7. Alcock, N. W.; Kjekshus, A. Acta Chem. Scand. 1965, 19, 79.

8. Wells, A. F. "Structural Inorganic Chemistry", 4th ed.; Clarendon: Oxford, England, 1975; page 459.

9. Torardi, C. C. Ph.D. Dissertation, Iowa State University, Ames, Iowa, 1981, Section IV.

10. Rohrbaugh, W. J.; Jacobson, R. A. Inorg. Chem. 1974, 13, 2535.

11. Jacobson, R. A. J. Appl. Crystallogr. 1976, 9, 115.

12. Lawton, S. L.; Jacobson, R. A. Inorg. Chem. 1968, 7, 2124.

13. Hubbard, C. R.; Babich, M. W.; Jacobson, R. A. "A PL/I Program System for Generalized Patterson Superpositions", 1977, US AEC Report IS-4106.

14. Lapp, R. L.; Jacobson, R. A. "ALLS, A Generalized Crystallographic Least Squares Program", 1979, US DOE Report IS-4708.

15. Powell, D. R.; Jacobson, R. A. "FOUR: A General Crystallographic Fourier Program", 1980, US DOE Report IS-4737.

16. Karcher, B. A. Ph.D. Dissertation, Iowa State University, Ames, Iowa, 1981.

17. Hanson, H. P.; Herman, F.; Lea, J. D.; Skillman, S. Acta Crystallogr. 1964, 17, 1040.

18. Templeton, D. H. In "International Tables for X-Ray Crystallography", 1st ed.; Macgillavry, C. H. and Rieck, G. D., Eds.; Kynoch Press: Birmingham, England, 1962; Vol. III, page 215.

19. Torardi, C. C. Ph.D. Dissertation, Iowa State University, Ames, Iowa, 1981, Section I.

20. Wright, D. A.; Williams, D. A. Acta Crystallogr. 1968, B24, 1107.

21. Ibers, J. A. Nature 1963, 197, 686.

22. Skarstad, P. M.; Geller, S. Mater. Res. Bull. 1975, 10, 791.

23. Chan, L. Y. Y.; Geller, S. J. Solid State Chem. 1977, 21, 331.

24. Torardi, C. C.; McCarley, R. E. J. Am. Chem. Soc. 1979, 101, 3963.

25. Torardi, C. C. Ph.D. Dissertation, Iowa State University, Ames, Iowa, 1981, Section IV.

26. Bursill, L. A.; Grzinic, G. Acta Crystallogr. 1980, B36, 2902.

27. McCarley, R. E. Ames Laboratory, Iowa State University, Ames, Iowa; unpublished work.

28. Murphy, D. W.; DiSalvo, F. J.; Carides, J. N.; Waszczak, J. V. Mater. Res. Bull. 1978, 13, 1395.

SECTION III. SYNTHESIS AND CRYSTAL STRUCTURE OF $NaMo_4O_6$. A METALLIC INFINITE-CHAIN POLYMER DERIVED BY CONDENSATION OF OCTAHEDRAL CLUSTERS

INTRODUCTION

Over the past several years, there has been considerable interest in solid state compounds containing discrete transition metal atom clusters and condensed transition metal atom clusters which form chain and sheet structures. Some examples of solid state compounds containing discrete clusters are NbO_2 (1), $LiZn_2Mo_3O_8$ (2), $Ba_{1.14}Mo_8O_{16}$ (3), and $PbMo_6S_8$ (4) with dimeric, trimeric, planar tetrameric and octahedral hexameric metal atom clusters, respectively. The halide compounds Gd_2Cl_3 (5), Sc_5Cl_8 (6) and Sc_7Cl_{10} (7) contain infinite chains of bonded metal atom clusters while the metal-rich compound ZrCl (8) is composed of sheets of Zr and Cl atoms in a double-layer stacking arrangement. The chain structure of Gd_2Cl_3 is derived from clusters of the type M_6X_8 (an octahedral metal atom cluster with X atoms bridging each face of the octahedron) sharing the metal atoms on opposite edges. The anionic chain structure in the compound $Sc_5Cl_8 = [ScCl_2^+][Sc_4Cl_6^-]$ can be conceptually formed by condensation of M_6X_{12} cluster units (X bridging all edges of the M_6 octahedron) with sharing of Sc and Cl atoms on trans edges as represented by the formula $[Sc_2Sc_{4/2}Cl_{8/2}Cl_{2/2}]Cl_{2/2}^-$. This compound was the first example of an M_6X_{12}-type of condensation.

This section reports the synthesis, single crystal structure, chemical and electrical properties of the recently described ternary oxide, $NaMo_4O_6$ (9). This compound contains infinite molybdenum-oxide cluster chains extended parallel to the c axis. The Na^+ ions occupy

sites in channels formed by four metal-oxide cluster chains crosslinked by molybdenum-oxygen bonds. The sodium can be replaced, in part, with lithium or potassium by ion-exchange in molten LiCl or KCl salts, respectively. The structure of $NaMo_4O_6$ is the second example of M_6X_{12} cluster condensation and provides evidence that the range of compounds with such structures may extend over numerous metal-nonmetal combinations.

EXPERIMENTAL

Materials

Sodium molybdate dihydrate (Fisher Certified A.C.S.) was dehydrated by drying in a 120°C oven for several days and then stored over $CaSO_4$. The KCl (Fisher Certified A.C.S.) was dried at 120°C for a few hours just before use. Lithium chloride was dried by heating slowly under vacuum to a final temperature of 500°C (over a period of one day) and then stored in a dry box. Molybdenum dioxide was prepared by the hydrogen reduction of MoO_3 (Fisher Certified A.C.S.) at 460°C for 48 hours. The MoO_2 was washed several times with alternate portions of 3M NH_4OH, deionized water, and 3M HCl until the washings were colorless, and finally dried in vacuo at 110°C. Chemical analyses for molybdenum were performed gravimetrically by oxidizing weighed samples of MoO_2 to MoO_3. Anal. Calculated for MoO_2: Mo, 74.99. Found: Mo, 74.96. Molybdenum tubing was obtained from Thermo-Electron Corp. (99.97%), Mo sheet from Rembar Co. (99.95%), and Mo powder from Aldrich (99.99%).

Syntheses

$NaMo_4O_6$

This phase was first discovered as one product obtained from a reaction of Na_2MoO_4, MoO_2, and ZnO in mole ratio 1:5:2. The reactant mixture was ground in a mortar, pelletized under 700 Kg/cm^2, electron beam welded in an evacuated molybdenum tube (2.5 cm long x 1.9 cm diam) which, in turn, was sealed in an evacuated fused quartz protection tube,

and fired at 1100°C for 2 days. The new compound grew from the surface of the pressed reaction pellet and molybdenum container walls as thin, metallic-colored needles. The other identified product that was formed in the pressed pellet was the well-known compound $Zn_2Mo_3O_8$ (10). Electron microprobe analysis of the needles established that Na and Mo were the only metallic elements present. The composition of $NaMo_4O_6$ was determined from single crystal x-ray diffraction data (see below). Subsequent work showed that essentially pure $NaMo_4O_6$ could be prepared from the stoichiometric quantities of Na_2MoO_4, MoO_2, and Mo with a two percent by weight excess of Na_2MoO_4. This reactant mixture was pressed into a pellet, sealed in an evacuated Mo tube, and fired at 1100°C for 7 days (shorter reaction times were not investigated). The product pellet was powdered, washed several times with deionized water, rinsed with methanol, and vacuum dried at 110°C. A Guinier x-ray powder diffraction pattern of the washed product contained the lines of $NaMo_4O_6$ and faintly showed the strongest line of Mo metal. In order to obtain a net oxidation state of the product, oxidation-reduction titrations were performed by dissolving weighed samples in aliquots of standardized ceric sulfate - 3M H_2SO_4 solution and titrating the unreacted Ce(IV) with standard Fe(II) solution after complete oxidation of molybdenum to Mo(VI). The analyses, based on the calculated value of 76.3% Mo for $NaMo_4O_6$, resulted in a molybdenum oxidation state of +2.74 compared to the calculated formal oxidation state of +2.75. Therefore, the amount of Mo metal impurity was assumed to be very small.

$\underline{Li_{1-x}Na_xMo_4O_6}$

Reactions between solid $NaMo_4O_6$ and molten LiCl resulted in a partial ion exchange of sodium by lithium ions (x is approximately equal to 0.25), and a change in structure from tetragonal to orthorhombic symmetry. In a typical reaction, 500 mg of $NaMo_4O_6$ powder and 8.5 g LiCl were sealed in an evacuated fused quartz ampoule and held at 700°C for 18 to 48 hours. After cooling to room temperature, the contents of the ampoule were placed in a beaker of deionized water until all of the LiCl was dissolved; then the black solid was washed with several portions of deionized water and air dried. Guinier x-ray powder diffraction patterns of the products were all the same regardless of reaction time. They showed the lines of a new $NaMo_4O_6$-related orthorhombic phase (see x-ray powder diffraction data), MoO_2, and Mo metal which was an impurity in the starting material (see above), but lines for tetragonal $NaMo_4O_6$ were not observed. Chemical analyses were obtained for Li and Na by atomic absorption spectroscopy, and Mo spectrophotometrically on the product of a 48 hour ion-exchange reaction. Found: Li, 1.0; Na, 1.1; Mo, 77.7. These results established a Li/Na ratio of 3.0, and a Mo/Li ratio of 4/0.71. Calculated values for an assumed formula $Li_{0.75}Na_{0.25}Mo_4O_6$ are: Li, 1.1; Na, 1.2; Mo, 78.2. A ten percent by weight impurity of MoO_2 would lower these calculated values to those found by chemical analyses. The reason for MoO_2 formation was not apparent but it could have been formed from residual moisture or oxide-hydroxide impurities in the LiCl, or from water adsorbed on the walls of the fused quartz

ampoule. For example, the following reaction:

$$2\ NaMo_4O_6 + 6\ H_2O \longrightarrow Na_2MoO_4 + 7\ MoO_2 + 6\ H_2$$

would require 6.0 mg H_2O to give a ten percent MoO_2 impurity in the ion-exchange reactions described above, and the reaction:

$$4\ NaMo_4O_6 + 2\ H_2O \longrightarrow 11\ MoO_2 + 5\ Mo + 4\ NaOH$$

would only require 1.3 mg H_2O to give the estimated level of MoO_2.

$\underline{Na_xK_{1-x}Mo_4O_6}$

A reaction between solid $NaMo_4O_6$ and molten KCl resulted in some ion exchange of sodium with potassium ions and an increase in the tetragonal unit cell volume. Two ion exchange reactions were conducted each consisting of 500 mg of powdered $NaMo_4O_6$ and 11 g KCl sealed in an evacuated fused quartz tube and held at 800°C for 24 hours in a tube furnace and 85 hours in a rocking furnace, respectively. The contents of the tubes were placed in beakers and covered with deionized water until the KCl dissolved; then the black products were washed several times with deionized water and air dried. Guinier x-ray powder diffraction patterns for the two products were essentially the same. They contained the lines of $NaMo_4O_6$, MoO_2, Mo, and a set of lines like those of $NaMo_4O_6$ positioned at slightly lower diffraction angles and with approximately equal intensities (see x-ray powder diffraction data below). Chemical analyses of the mixed product obtained from the 85 hour ion-exchange reaction established a Na/K ratio of 1.2. However,

it was not possible to determine whether the potassium was present as pure KMo_4O_6 or as a mixed alkali metal compound. Also, the origin of molybdenum dioxide formation was not apparent but assumed to be a result of reaction with residual moisture as described above for the LiCl ion-exchange reactions.

Physical and Chemical Properties

Crystals of $NaMo_4O_6$ were grown up to 1 mm in length but only 0.02 mm in width and they exhibited a tendency to separate into thinner whiskers along the c axis (long dimension). It was determined that $NaMo_4O_6$ is stable in air up to at least 300°C by viewing crystals on a hot stage microscope. The compound $NaMo_4O_6$ in powder form appeared stable to concentrated hydrochloric acid but was decomposed in 3M HNO_3 with gas evolution.

X-Ray Powder Diffraction Data

An Enraf Nonius Delft triple focusing Guinier x-ray powder diffraction camera was used with Cu $K\alpha_1$ radiation (λ = 1.54056 Å) to obtain unit cell data. National Bureau of Standards silicon powder was mixed with all samples as an internal standard. The lattice parameters for $NaMo_4O_6$, $Li_{1-x}Na_xMo_4O_6$ and $K_{1-x}Na_xMo_4O_6$ were calculated by a least squares method and are listed in Table III-1. Lattice parameters for $NaMo_4O_6$, calculated using the strongest 17 lines observed in the x-ray powder pattern, compare very well with those obtained from single crystal data. The compound $Li_{1-x}Na_xMo_4O_6$ was indexed on the basis of

Table III-1. Lattice parameters for $NaMo_4O_6$, $Li_{1-x}Na_xMo_4O_6$, and $K_{1-x}Na_xMo_4O_6$

Compound	a, Å	b, Å	c, Å	V, Å^3
$NaMo_4O_6$	9.570(3)	9.570(3)	2.8634(8)	262.2[a]
	9.567(1)	9.567(1)	2.8618(2)	261.9[b]
$Li_{1-x}Na_xMo_4O_6$	9.578(4)	9.726(3)	2.832(1)	263.8[b]
$K_{1-x}Na_xMo_4O_6$	9.642(1)	9.642(1)	2.8772(2)	267.5[b]

[a]From single crystal x-ray diffraction data.

[b]From powder x-ray diffraction data.

an orthorhombic unit cell and $K_{1-x}Na_xMo_4O_6$ on the basis of a tetragonal unit cell. The lattice parameters for both compounds were calculated using all of the reflections remaining when the lines of all other known phases were removed. These data are shown in Tables III-2 and III-3.

Pressed Pellet Electrical Resistivity Measurement

A pellet of $NaMo_4O_6$ powder, 0.48 cm thick and 0.64 cm in diameter, containing less than one percent of Mo metal impurity was pressed under 700 Kg/cm^2 and four platinum wire connections made with silver adhesive. Electrical resistivity measurements were made using a standard four probe a.c. (27.5 Hz) method by recording the voltage across the pressed pellet as a function of temperature. The cooling rate was adjusted to 1-2 degrees/minute and temperature readings were provided by Pt and Ge resistance thermometers. Voltage readings were recorded approximately every 2.5 degrees in the interval 20-280 K and at least every degree from 20 to 2.4 K. The voltage across a calibrated standard resistor was measured periodically and showed no significant change during the experiment. The ratio of the measured resistivity to that measured at 280 K was graphed as a function of temperature.

Table III-2. X-ray powder diffraction data for $Li_{1-x}Na_xMo_4O_6$

h	k	ℓ	d_{obsd}	d_{calcd}	I_{obsd}[a]
1	1	0	6.842	6.825	s
2	1	0	4.299	4.297	vw
1	3	0	3.072	3.071	m
3	1	0	3.038	3.034	m
2	3	0	2.688	2.685	m
1	1	1	2.618	2.616	m
1	2	1	2.371	2.371	s
2	1	1	2.365	2.365	s
3	3	0	2.275	2.275	w
2	2	1	2.181	2.179	w
1	3	1	2.083	2.082	m
2	3	1	1.948	1.948	m
3	2	1	1.942	1.942	s
3	4	0	1.934	1.934	m
2	5	0	1.802	1.802	w
3	3	1	1.773	1.774	w
1	5	1	1.581	1.581	w
5	2	1	1.508	1.509	w
0	0	2	1.416	1.416	m

[a] s = strong, m = medium, w = weak, vw = very weak.

Table III-3. X-ray powder diffraction data for $K_{1-x}Na_xMo_4O_6$

h	k	ℓ	d_{obsd}	d_{calcd}	I_{obsd}[a]
1	1	0	6.828	6.818	s
2	1	0	4.312	4.312	vw
3	1	0	3.047	3.049	m
3	2	0	2.674	2.674	w
1	1	1	2.651	2.651	w
2	0	1	2.470	2.471	m
2	1	1	2.394	2.393	s
3	3	0	2.273	2.273	vw
2	2	1	2.199	2.199	w
3	1	1	2.092	2.093	w
3	2	1	1.958	1.959	s
4	3	0	1.929	1.928	w
4	4	0	1.704	1.704	vw
5	2	1	1.521	1.520	vw
0	0	2	1.439	1.439	m
1	1	2	1.408	1.408	w
3	1	2	1.301	1.301	w

[a] s = strong, m = medium, w = weak, vw = very weak.

Photoelectron Spectra

The valence band ultraviolet photoelectron spectrum of $NaMo_4O_6$ was obtained with an AEI-200B instrument using monochromatic HeI radiation (21.2 eV). The valence band x-ray photoelectron spectrum was obtained with the same instrument using Al Kα radiation (1486.6 eV). Photoelectron binding energies were referenced against silver metal. The powdered sample of $NaMo_4O_6$, which contained less than one percent of Mo metal impurity, had been washed several times with deionized water and dried in vacuo at 110°C.

X-Ray Data Collection

A single crystal of $NaMo_4O_6$ in the shape of a thin needle with dimensions 0.36 x 0.02 x 0.02 mm was selected for x-ray data collection and was mounted with epoxy adhesive on the tip of a glass fiber with the c axis (long dimension) parallel with the long fiber axis. The crystal was indexed as tetragonal on a four-circle x-ray diffractometer (designed and built in Ames Laboratory) (11) with an automatic indexing program (12) that uses reflections obtained from several ω-oscillation photographs at various χ and φ settings as input. The data set was collected at room temperature on the same x-ray diffractometer using Mo Kα radiation (λ = 0.71034 Å) monochromatized with a graphite single crystal. An ω-scan mode was used to collect all data in the HKL, $\bar{H}\bar{K}L$, $\bar{H}K\bar{L}$, and $H\bar{K}\bar{L}$ octants with $2\theta \leq 60°$. The peak heights of three standard reflections which were remeasured every 75 reflections did not show any significant change over the period of data collection. Final cell

parameters and their standard deviations were obtained from the same crystal by a least-squares refinement of $\pm 2\theta$ values of 7 independent reflections randomly distributed in reciprocal space having $2\theta > 28°$. The results are listed in Table III-1.

Structure Determination and Refinement

The observed intensities were corrected for Lorentz-polarization effects and standard deviations calculated (13) to give 1497 reflections with $I > 3\sigma(I)$. Examination of the data set revealed the systematic nonextinction condition $0k\ell$: $k = 2n$. The data were averaged in 4/mmm Laue symmetry to yield a total of 216 independent reflections for the final data set.

A Patterson-superposition method (14) was used to locate the positions of all 8 molybdenum atoms contained in the unit cell. Space group P4/mbm (no. 127) was selected and the molybdenum atoms assigned to mirror planes with site symmetry mm at z = 0 and ½. A full-matrix least-squares refinement (15) on the positional and isotropic thermal parameters of the molybdenum atoms resulted in a residual $R = \Sigma\left||F_o|-|F_c|\right|/\Sigma|F_o|$ of 0.262. Oxygen atom positions were located from an electron density Fourier map (16) and subsequent refinement of Mo and O positional and isotropic thermal parameters converged to give $R = 0.081$ and $R_w = 0.111$ where $R_w = [\Sigma\omega(|F_o|-|F_c|)^2/\Sigma\omega|F_o|^2]^{\frac{1}{2}}$ and $\omega = \sigma_F^{-2}$. At this point, an electron density map revealed four peaks of sodium electron density spaced at ca. 0.5 Å from one another in a square pattern around the special position 0, 0, 1/2 and with very

shallow minima between peaks. This implied that the sodium ions were statistically disordered around that special position. Attempts to refine the structure with sodium at these positions resulted in very large positional shifts and a diverging refinement. The sodium was then constrained at the position 0, 0, 1/2 and a full isotropic refinement gave R = 0.062 and R_w = 0.076 with a sodium isotropic temperature factor of 7.3 $Å^2$. Further refinement of the scale factor, positional parameters, sodium multiplier and all anisotropic thermal parameters gave convergence at R = 0.045 and R_w = 0.054 with a sodium atom occupancy per site of 1.02(6). An absorption correction was not considered necessary because the calculated transmission factors varied from only 0.85 to 0.87 over all crystal orientations. A final difference Fourier synthesis map was flat to $\leq$ 1.5e/$Å^3$. The atomic scattering factors used were those of Hanson et al. (17) for neutral atoms and molybdenum was corrected for the real and imaginary parts of anomalous dispersion (18).

RESULTS

Structure Description

The final positional parameters for $NaMo_4O_6$ are given in Table III-4, thermal parameters in Table III-5, and important interatomic distances and angles in Table III-6. Observed and calculated structure factors are available as supplementary material.

Figure III-1 is an ORTEP drawing, with labels referring to Table III-6, of a section of one metal-oxide cluster chain showing the repeat unit along the c axis. Bonds between molybdenum atoms are represented by the solid-filled lines and Mo-O bonding by the open unfilled lines. All Mo1 and O2 atoms lie in mirror planes perpendicular to the c axis at z = 0 and 1, while the Mo2 and O1 atoms lie in a mirror plane at z = 1/2. Two other mirror planes are present in this structure; one contains all of the Mo1 atoms as well as O1a and O1b, the other mirror contains the Mo2, O1c and O1d atoms and bisects the bonds between Mo1a - Mo1b and Mo1c - Mo1d. The atoms Mo1, Mo2, and O1, therefore, lie on sites of mm symmetry while the O2 atoms reside on sites of m symmetry. Note that if atoms O1c and d were removed and oxygen atoms placed so as to bridge the edges Mo1a - Mo1b and Mo1c - Mo1d, then the Mo_6O_{12} 'building block' would result. However, in this condensed cluster system, the atoms at z = 0 and 1 also constitute parts of neighboring unit cells.

An extended view of one of the chains running parallel to the c axis is provided in Figure III-2. This drawing shows the architecture

Table III-4. Positional parameters for $NaMo_4O_6$

Atom	Position[a]	Multiplier	x	y	z
Mo1	4g	0.250	0.6017(2)	0.1017	0.00
Mo2	4h	0.250	0.1438(2)	0.6438	0.50
O1	4h	0.250	0.293(2)	0.793	0.50
O2	8i	0.50	0.0457(9)	0.7599(9)	0.00
Na1	2b	0.127(8)	0.00	0.00	0.50

[a]Space group P4/mbm (no. 127).

Table III-5. Thermal parameters for $NaMo_4O_6$[a]

Atom	B_{11}	B_{22}	B_{33}	B_{12}
Mo1	0.59(4)	0.59	0.72(5)	0.01(3)
Mo2	0.60(4)	0.60	1.45(6)	-0.03(4)
O1	1.02(25)	1.02	1.20(46)	-0.43(33)
O2	1.36(31)	1.22(30)	0.91(28)	-0.15(25)
Na1	9.0(11)	9.0	2.9(7)	0.00

[a]The general thermal parameter expression used is $\exp[-1/4(B_{11}h^2a^{*2} + B_{22}k^2b^{*2} + \ldots 2B_{23}k\ell b^*c^*)]$, however, $B_{13} = B_{23} = 0$ by symmetry.

Table III-6. Interatomic distances and angles in $NaMo_4O_6$[a]

Interatomic Distances (Å)

Mo1a-Mo1b	2.753(3)	Mo1a-O2a	2.068(8)
Mo1a-Mo2	2.780(2)	Mo1a-O1a	2.015(8)
Mo1a-Mo1c	2.8618(2)	Mo2-O1c	2.024(11)
Mo1a-Mo1d	3.971(2)	Mo2-O2a	2.040(6)
Mo2-Mo2	3.892(3)		
O1a-O2a	2.852(15)	Na1-O1	3.433(9)
O1c-O2a	2.787(15)	Na1-O2	2.742(8)
O2a-O2b	2.898(17)		
O2a-O2e	2.8618(2)		

Bond Angles (deg)

Mo1a-Mo1b-Mo1d	90.00	O1a-Mo1a-O2a	88.6(4)
Mo1a-Mo2-Mo1b	58.35(5)	O2a-Mo1a-O2c	176.0(5)
Mo1a-Mo2-Mo1c	61.95(5)	O1c-Mo2-O2a	86.6(3)
Mo1b-Mo1a-Mo2	60.32(4)	O2a-Mo2-O2b	90.5(3)
Mo1c-Mo1a-Mo2	59.02(2)	O2a-Mo2-O2e	89.1(3)
		O2a-Mo2-O2f	173.2(5)
Mo1a-O2a-Mo2	85.2(3)		
Mo1a-O1a-Mo1c	90.5(4)		

[a]Calculated using the unit cell parameters obtained from Guinier x-ray powder diffraction data.

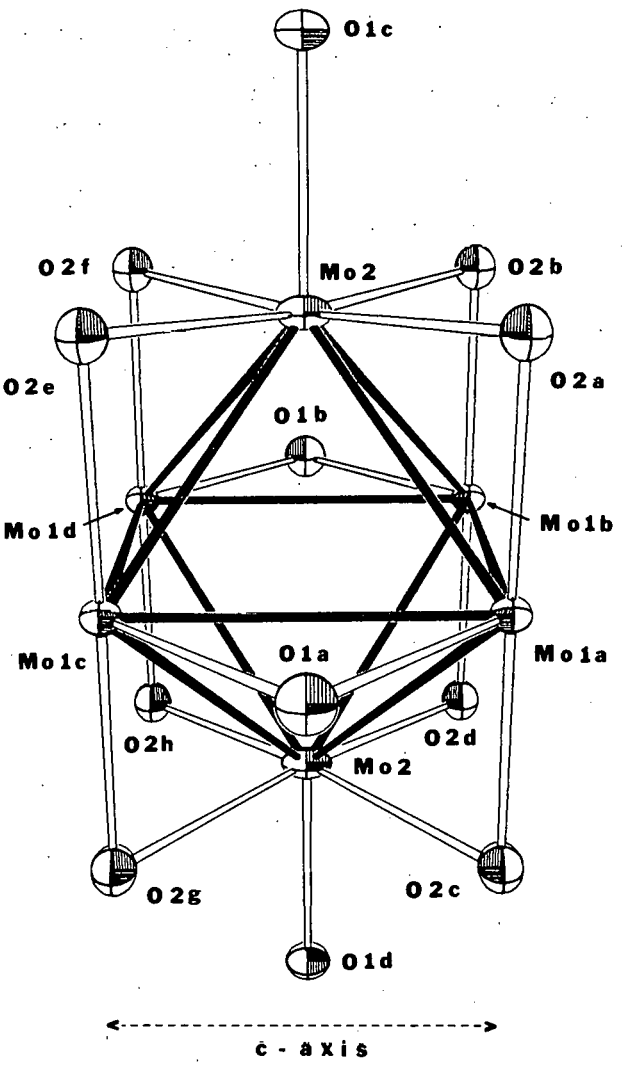

Figure III-1. A section of one molybdenum-oxide cluster chain in $NaMo_4O_6$ showing the repeat unit along the c axis. Fifty percent probability anisotropic thermal ellipsoids are shown

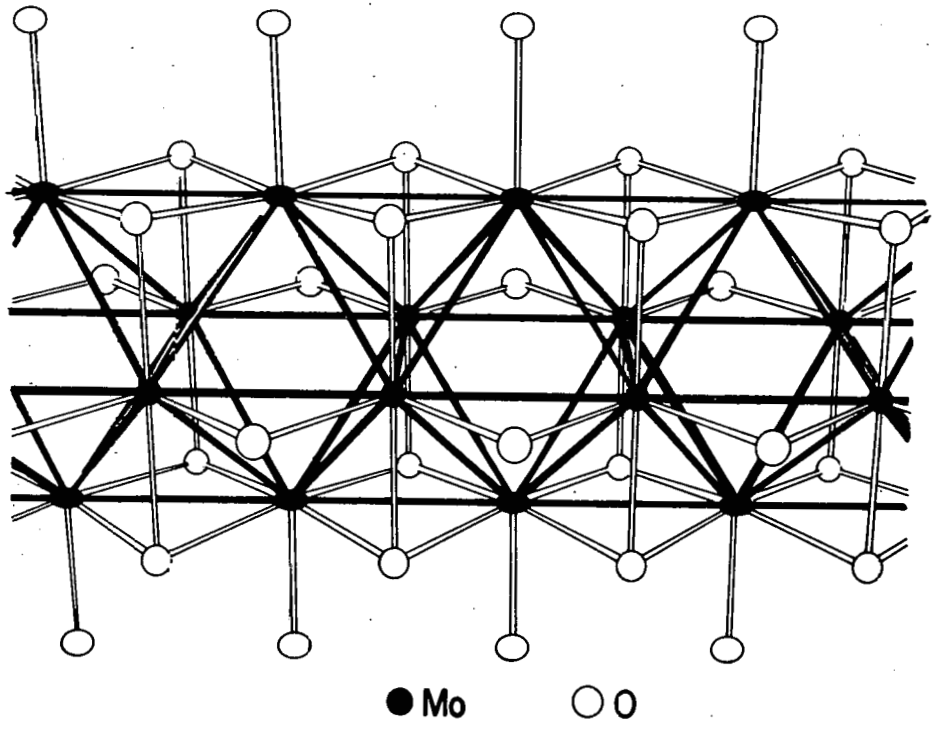

Figure III-2. A view of one molybdenum-oxide cluster chain, $[Mo_2Mo_{4/2}O_{8/2}O_{2/2}]O_{2/2}^-$, extended parallel to the c axis

of the chains as comprised of Mo_6O_{12}-type clusters fused at opposite edges by removal of two edge-bridging O atoms and sharing of the metal and remaining oxygen atoms between cluster units. The doubly bridging and exo oxygen atoms, labeled as O1 in Figure III-1, are bonded to and consequently connect neighboring metal-oxide cluster chains as indicated by the formulation $Na^+[Mo_2Mo_{4/2}O_{8/2}O_{2/2}]O_{2/2}^-$. The structure of these chains is essentially the same as that in the anion of $[ScCl_2^+][Sc_4Cl_6^-]$. However, because of the greater number of valence electrons available per repeat unit for metal-metal bonding in the Mo chains, 13 in $[Mo_4O_6^-]$ vs 7 in $[Sc_4Cl_6^-]$, the metal-metal bonds are stronger and closer to being equivalent over the various edges of the octahedral units. The shortest Mo-Mo bond length, 2.753(3) Å, is found on the shared edges of the octahedral units perpendicular to the c axis direction while the longest Mo-Mo bond distance, 2.8618(2) Å, is equal and parallel to the length of the c axis. The bonds between waist and apex molybdenum atoms, Mo1-Mo2, are intermediate in length, 2.780(2) Å. The Mo-Mo bond distances within the repeat unit, 2.753(3)(1X), 2.8618(2)(4X) and 2.780(2)(8X) Å, result in an average distance of 2.803 Å which is only 0.078 Å longer than the distance between nearest neighbors in bcc molybdenum metal. These 13 Mo-Mo bonds within the Mo_4O_6 repeat unit contain 13 electrons and result in an average bond order of 0.5. The metal-oxide cluster chains contain molybdenum in two different environments, both eleven coordinate; the waist Mo atoms, Mo1, are bonded to seven molybdenum and four oxygen atoms, and the apical Mo atoms, Mo2, which are bonded to six molybdenum and five oxygen atoms.

The oxygen atoms in this structure are each strongly bonded to three Mo atoms in two different geometries. Oxygen atoms, O2 in Figure III-1, which are shared between octahedral units within the chains are each in a trigonal pyramidal-like coordination to two apical molybdenum atoms, Mo2, and one waist molybdenum atom, Mo1. The doubly, edge-bridging oxygen atoms in Figure III-2 are also the exo-bonded oxygen atoms on a neighboring metal-oxide cluster chain just as the exo oxygen atoms pictured are doubly bridging to molybdenum atoms along the edge of another neighboring cluster chain. The result is a trigonal planar-like arrangement of Mo atoms around these equivalent, interchain bridging oxygen atoms, O1 in Figure III-1. The arrangement of oxygen atoms within and between cluster chains is more clearly depicted in Figure III-3 which is a view of the structure down the c axis and perpendicular to the a-b plane. The average intrachain Mo-O bond length is 2.049 Å compared to the shorter average interchain Mo-O bond distance of 2.018 Å.

Figure III-3 also shows that the Na^+ ions occupy sites in channels formed by four metal-oxide cluster chains crosslinked by metal-oxygen bonds as described above. Each sodium ion is surrounded by eight intrachain oxygen atoms at a distance of 2.742(8) Å in tetragonal symmetry. The eight O atoms in the coordination sphere of Na^+ form a square box compressed along the c axis with O-O distances of 2.862 and 3.307 Å. The Na-O distance is ca. 0.16 Å longer than the sum of ionic radii, 2.58 Å using the ionic radii of Shannon and Prewitt (19), and the Na^+ ions exhibit large thermal parameters in the a-b plane,

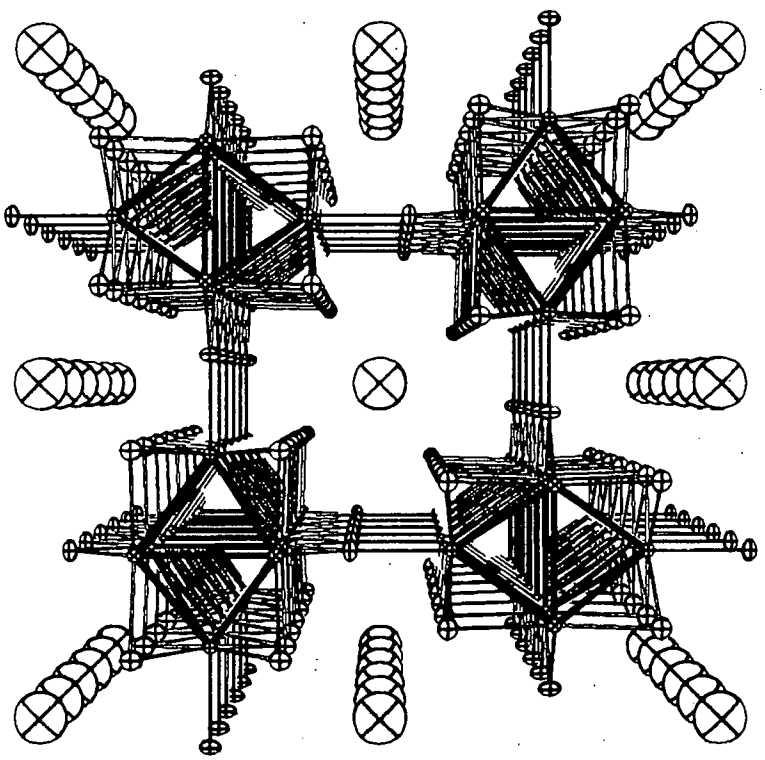

Figure III-3. The structure of $NaMo_4O_6$ as viewed down the c axis showing the interlinking of cluster chains and sodium ion positions along the channels

9.0(11) $Å^2$. However, as mentioned previously, the sodium ions may not actually reside on these sites of 4/m symmetry but may be statistically disordered in the a-b plane around this inversion center. Some of the Na-O distances would then be shorter and some longer than 2.74 Å and the individual sodium thermal parameters would be much smaller than 9.0 $Å^2$. Perhaps low temperature x-ray diffraction data would prove useful in providing information on the sodium ion positions.

Electrical Resistivity Measurement

A pressed pellet electrical resistivity ratio *vs* temperature curve for $NaMo_4O_6$ is shown in Figure III-4. The value of the pressed pellet electrical resistivity at room temperature is *ca.* 10^{-2} ohm-cm and represents some kind of averaged ($\rho_{||}$ and $\rho_{\perp}$) electrical resistance. The resistivity increases slowly, at first, as the temperature is lowered, but it is not an exponential increase indicative of a semiconductor. The increase in resistivity becomes more rapid starting at approximately 100 K and reaches a maximum value at T = 11 K with roughly eight times the room temperature electrical resistance. The resistivity then drops sharply in the temperature range 10 to 2.4 K. However, a superconducting transition for $NaMo_4O_6$ was not observed during a.c. susceptibility measurements taken in the temperature interval 1.1 - 30 K. There was also no evidence for a magnetic phase transition within this temperature range. The maximum in the resistivity ratio *vs* temperature curve could be due to a structural phase transition. If such a transition occurs, it should be detectable

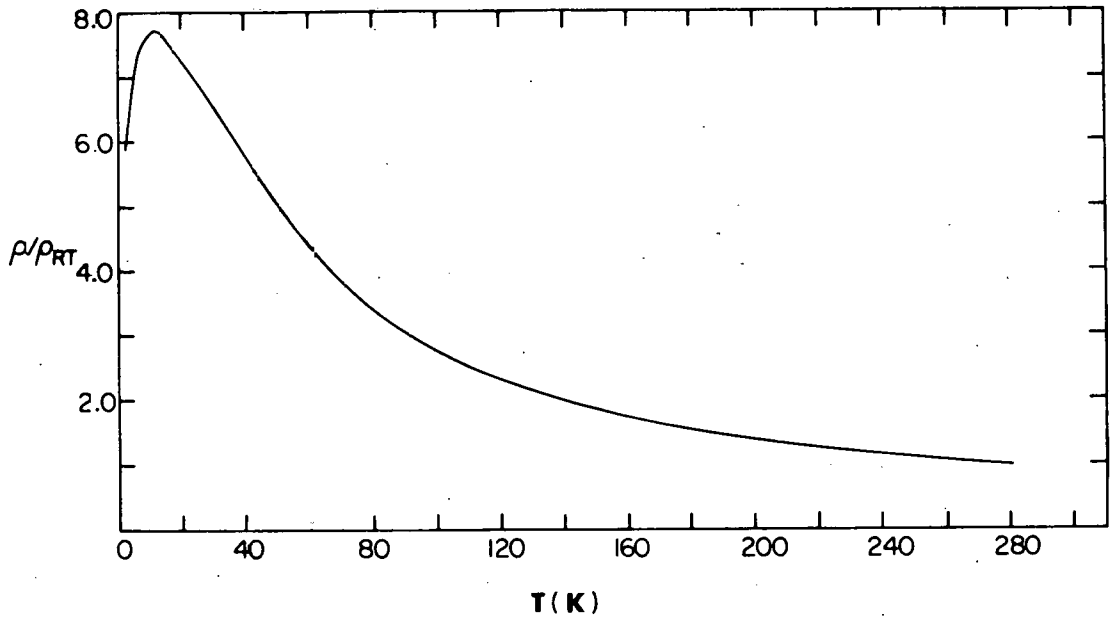

Figure III-4. Resistivity ratio vs temperature curve for a pressed pellet of $NaMo_4O_6$

by heat capacity experiments or by low temperature x-ray diffraction studies.

Ultraviolet Photoelectron Spectrum

The valence band ultraviolet photoelectron spectrum of $NaMo_4O_6$ is shown in Figure III-5. The spectrum contains two broad overlapping bands which are approximately 3.5 - 4 eV wide. Maxima in the spectrum occur at 2 and 5.5 eV below the Fermi level. The presence of electron density at the Fermi level of $NaMo_4O_6$ is indicative of a metallic compound, but the density of states near E_F is low. The maximum of this band is observed at a relatively high binding energy of 2 eV. A similar spectrum for the valence band of $NaMo_4O_6$ was obtained using x-ray photoelectron spectroscopy. The observed spectra may, however, reflect a surface contamination due to the handling and treatment of the sample as described above.

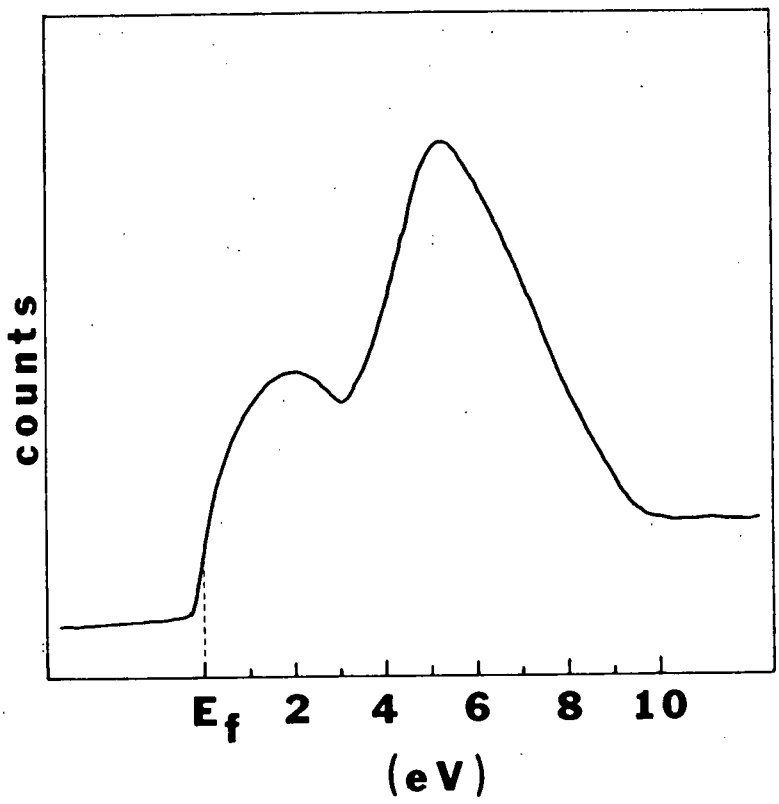

Figure III-5. Valence band ultraviolet photoelectron spectrum of $NaMo_4O_6$

DISCUSSION AND CONCLUSIONS

The infinite-chain, polymeric structure of $NaMo_4O_6$ is clearly dominated by strong Mo-Mo bonding. Within the chains, each Mo_4O_6 repeat unit has available 13 electrons to participate in Mo-Mo bonding and each unit has 13 metal-metal bonds. If all 13 electrons reside in bonding orbitals, then the average Mo-Mo bond order is 0.5. Use of the Pauling empirical equation (20), $D_n = D_1 - 0.6 \log n$, permits calculation of the bond order n associated with each Mo-Mo bond in the repeat unit of length D_n relative to the length of a single Mo-Mo bond, $D_1 = 2.614$ Å (21). When averaged over all 13 Mo-Mo bonds, the result is n = 0.49 which provides evidence that the 13 electrons reside in bonding orbitals.

Several other features of this structure should be noted. One feature is that the repeat distance between units of 2.862 Å constitutes both the bonded Mo-Mo and nonbonded O-O distance along the direction of the chain. Another feature is that the relatively longer average Mo-O distance of 2.049 Å for the intrachain oxygen atoms results, in part, from their sp^3-like geometry and coordination to sodium. The shorter average Mo-O bond length of 2.018 Å for the interchain oxygen atoms may result from their sp^2-like hybridization and resultant ability to form pi bonds to the molybdenum cluster chains.

A pi bonding interaction could serve as a mechanism for electron delocalization from chain to chain and be responsible for the fact that crystals of $NaMo_4O_6$ are opaque to polarized light perpendicular to

the c axis. A single crystal electrical resistivity measurement along the c axis has shown $NaMo_4O_6$ to be a moderately good electrical conductor with ρ ca. 10^{-4} ohm-cm, but the resistivity perpendicular to the c axis, which would provide information regarding interchain electronic transport properties, has not been measured because of the very small crystal dimension ($\leq$ 0.02 mm).

Another interesting structural feature of $NaMo_4O_6$ is the relatively large site occupied by Na^+ ions within the channels. This site appeared to be of sufficient size to accommodate ions as large as Ba^{2+} and possibly K^+, and because of the 'loose fit' of the Na^+ ions, the question also arose as to whether a smaller cation such as Li^+ could be placed in the channels. A reaction designed to prepare the isoelectronic compound $Ba_{0.5}Mo_4O_6$ was successful in preparing the new compound $Ba_{0.62}Mo_4O_6$ (22) which also contains a commensurate superlattice ordering of barium ions. Attempts to prepare KMo_4O_6 always resulted in the formation of a new phase tentatively formulated as $K_{2+x}Mo_{12}O_{19}$ (23). Reactions balanced to give $LiMo_4O_6$ gave instead a new lithium molybdenum oxide which is presently under investigation.

The possibility of ion exchanging the sodium for K^+ or Li^+ was also considered. Aqueous ion exchange reactions at room temperature using KCl and LiCl solutions were unsuccessful. However, an ion-exchange reaction between $NaMo_4O_6$ and molten LiCl at 700°C was successful in forming $Li_{1-x}Na_xMo_4O_6$ with x ca. 0.25. The lithiated structure was lowered in symmetry from tetragonal to orthorhombic, see Table III-1, but no explanation for this structural transition is

apparent. If the transition results from a change in the number of electrons per Mo_4O_6 repeat unit, then the structure must contain more or less than one alkali metal ion per site along the channels. It may be possible to reduce the molybdenum-oxygen cluster chains by inserting additional lithium into the channels to give some sites containing two Li^+ ions each in approximately four-coordination with oxygen. A certain amount of $NaMo_4O_6$ would also be oxidized, possibly forming some MoO_2. The 0.6% increase in unit cell volume of the lithiated compound relative to $NaMo_4O_6$ could, therefore, result from a small overall lengthening of Mo-Mo and Mo-O bonds. However, another reason for this volume increase could simply be the result of less efficient space filling by the atoms in the orthorhombic structure. Similar ion-exchange reactions between $NaMo_4O_6$ and molten KCl at 800°C were successful in exchanging some Na^+ with K^+ with a resultant 2% increase in the tetragonal unit cell volume (see Table III-1), but as mentioned earlier, it is not known whether the potassium is present as KMo_4O_6 or as a mixed alkali metal compound. The fact that 24 and 85 hour reaction times resulted in the same ratio of $NaMo_4O_6$ to $Na_xK_{1-x}Mo_4O_6$ implies that formation of the potassium compound becomes inhibited. This could be due to a coating of the potassium compound on the particles of $NaMo_4O_6$, thereby hindering further reaction. It can thus be concluded that the sodium ions are indeed exchangeable under the proper experimental conditions. It may also be possible to remove the Na^+ ions altogether in an oxidative process leaving intact the Mo_4O_6 structure with empty sites along the channels 2.5 - 3 Å in diameter or

to prepare compounds $M_x^{n+}[Mo_4O_6^{xn-}]$ with n = 2, x > 0.5, or n = 3, x > 0.33 such that the electron/metal ratio is varied over the range 3.0 - 3.75.

A final comment is made on the mechanism of crystal growth for $NaMo_4O_6$. The crystals grew not only from the pressed reaction pellet but also from the walls and ends of the molybdenum reaction vessel. This suggests a vapor transport mechanism. Under the conditions of the reaction, some possible vapor state species are $Na_2O(g)$, $MoO_3(g)$, $MoO_2(OH)_2(g)$ and H_2. The first two gaseous compounds could be generated by the thermal decomposition of Na_2MoO_4 and the latter two arising from the reaction of MoO_2 with residual moisture (24); but it is not possible to say at this time which, if any, are involved in single crystal growth.

REFERENCES

1. Marinder, B. O. Arkiv Kemi 1962, 19, 435.

2. Torardi, C. C. Ph.D. Dissertation, Iowa State University, Ames, Iowa, 1981, Section I.

3. Torardi, C. C. Ph.D. Dissertation, Iowa State University, Ames, Iowa, 1981, Section II.

4. Chevrel, R.; Sergent, M.; Prigent, J. J. Solid State Chem. 1971, 3, 515.

5. Lokken, D. A.; Corbett, J. D. Inorg. Chem. 1973, 12, 556.

6. Poeppelmeier, K. R.; Corbett, J. D. J. Am. Chem. Soc. 1978, 100, 5039.

7. Poeppelmeier, K. R.; Corbett, J. D. Inorg. Chem. 1977, 16, 1107.

8. Adolphson, D. G.; Corbett, J. D. Inorg. Chem. 1976, 15, 1820.

9. Torardi, C. C.; McCarley, R. E. J. Am. Chem. Soc. 1979, 101, 3963.

10. McCarroll, W. H.; Katz, L.; Ward, R. J. Am. Chem. Soc. 1957, 79, 5410.

11. Rohrbaugh, W. J.; Jacobson, R. A. Inorg. Chem. 1974, 13, 2535.

12. Jacobson, R. A. J. Appl. Crystallogr. 1976, 9, 115.

13. Lawton, S. L.; Jacobson, R. A. Inorg. Chem. 1968, 7, 2124.

14. Hubbard, C. R.; Babich, M. W.; Jacobson, R. A. "A PL/1 Program System for Generalized Patterson Superpositions", 1977, US AEC Report IS-4106.

15. Lapp, R. L.; Jacobson, R. A. "ALLS, A Generalized Crystallographic Least Squares Program", 1979, US DOE IS-4708.

16. Powell, D. R.; Jacobson, R. A. "FOUR: A General Crystallographic Fourier Program", 1980, US DOE Report IS-4737.

17. Hanson, H. P.; Herman, F.; Lea, J. D.; Skillman, S. Acta Crystallogr. 1964, 17, 1040.

18. Templeton, D. H. In "International Tables for X-Ray Crystallography", 1st ed.; Macgillavry, C. H. and Rieck, G. D., Eds.; Kynoch Press: Birmingham, England, 1962; Vol. III, page 215.

19. Shannon, R. D.; Prewitt, C. T. Acta Crystallogr. 1969, B25, 925.

20. Pauling, L. "The Nature of the Chemical Bond", 3rd ed.; Cornell University Press: New York, 1960; page 400.

21. McCarley, R. E. Ames Laboratory, Iowa State University, Ames, Iowa; private communication.

22. Torardi, C. C. Ph.D. Dissertation, Iowa State University, Ames, Iowa, 1981, Section IV.

23. Torardi, C. C. Ph.D. Dissertation, Iowa State University, Ames, Iowa, 1981, Section V.

24. Schafer, H.; Grofe, T.; Trenkel, M. J. Solid State Chem. 1973, 8, 14.

SECTION IV. THE SYNTHESIS AND CRYSTAL STRUCTURE OF $Ba_{0.62}Mo_4O_6$. A METALLIC INFINITE-CHAIN POLYMER DERIVED BY CONDENSATION OF OCTAHEDRAL CLUSTERS AND CONTAINING A SUPERLATTICE ORDERING OF BARIUM IONS

INTRODUCTION

The synthesis and structure of the compound $NaMo_4O_6$ was recently described (1) as containing octahedral molybdenum atom cluster units fused on opposite edges to form linear chains. Oxygen atoms bridge the outwardly exposed edges of the octahedral cluster chains and connect one chain to another through Mo-O-Mo bridges as indicated in the connectivity formula $Na^+[(Mo_2Mo_{4/2}O_{8/2}O_{2/2})O_{2/2}^-]$. These infinite chains are interlinked in such a manner that channels accommodating the Na^+ ions are provided. This structure possesses many interesting features, but the strong metal-metal bonding clearly dominates in determining the architecture of the chains. In the course of further research dealing with this structure type, a related barium compound was synthesized (2). This section reports the preparation and crystal structure of the compound $Ba_{0.62}Mo_4O_6$. The new compound exhibits a superlattice ordering of barium ions within the channels. Efforts made to solve the superstructure of this compound from single crystal x-ray diffraction data are also discussed.

EXPERIMENTAL

Materials

Barium molybdate was prepared by mixing an aqueous solution of $BaCl_2 \cdot 2H_2O$ ('Baker Analyzed' Reagent, 99.6%) with an aqueous solution containing the stoichiometric quantity of ammonium heptamolybdate tetrahydrate ('Baker Analyzed' Reagent, 83.0% as MoO_3) and ammonium hydroxide. The white precipitate was filtered, washed several times with deionized water, dried at 120°C for 20 hours, and stored over P_4O_{10}. Molybdenum dioxide was prepared by the hydrogen reduction of MoO_3 (Fisher Certified A.C.S.) at 460°C for 40 hours. The reduced material was washed several times with alternate portions of 3M NH_4OH, deionized water, and 3M HCl until the washings were colorless, and finally dried in vacuo at 110°C. Anal. Calculated for MoO_2: Mo, 74.99. Found: Mo, 74.96. Molybdenum tubing was obtained from Thermo-Electron Corp. (99.97%), Mo sheet from Rembar Co. (99.95%), and Mo powder from Aldrich (99.99%).

Synthesis

An attempt was made to prepare the compound $Ba_{0.5}Mo_4O_6$ (which would be isoelectronic with the $NaMo_4O_6$ phase) using $BaMoO_4$, MoO_2, and Mo powder in a 1:4:3 mole ratio. The reaction mixture was ground in a mortar, pelletized under 700 kg/cm^2, sealed in an evacuated molybdenum tube (3 cm long x 1 cm diam) which, in turn, was sealed in an evacuated inconel protection tube, and held at 1100°C for one week. The product

pellet was covered with small, needle-shaped crystals possessing metallic luster. Some of these crystals were scraped from the pellet and powdered in a mortar. An x-ray powder diffraction pattern of this material contained the lines of a new phase related to tetragonal $NaMo_4O_6$ as well as the strongest lines of MoO_2 and Mo metal. The composition of the new phase was determined as $Ba_{0.62}Mo_4O_6$ from single crystal x-ray diffraction data (see below). The experiment was repeated using a 5 day reaction time and identical results were obtained. If the compound $Ba_{0.62}Mo_4O_6$ were the only phase formed in the reaction, then unreacted MoO_2 and Mo would be expected.

X-Ray Data Collection for the $Ba_{0.62}Mo_4O_6$ Subcell

A single crystal of $Ba_{0.62}Mo_4O_6$ in the shape of a thin needle with dimensions 0.22 x 0.02 x 0.02 mm was selected for x-ray data collection and was mounted in a 0.2 mm Lindemann glass capillary with a small amount of silicone grease. The crystal was aligned with its long dimension nearly collinear with the phi-circle axis on a four-circle x-ray diffractometer designed and built in the Ames Laboratory (3). Four ω-oscillation photographs were then taken at various χ and ϕ settings. Reflections obtained from these photographs were input into an automatic indexing program (4) from which an orthorhombic unit cell was calculated with lattice parameters similar to those of $NaMo_4O_6$. The data set was collected at ambient temperature on the same x-ray diffractometer using Mo Kα radiation (λ = 0.71034 Å) monochromatized with a graphite single crystal. An ω-scan mode was used to collect all

data in the HKL, $\bar{H}\bar{K}L$, and $\bar{H}K\bar{L}$ octants with $2\theta \leq 60°$. The peak heights of three standard reflections which were remeasured every 75 reflections did not show any significant change over the period of data collection. Final cell parameters and their standard deviations were obtained from the same crystal by a least-squares refinement of $\pm 2\theta$ values of 16 independent reflections randomly distributed in reciprocal space having $2\theta > 27°$. The results were a = 9.509(2) Å, b = 9.825(2) Å, c = 2.853(1) Å, and V = 266.5 $Å^3$.

Structure Refinement of the $Ba_{0.62}Mo_4O_6$ Subcell

The observed intensities were corrected for Lorentz and polarization effects and standard deviations calculated as described previously (5) to give 1076 reflections with $I > 3\sigma(I)$. Examination of the data set revealed the systematic nonextinction conditions hOℓ: h = 2n, and Okℓ: k = 2n. The data were averaged in mmm Laue symmetry to yield a total of 394 independent reflections for the final data set.

The positional parameters of $NaMo_4O_6$ were used as the starting set of positions for the new barium compound in space group Pbam (no. 55). Barium was constrained on the 2b positions $(0,0,\frac{1}{2};\ \frac{1}{2},\frac{1}{2},\frac{1}{2})$ and its multiplier fixed to give an occupancy of one Ba atom per unit cell (i.e., $Ba_{0.5}Mo_4O_6$). A full-matrix least-squares isotropic refinement (6) resulted in a residual $R = \Sigma\left||F_o|-|F_c|\right|/\Sigma|F_o|$ of 0.212 with a large barium isotropic thermal parameter of 3.6 $Å^2$. The barium atom was removed from the atomic parameter list and an electron density Fourier

map was calculated (7) using only the phases derived from the Mo and O positions. This map clearly showed a region of electron density, elongated along the c axis, consisting of two peaks symmetrically related at $(0,0,\pm z)$ with z approximately 0.375. Therefore, these 4e positions, rather than 2b sites, were assigned to the barium atom with an initial multiplier value of 0.125 (1 Ba atom/cell). An isotropic refinement including the barium atom position and multiplier converged to give R = 0.093 and R_w = 0.149 where $R_w = [\Sigma\omega(|F_o|-|F_c|)^2/\Sigma\omega|F_o|^2]^{\frac{1}{2}}$ and $\omega = \sigma_F^{-2}$. An absorption correction was made (μ = 121 cm^{-1}) using an empirical ϕ-scan method (8) where the intensity of a selected reflection at χ approximately 90° was measured every 10° in ϕ with the aid of the x-ray diffractometer; however, this correction made no significant change in the refinement. A full anisotropic refinement gave R = 0.081 and R_w = 0.123 with a total barium occupancy of 1.25(3) atoms/cell. A large barium B_{33} thermal parameter of 2.6(3) $Å^2$ also resulted from the refinement. A final difference Fourier synthesis map contained electron densities as high as 7.5e/$Å^3$ on molybdenum sites and 3.3e/$Å^3$ on the inversion center at $(0,0,\frac{1}{2})$.

It was observed that the high angle data ($\sin\theta/\lambda > 0.6$) refined to a relatively high residual R of 0.14. A full anisotropic refinement using only data with $2\theta \leq 50°$ (265 reflections) resulted in R = 0.056 and R_w = 0.091 with no significant change in the barium atom multiplier; there was also no increase in the positional and thermal parameter standard deviations. An electron density difference map was generated after this refinement and it revealed electron peak densities

of $5e/Å^3$ on all molybdenum atom sites, and $3e/Å^3$ at the positions $(0,0,\frac{1}{2};\ \frac{1}{2},\frac{1}{2},\frac{1}{2})$. The residual electron density, fractional occupation of barium, and large B_{33} thermal parameter for barium all suggested the possibility of a superlattice ordering of barium ions within the channels. It was believed that the barium ion ordering could affect the cluster chains and result in several slightly different molybdenum and oxygen atomic positions along the chains in the supercell.

The atomic scattering factors used were those of Hanson et al. (9) for neutral atoms. Molybdenum and barium were corrected for the real and imaginary parts of anomalous dispersion (10).

Superlattice Determination

Several crystals of $Ba_{0.62}Mo_4O_6$ were mounted in 0.2 mm Lindemann glass capillaries, and oscillation photographs along the c axis (long dimension) were obtained. They all showed the presence of weak superlattice layers, consisting of discrete diffraction spots, indicating the true unit cell dimension along the c axis to be 8(2.853) Å. This suggested a commensurate superlattice ordering with barium ions occupying five of the eight possible cation sites along each channel in the supercell. This occupation scheme would result in the stoichiometry $Ba_5Mo_{32}O_{48} = Ba_{0.625}Mo_4O_6$ as observed from the single crystal structure analysis described above.

X-Ray Data Collection for the $Ba_{0.62}Mo_4O_6$ Supercell

A crystal of $Ba_{0.62}Mo_4O_6$ of dimensions 0.18 x 0.02 x 0.02 mm was selected for x-ray data collection. The crystal was mounted on the four-circle x-ray diffractometer and indexed as orthorhombic with the same lattice parameters previously obtained for the subcell. The crystal's orientation matrix was transformed to give a c axis which was eight times the length of the subcell c axis. The data set was collected at room temperature using Mo Kα radiation (λ = 0.71034 Å) monochromatized with a graphite single crystal. An ω-scan mode was used to collect all data in the HKL and $\bar{H}\bar{K}$L octants with $2\theta \leq 60°$. The peak heights of three standard reflections which were remeasured every 75 reflections did not show any significant change over the period of data collection. Final cell parameters and their standard deviations were obtained from the same crystal by a least-squares refinement of $\pm 2\theta$ values of 17 independent reflections randomly distributed in reciprocal space having $2\theta > 27°$. The results were a = 9.517(1) Å, b = 9.822(1) Å, c = 22.813(4) Å, and V = 2132.4 $Å^3$.

Structure Refinement of the $Ba_{0.62}Mo_4O_6$ Supercell

Examination of the data set revealed that all observed reflections satisfied the nonextinction conditions h0ℓ: h = 2n, and 0kℓ: k = 2n. An absorption correction was made using an empirical ϕ-scan method (as described above for the $Ba_{0.62}Mo_4O_6$ subcell), and the intensities were

corrected for Lorentz-polarization effects to yield 1121 reflections with $I > 3\sigma(I)$. The data were finally averaged in mm2 symmetry to give 639 independent reflections for the final data set.

The starting set of molybdenum and oxygen positions were taken from the $Ba_{0.62}Mo_4O_6$ subcell refinement; only the z fractional coordinates were changed to form 8 subcells stacked into one supercell. With all of the Mo and O atoms fixed in these positions, a refinement of only the scale factor in the noncentrosymmetric space group Pba2 (no. 32) gave an R of 0.42. Because of pseudosymmetry created by the molybdenum atom positions, a centric electron density map resulted from this refinement; all eight subcells contained barium electron density elongated along the c axis. To disperse this pseudosymmetry, the molybdenum atom positions were next allowed to vary, but severe positional correlations among the Mo atoms caused a diverging refinement. This problem was circumvented by employing a cyclic process where the molybdenum atoms were varied in groups of two or three while all other atoms remained fixed in position. In this manner, a residual R of 0.34 was obtained. A difference map now displayed a range of barium electron density in the eight sites along each channel. The position of the strongest peak in this map was assigned to a barium ion and it was refined along with the molybdenum atom positions through the atomic cycling process; then another electron density difference map was generated. This procedure was repeated until a fifth barium ion was located and a difference map showed only low levels of residual electron density along the channels. The least-squares full-matrix

refinement gave R = 0.125 at this point. A study of the atomic positions indicated that the structure was actually centrosymmetric; therefore, the origin of the cell was changed and a barium atom constrained on the inversion center at $(0,0,\frac{1}{2})$, with the remaining barium atoms on 4e positions $(0,0,\pm z)$. An essentially identical refinement resulted in space group Pbam, with the added benefit of a decrease in positional correlations and overall standard deviations.

The oxygen atom positions were next refined through the cycling process until all positional shifts were less than the positional standard deviations. The isotropic thermal parameters for oxygen had been constrained to 1.0 Å^2 and remained fixed at this value for the entire structural refinement. The barium and molybdenum isotropic thermal parameters were then included in the cyclic process of refinement. After many individual barium, molybdenum, and oxygen cycles, the isotropic refinement converged at R = 0.072 and R_w = 0.091 where $R_w = [\Sigma\omega(|F_o|-|F_c|)^2/\Sigma\omega|F_o|]^{\frac{1}{2}}$ and $\omega = \sigma_F^{-2}$. Further cyclic refinement of atomic positions and heavy atom anisotropic thermal parameters, which were very sensitive to correlation effects, resulted in R = 0.066 and R_w = 0.083. All positional, thermal, and occupational parameter standard deviations were also lowered by the anisotropic treatment. Variation of the occupation parameters for the three independent barium ion sites gave converged values of 1.028(24), 1.020(20), and 0.936(16). A difference map disclosed two small inversion-related peaks with densities of 6e/Å^3 in one of the 'empty' barium sites. This site was adjacent to that of the barium ion possessing the low occupation number.

A fourth Ba atom was placed at this new position and assigned a low value for its multiplier. The cyclic process of refinement was again employed and included the occupation parameters of the fourth Ba atom and its neighbor. A residual R = 0.064 and R_w = 0.077 was obtained with occupation values of 0.10(2) and 0.88(2) for the two barium ion sites. This result implied that the true barium ion superlattice ordering was more complicated than had been anticipated. A final electron density difference map was flat to $\leq 3e/\AA^3$. (A final anisotropic refinement of the four barium ion positions in a supercell containing anisotropic molybdenum and isotropic oxygen atoms, constrained using the equivalent subcell positional and thermal parameters, resulted in R = 0.135 and R_w = 0.190.)

Positional parameter standard deviations were obtained from one cycle of least-squares full-matrix refinement where all atomic positions were simultaneously varied. Thermal parameter standard deviations are those obtained from the atomic cycling process; therefore, the values are slightly lower than those that would have been obtained from a simultaneous refinement. Atomic scattering factor tables and corrections for anomalous dispersion used in the structural refinement were as described for the $Ba_{0.62}Mo_4O_6$ subcell refinement.

RESULTS AND DISCUSSION

Structure Description and Discussion of the $Ba_{0.62}Mo_4O_6$ Subcell

The final positional parameters for the $Ba_{0.62}Mo_4O_6$ subcell are listed in Table IV-1, and thermal parameters are given in Table IV-2. Important interatomic distances and angles are given in Table IV-3. The atomic labels in this table correspond to those in Figure IV-1. The information listed in these tables is the result of the refinement where R = 0.081 and R_w = 0.123. Observed and calculated structure factors are available as supplementary material.

Figure IV-1 is an ORTEP drawing of a section of one molybdenum-oxide cluster chain showing the repeat unit along the c axis. Bonds between molybdenum atoms are represented by the solid, filled lines; Mo-O bonding is represented by the open, unfilled lines. From this figure, it can be seen that the molybdenum-oxide cluster chains in $Ba_{0.62}Mo_4O_6$ are essentially the same as those in $NaMo_4O_6$ (11), except the former possess lower symmetry. All molybdenum and oxygen atoms lie on sites of m symmetry in this subcell refinement. The Mo1, O2, and O3 atoms lie in mirror planes perpendicular to the c axis at z = 0 and 1, while the Mo2 and O1 atoms lie in a mirror plane at z = 1/2. There is also a two-fold rotation axis running parallel with the c axis and passing through the midpoint of the bonds between Mo1a - Mo1b and Mo1c - Mo1d. Consequently, inversion centers are located at the midpoint of these two Mo-Mo bonds as well as in the center of the octahedral cluster repeat unit.

Table IV-1. Positional parameters for the $Ba_{0.62}Mo_4O_6$ subcell[a]

Atom	Position[b]	Multiplier	x	y	z
Ba1	4e	0.156(4)	0.00	0.00	0.369(2)
Mo1	4g	0.50	0.6102(2)	0.0935(2)	0.00
Mo2	4h	0.50	0.1345(2)	0.6501(2)	0.50
O1	4h	0.50	0.2727(18)	0.8147(20)	0.50
O2	4g	0.50	0.0290(16)	0.7562(15)	0.00
O3	4g	0.50	0.2427(17)	0.0613(15)	0.00

[a]Positional parameters obtained from the refinement using all collected data with $2\theta \leq 60°$ ($R = 0.081$; $R_w = 0.123$).

[b]Space group Pbam (no. 55).

Table IV-2. Thermal parameters for the $Ba_{0.62}Mo_4O_6$ subcell[a,b]

Atom	B_{11}	B_{22}	B_{33}	B_{12}
Ba1	1.11(14)	0.94(15)	2.63(25)	-0.02(9)
Mo1	0.71(8)	0.99(8)	0.64(8)	0.07(4)
Mo2	0.87(8)	0.62(8)	1.69(9)	-0.04(4)
O1	0.97(62)	1.59(66)	1.17(74)	-0.16(52)
O2	1.54(52)	0.79(47)	1.50(76)	-0.49(39)
O3	1.33(53)	0.34(45)	0.91(61)	-0.08(41)

[a]The general thermal parameter expression used is $\exp[-1/4(B_{11}h^2a^{*2} + B_{22}k^2b^{*2} + \ldots 2B_{23}k\ell b^*c^*)]$, however, $B_{13} = B_{23} = 0$ by symmetry.

[b]Thermal parameters obtained from the refinement using all collected data with $2\theta \leq 60°$ ($R = 0.081$; $R_w = 0.123$).

Table IV-3. Interatomic distances and angles in the $Ba_{0.62}Mo_4O_6$ subcell[a]

	Distances (Å)		
Mo1a-Mo1b	2.787(4)	Mo1a-O1a	2.022(13)
Mo1a-Mo1c	2.853(1)	Mo1a-O2a	2.075(15)
Mo1a-Mo2a	2.785(2)	Mo1a-O3b	2.067(16)
Mo1a-Mo1d	3.988(3)	Mo2a-O1c	2.084(19)
Mo1b-Mo2a	2.795(2)	Mo2a-O2a	2.032(11)
Mo2a-Mo2b	3.904(4)	Mo2a-O3a	2.039(11)
O1a-O2a	2.908(20)	Ba1-O2	2.632(14)
O1a-O3b	2.826(21)	Ba1-O2	3.009(13)
O1c-O2a	2.782(20)	Ba1-O3	2.607(15)
O1c-O3a	2.873(22)	Ba1-O3	2.987(13)
O2a-O2c	2.853(1)	Ba1-O1	3.190(18)
O2a-O3a	2.895(22)	Ba1-O1	3.791(19)
	Angles (deg)		
Mo1a-Mo1c-Mo1d	90.00	O1a-Mo1a-O2a	90.4(6)
Mo1a-Mo1c-Mo2a	59.19(3)	O1a-Mo1a-O3b	87.5(6)
Mo1a-Mo1c-Mo2b	59.32(3)	O2a-Mo1a-O3b	177.0(6)
Mo1a-Mo1b-Mo2a	59.87(7)	O2a-Mo2a-O3a	90.6(4)
Mo1a-Mo2a-Mo1b	59.91(7)	O2a-Mo2a-O1c	85.0(6)
Mo1a-Mo2a-Mo1c	61.62(6)	O2a-Mo2a-O2c	89.2(6)
Mo1a-Mo2b-Mo1c	61.37(6)	O2a-Mo2a-O3c	173.3(6)
Mo1b-Mo1a-Mo2a	60.22(7)	O3a-Mo2a-O3c	88.8(6)
Mo2a-Mo1a-Mo2b	88.78(7)	O3a-Mo2a-O1c	88.3(6)
Mo1a-O1a-Mo1c	89.7(7)		
Mo1a-O2a-Mo2a	85.4(5)		
Mo1a-O3b-Mo2b	85.8(5)		

[a]Distances and angles obtained using the positional parameters in Table IV-1.

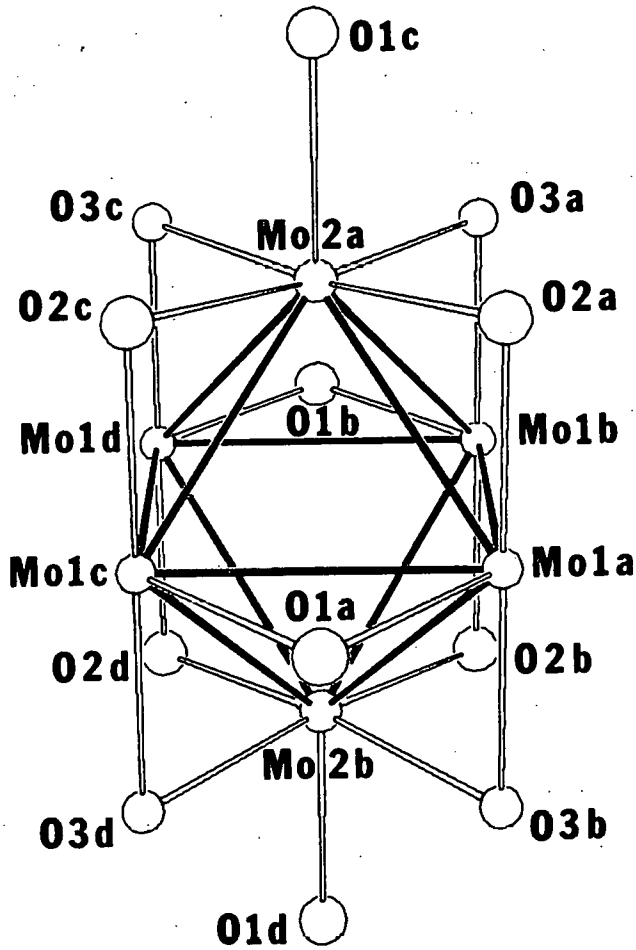

Figure IV-1. A section of one molybdenum-oxide cluster chain in the $Ba_{0.62}Mo_4O_6$ subcell showing the repeat unit along the c axis (parallel with the Mola-Molc bond). The fifty percent probability isotropic thermal ellipsoids are shown

An extended view of one of the cluster chains running parallel with the c axis is provided in Figure IV-2. The architecture of the chains is comprised of clusters of the type Mo_6O_{12} fused at opposite edges by removal of two edge-bridging oxygen atoms and sharing of the metal and remaining oxygen atoms on those edges between cluster units. The doubly-bridging and exo oxygen atoms, O1 atoms in Figure IV-1, are structurally equivalent, and connect each metal-oxide cluster chain to four other adjacent cluster chains. The connectivity within and between chains can be represented by the formulation $Ba^{2+}_{0.62}[(Mo_2Mo_{4/2}O_{8/2}O_{2/2})O^{1.24-}_{2/2}]$. The molybdenum-oxide cluster chains contain two types of molybdenum atoms, both eleven coordinate; the waist Mo atoms, Mo1, which are bonded to seven Mo and four O atoms, and the apical Mo atoms, Mo2, which are bonded to six Mo and five O atoms. One of the shortest Mo-Mo bond lengths, 2.787(4) Å, is found on the shared edges of the octahedral units perpendicular to the c axis direction. The longest Mo-Mo bond distance, 2.853(1) Å, is equal and parallel to the length of the c axis. There are two different Mo-Mo bond lengths of 2.785(2) Å and 2.794(2) Å between molybdenum atoms Mo1 and Mo2. The molybdenum bond distances within the repeat unit, 2.787(4)(1X), 2.853(1)(4X), 2.785(2)(4X), and 2.794(2)(4X) Å, result in an average distance of 2.809 Å. This value is only 0.004 Å longer than the average distance in $NaMo_4O_6$, and 0.082 Å longer than the distance between nearest neighbors in bcc molybdenum metal.

The oxygen atoms in this structure are each bonded to three molybdenum atoms in two different geometries. Oxygen atoms O2 and O3

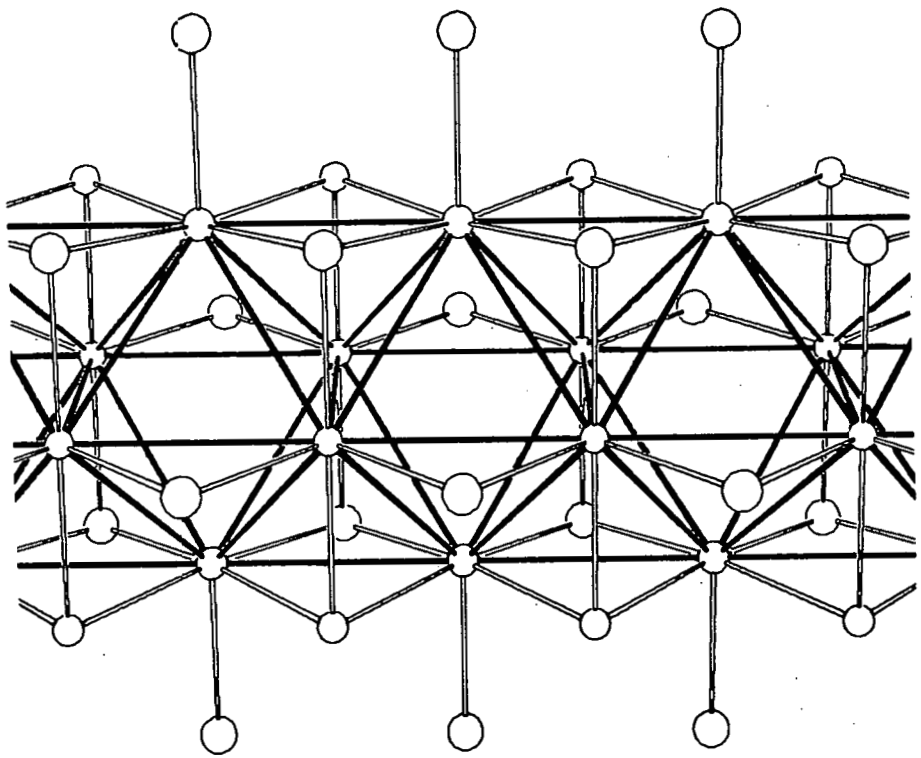

Figure IV-2. A view of one molybdenum-oxide cluster chain in $Ba_{0.62}Mo_4O_6$ = $Ba^{2+}_{0.62}[(Mo_2Mo_{4/2}O_{8/2}O_{2/2})O^{1.24-}_{2/2}]$ extended parallel with the c axis. Fifty percent probability isotropic thermal ellipsoids are shown

(Figure IV-1) are shared between octahedral units within the chains, as depicted in Figure IV-2, and are in a trigonal pyramidal-like coordination with two Mo2 atoms and one Mol atom. The doubly-bridging oxygen atoms in Figure IV-2 are also the singly-bonded oxygen atoms on a neighboring metal-oxide cluster chain; just as the singly-bonded oxygen atoms pictured are doubly-bridging to molybdenum atoms along the edge of another adjacent cluster chain. As a result, the molybdenum atoms are arranged around these interchain oxygen atoms in approximately trigonal planar coordination. A view of the structure down the c axis, Figure IV-3, shows the arrangement of oxygen atoms within and between cluster chains. The average intrachain Mo-O bond length of 2.053 Å in this compound is quite comparable to the value of 2.049 Å found in $NaMo_4O_6$. However, the interchain Mo-O bond lengths consisting of two short bonds, 2.022(13) Å, and one long bond, 2.084(19) Å, result in a longer average Mo-O distance relative to that observed in $NaMo_4O_6$, viz., 2.043 Å vs. 2.018 Å. The two short Mo-O bonds involve the Mol atoms where the interchain oxygen atom is doubly-bridging on an edge of the octahedral cluster repeat unit.

It can also be seen from Figure IV-3 that the principal features of this structure are exactly like those of $NaMo_4O_6$ except the unit cell is distorted from tetragonal to orthorhombic symmetry. In part, this is a result of a slight rotation of each Mo_4O_6 chain about its own axis parallel to the c axis. The rotation of each chain is in a direction opposite to that of each of its neighbors. Thus, the O-O distances between atoms in neighboring chains are reduced in one direction and increased in the other direction within the a-b plane.

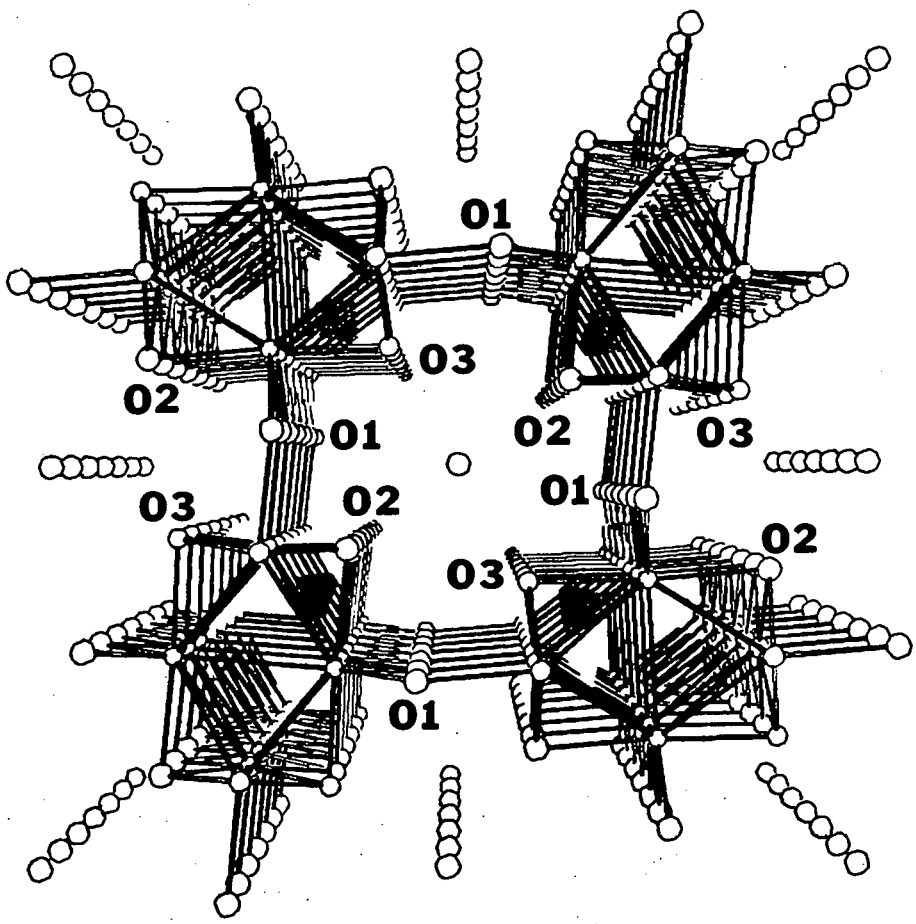

Figure IV-3. The structure of $Ba_{0.62}Mo_4O_6$ (subcell refinement) as viewed down the c axis showing the crosslinking of cluster chains and barium ion positions along the channels

Figure IV-3 also shows that the Ba^{2+} ions occupy sites in channels formed by four metal-oxide cluster chains crosslinked by Mo-O-Mo bonds as described above. Each barium ion is surrounded by eight intrachain oxygen atoms, O2 and O3, forming a rectangular box (angles in the a-b mirror plane are actually 90.6° and 89.4°) compressed along the c axis with O-O distances of 2.853(1), 3.144(22), and 3.622(22) Å. This box contains two barium ion sites symmetrically related through the inversion center located at the center of the box. Only one of these two sites, which are 0.74 Å apart, can be occupied by a barium ion at any time. The barium ion position gives rise to two average Ba-O distances of 2.620 Å and 2.998 Å. In addition, there are two interchain oxygen atoms, O1 in Figure IV-3, as next-nearest neighbors to barium each with a Ba-O distance of 3.19 Å.

The cause of the reduction in symmetry from tetragonal for $NaMo_4O_6$ to orthorhombic for $Ba_{0.62}Mo_4O_6$ is not obvious. If the effect is electronically driven, then it results from only an additional 0.24 electrons per Mo_4O_6 unit. A lowering of the structural symmetry could also be due to the presence of the more highly charged Ba^{2+} ions. In $NaMo_4O_6$, the sp^2-like oxygen atoms, each bridging two individual cluster chains, possess the capability of pi bonding to the molybdenum chains through the unhybridized p orbitals. In $Ba_{0.62}Mo_4O_6$, these lone pair p orbitals weakly interact with the Ba^{2+} ions as evidenced by the Ba-O1 interatomic distance of 3.19 Å. This distance is approximately 0.35 Å longer than the sum of ionic radii (12) for barium and oxygen. Each barium ion can attract electron density from the unhybridized

p orbitals of two interchain oxygen atoms through opposite faces of the surrounding rectangular box of intrachain oxygen atoms. Only one lobe of each lone pair p orbital is properly directed and close enough for interaction with barium. The resulting polarization of electron density in these orbitals towards the divalent cation could, therefore, cause loss of the sp^2-like planarity, and reduction in overall structural symmetry as shown in Figure IV-3.

Structure Description and Discussion of the $Ba_{0.62}Mo_4O_6$ Supercell

The final positional parameters for the $Ba_{0.62}Mo_4O_6$ supercell are listed in Table IV-4. Thermal parameters are given in Table IV-5; however, the significance of these numbers is questionable due to strong correlation effects in the structural refinement. Important molybdenum interatomic distances are listed in Table IV-6, and Mo-Mo-Mo bond angles are given in Table IV-7. The atomic labels in these two tables correspond to those shown in Figure IV-4. Molybdenum-oxygen and barium-oxygen interatomic distances are not tabulated because of their very high standard deviations, 0.08 Å (ave); all of the Mo-O bond distances are well within 3σ of being equivalent. The Mo-O-Mo bond angles are not listed because they possess large standard deviations of 3-4 degrees. The high standard deviations for the metal-oxygen distances and Mo-O-Mo angles are also a consequence of the correlation problem encountered during the structural refinement. Observed and calculated structure factors are available as supplementary material.

Table IV-4. Positional parameters for the $Ba_{0.62}Mo_4O_6$ supercell

Atom	x	y	z
Ba1	0.00	0.00	0.50
Ba2	0.00	0.00	0.1083(4)
Ba3	0.00	0.00	0.2686(3)
Ba4	0.00	0.00	0.0289(18)
MoA1	0.1318(18)	0.6605(15)	0.00
MoA2	0.1279(7)	0.6463(11)	0.1319(3)
MoA3	0.1419(10)	0.6507(14)	0.2474(4)
MoA4	0.1326(9)	0.6457(10)	0.3803(3)
MoA5	0.1412(11)	0.6565(14)	0.50
MoB1	0.6087(14)	0.0884(13)	0.0660(3)
MoB2	0.6146(10)	0.0982(9)	0.1863(5)
MoB3	0.6076(9)	0.0922(8)	0.3170(3)
MoB4	0.6110(15)	0.0920(13)	0.4347(3)
OA1	0.280(12)	0.799(10)	0.00
OA2	0.273(10)	0.822(7)	0.124(3)
OA3	0.265(9)	0.810(11)	0.251(4)
OA4	0.276(9)	0.827(6)	0.375(3)
OA5	0.271(16)	0.803(11)	0.50
OB1	0.041(8)	0.755(10)	0.061(3)
OB3	0.011(8)	0.760(6)	0.191(3)
OB5	0.024(5)	0.745(6)	0.315(3)
OB7	0.021(11)	0.764(11)	0.442(3)
OB2	0.238(9)	0.064(12)	0.061(3)
OB4	0.226(5)	0.055(6)	0.194(2)
OB6	0.253(7)	0.066(8)	0.311(4)
OB8	0.251(7)	0.058(9)	0.439(2)

Table IV-5. Thermal parameters for the $Ba_{0.62}Mo_4O_6$ supercell[a,b]

Atom	B_{11}	B_{22}	B_{33}	B_{12}	B_{13}	B_{23}
Ba1	0.67(28)	0.80(30)	3.47(42)	-0.56(30)	0.00	0.00
Ba2	1.34(22)	1.13(23)	2.61(33)	0.70(22)	0.00	0.00
Ba3	0.46(15)	1.22(19)	1.45(20)	0.03(17)	0.00	0.00
Ba4[c]	0.29(123)					
MoA1	1.16(29)	0.47(29)	1.32(27)	0.13(24)	0.00	0.00
MoA2	0.16(14)	0.69(18)	0.98(19)	-0.18(14)	0.34(15)	-0.15(18)
MoA3	1.04(19)	0.46(18)	1.22(21)	-0.24(15)	-0.38(18)	-0.41(21)
MoA4	0.09(12)	0.19(14)	0.10(13)	-0.03(12)	0.05(13)	-0.06(13)
MoA5	0.02(22)	0.41(27)	1.07(24)	-0.01(25)	0.00	0.00
MoB1	0.87(16)	1.17(19)	0.02(18)	0.12(14)	-0.02(18)	-0.06(18)
MoB2	0.65(14)	0.46(15)	0.48(14)	0.19(12)	-0.27(15)	-0.26(15)
MoB3	0.14(13)	0.57(15)	0.21(15)	-0.09(11)	-0.13(15)	-0.17(15)
MoB4	0.78(17)	0.47(17)	0.30(16)	-0.12(13)	-0.33(15)	-0.06(15)

[a]The general thermal parameter expression used is $\exp[-1/4(B_{11}h^2a^{*2} + B_{22}k^2b^{*2} + \ldots 2B_{23}k\ell b^*c^*)]$.

[b]Oxygen atoms constrained isotropically with B = 1.0 $Å^2$.

[c]Isotropic value.

Table IV-6. Molybdenum-molybdenum bond distances (Å) in the $Ba_{0.62}Mo_4O_6$ supercell

A1-A2	3.014(7)	A4-B3'	2.757(12)
A1-B1	2.830(18)	A4-B4	2.682(15)
A1-B1'	2.880(17)	A4-B4'	2.652(15)
A2-A3	2.637(11)	A5-B4	2.895(15)
A2-B1	2.767(13)	A5-B4'	2.874(17)
A2-B1'	2.759(15)	B1-B1'	2.700(26)
A2-B2	2.661(12)	B1'-B1"	3.012(12)
A2-B2'	2.705(14)	B1-B2	2.746(13)
A3-A4	3.033(11)	B2-B2'	2.912(18)
A3-B2	2.858(14)	B2-B3	2.985(13)
A3-B2'	2.826(16)	B3-B3'	2.734(17)
A3-B3	2.914(12)	B3-B4	2.684(10)
A3-B3'	2.885(15)	B4-B4'	2.780(27)
A4-A5	2.735(6)	B4-B4"	2.981(15)
A4-B3	2.754(11)		

Table IV-7. Selected Mo-Mo-Mo bond angles (deg) in the $Ba_{0.62}Mo_4O_6$ supercell

B1-A1-B1'	56.4(5)	A3-B2-B2'	58.7(4)
B1'-A1'-B1"	64.3(5)	A3-B2-B3	59.8(3)
B1'-A1-B1"	63.1(5)	A3-B2'-B2	59.7(3)
B1-A2-B1'	58.5(5)	A3'-B2-B3	59.5(3)
B1-A2-B2	60.7(3)	B1-B2-B2'	87.8(3)
B1-A2'-B2	60.3(4)	B1-B2-B3	176.0(5)
B2-A2-B2'	65.7(4)	B2'-B2-B3	88.3(2)
B2-A3-B2'	61.6(4)	A3-B3-A3'	87.4(4)
B2-A3-B3	62.3(3)	A3-B3-B2	57.9(3)
B2-A3'-B3	63.0(4)	A3-B3-B3'	61.3(4)
B3-A3-B3'	56.3(4)	A3'-B3-B2	57.5(3)
B3-A4-B3'	59.5(4)	A3-B3'-B3	62.4(3)
B3-A4-B4	59.2(3)	A4-B3-A4'	87.7(4)
B3-A4'-B4	59.5(3)	A4-B3-B3'	60.3(3)
B4-A4-B4'	62.8(5)	A4-B3-B4	59.1(4)
B4-A5-B4'	57.6(5)	A4-B3'-B3	60.2(3)
B4-A5-B4"	62.0(4)	A4'-B3-B4	58.3(3)
B4-A5'-B4"	62.5(5)	B2-B3-B3'	91.7(2)
A1-B1-A1'	89.8(5)	B2-B3-B4	177.8(5)
A1-B1-B1'	62.7(5)	B3'-B3-B4	90.5(3)
A1-B1'-B1	60.9(5)	A4-B4-A4'	91.4(5)
A2-B1-B1'	60.6(5)	A4-B4-B3	61.8(3)

Table IV-7. (Continued)

A2-B1-B2	57.7(3)	A4-B4-B4'	58.1(5)
A2-B1'-B1	60.9(4)	A4'-B4-B3	62.2(3)
A2'-B1-B2	58.9(3)	A4-B4'-B4	59.1(4)
A2-B1-A2'	86.0(4)	A5-B4-A5'	90.1(5)
B1'-B1-B2	92.2(3)	A5-B4-B4'	60.8(5)
A2-B2-A2'	89.2(4)	A5-B4-B4"	59.0(2)
A2-B2-B1	61.5(4)	A5-B4'-B4	61.6(4)
A2-B2-B2'	57.9(4)	A5'-B4-B4"	58.8(2)
A2'-B2-B1	60.8(4)	B3-B4-B4'	89.5(3)
A2-B2'-B2	56.4(3)	B3-B4-B4"	179.3(4)
A3-B2-A3'	89.6(5)	B4'-B4-B4"	90.0

Figure IV-4 is an ORTEP drawing of a section of one molybdenum-oxide cluster chain showing five of the eight subcell units extended along the c axis. Bonds between molybdenum atoms are represented by the solid, filled lines, while Mo-O bonding is represented by the open, unfilled lines; only the molybdenum atoms are labeled. Atoms A1 and A5 lie in mirror planes perpendicular to the c axis at z = 0 and 1/2, respectively, and all other Mo atoms occupy general positions in space group Pbam. There is a two-fold axis of rotation running parallel with the c axis and passing through the midpoint of the bonds between atoms B1-B1', B2-B2', etc. However, inversion centers in these cluster chains are only located midway between molybdenum atoms A1-A1' and A5-A5'.

It can be seen from this figure that the supercell molybdenum-oxide cluster chains are distorted from the highly symmetric chains found in $NaMo_4O_6$ (11). The architecture of the chains and the connectivity within and between cluster chains is basically the same as described for the $Ba_{0.62}Mo_4O_6$ subcell (see above). The most obvious structural difference between these distorted chains and those of the subcell is the alternating long-short-long molybdenum bond distances along the c axis direction of the supercell (see Table IV-6). The average molybdenum bond lengths per octahedral unit also alternate along the chain. Of the five bonded octahedral cluster units shown in Figure IV-4, the first, third, and fifth have an average Mo-Mo bond length of 2.880 Å; the second and fourth octahedral units have an average bond length of 2.743 Å. The overall average molybdenum bond distance within the supercell repeat unit is 2.811 Å, which compares favorably with the

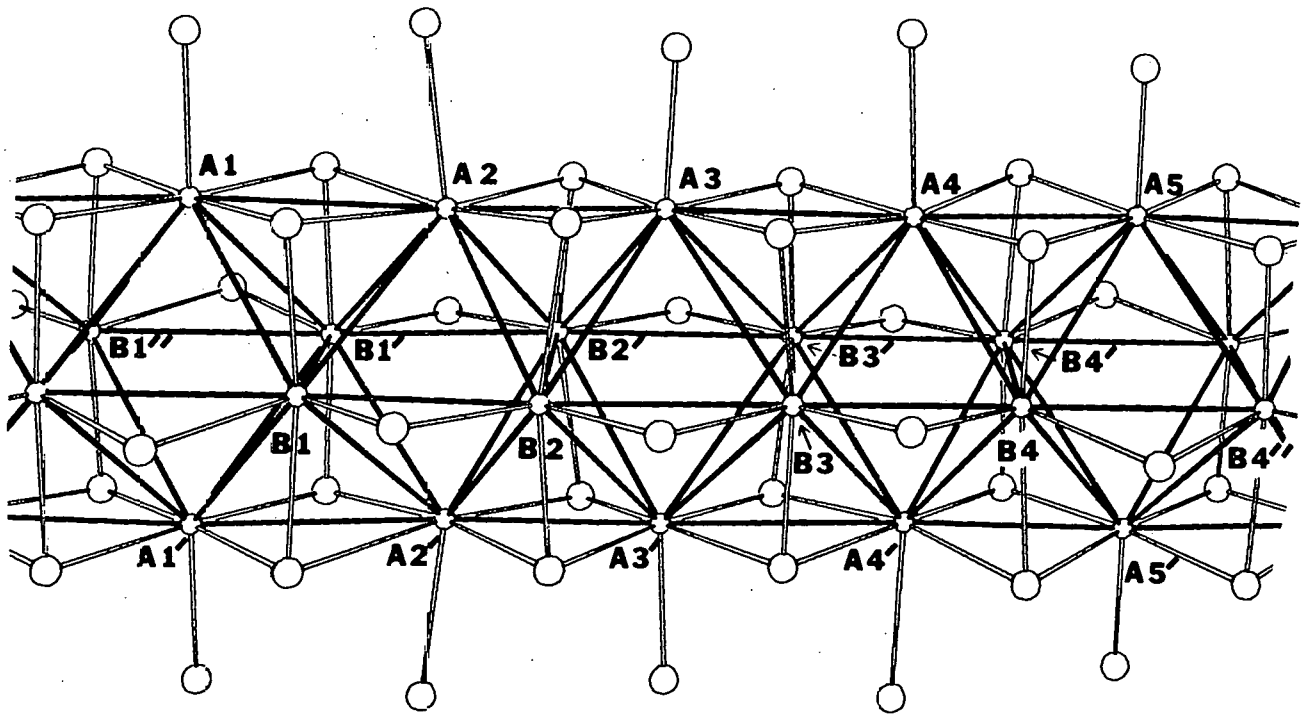

Figure IV-4. A section of one molybdenum-oxide cluster chain in the $Ba_{0.62}Mo_4O_6$ supercell showing one-half of the repeat unit along the c axis between atoms A1(A1') and A5(A5'). Only the molybdenum atoms are labeled. An average isotropic value for molybdenum and oxygen are represented by the fifty percent probability thermal ellipsoids

subcell average bond length of 2.809 Å. Within and between the infinite chains, the average Mo-O bond distances remain quite comparable to those in the $Ba_{0.62}Mo_4O_6$ subcell, viz., 2.053 and 2.043 Å in the subcell vs. 2.059 and 2.047 Å in the supercell, for the intrachain and interchain oxygen atoms, respectively.

A three-dimensional view of the superstructure down the c axis is given in Figure IV-5. This drawing shows the crosslinking of the distorted molybdenum-oxide cluster chains and the resulting barium ion sites along the channels. Each barium ion is surrounded by eight intrachain oxygen atoms forming a distorted rectangular box compressed along the c axis. To a first approximation, only five of the eight boxes stacked along the c axis of the unit cell are occupied by barium ions. The arrangement of these barium ions along one channel of the unit cell is shown in Figure IV-6. The barium ion at the center of the channel, Ba1, lies on an inversion center at (0,0,1/2); its two adjacent sites are empty. The average Ba-O bond distance for this atom is 2.75(8) Å. The two Ba2 ions and the two Ba3 ions are related through the inversion center at (0,0,1/2). Barium ions Ba2 and Ba3 occupy adjacent sites along the channel, but they are shifted away from each other along the c axis to minimize electrostatic repulsion. The positions of these cations along the channels result in a short and long average barium-oxygen bond distance for each; 2.63(9) Å and 2.99(6) Å for Ba2, and 2.70(7) Å and 2.88(6) Å for Ba3. The refined occupation numbers of 1.03(2) for Ba1 and 1.02(2) for Ba3 indicate full occupancy for these two cations, whereas a partial occupation value of

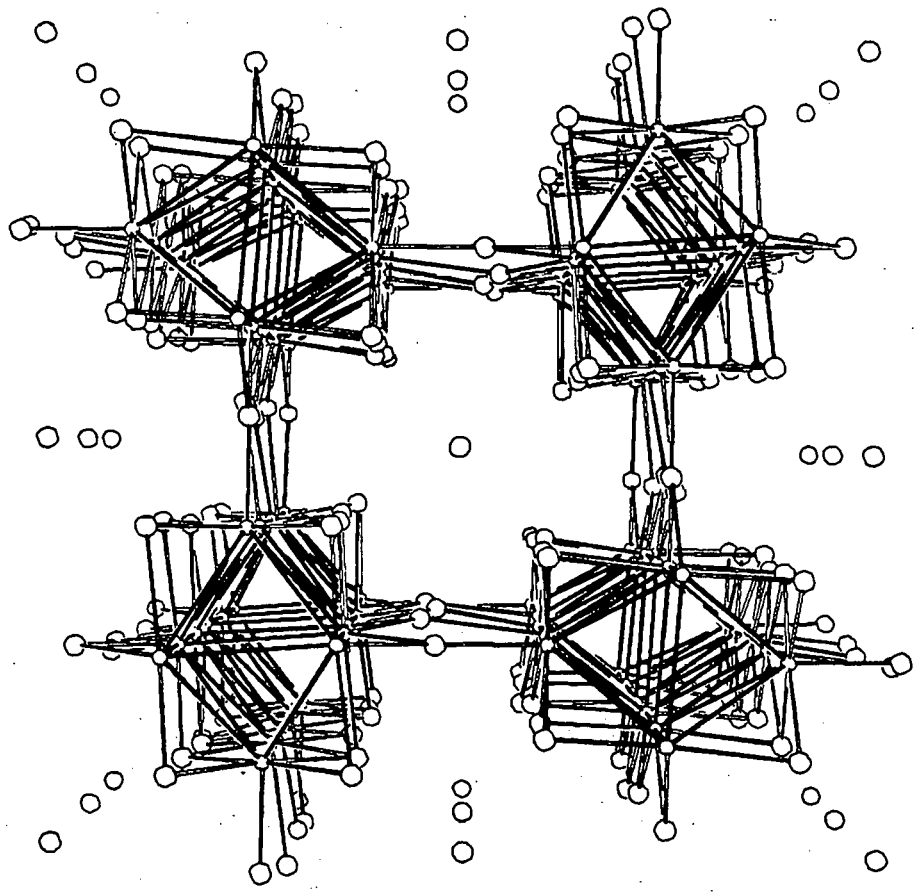

Figure IV-5. The superstructure of $Ba_{0.62}Mo_4O_6$ as viewed down the c axis showing the crosslinking of cluster chains and barium ion positions along the channels

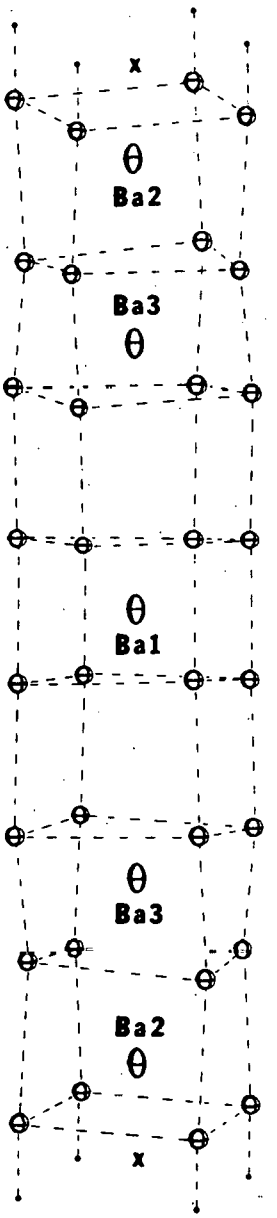

Figure IV-6. The arrangement of the five barium ions in the eight sites available along one channel of the $Ba_{0.62}Mo_4O_6$ supercell

0.88(2) for Ba2 was obtained. A fourth barium ion site was discovered from the structural refinement (Ba4 in Table IV-4), and is labeled with an x in Figure IV-6. This site, which is adjacent to the Ba2 site, is only partially occupied with a refined occupation number of 0.10(2). Thus, it appears that the Ba2 ion is statistically disordered between two neighboring sites with a distribution ratio of 9:1. This apparent disorder in the supercell suggests the existence of an even larger supercell where all of the barium ions are ordered in fully occupied sites.

CONCLUSIONS

The Mo_4O_6 structure type is now known to incorporate Li, Na, K, and Ba ions within its channels (2,11). Compared to $NaMo_4O_6$, the $Ba_{0.62}Mo_4O_6$ phase is slightly more reduced by ca. 0.25 electrons. The longer overall average Mo-Mo bond distance in this compound, viz., 2.810 Å for $Ba_{0.62}Mo_4O_6$ vs. 2.803 Å for $NaMo_4O_6$, suggests that the additional electrons occupy antibonding orbitals (or bands), but other effects could also be responsible for this small difference (e.g., size and charge of the cation within the channels, or extent of Mo-O pi bonding). The longer average Mo-O bond distance for the interchain oxygen atoms in the barium compound, relative to $NaMo_4O_6$, could result from a diminished pi bonding interaction or from the reduction of symmetry from tetragonal to orthorhombic. However, explanations for the adoption of orthorhombic symmetry and its affect on the structural details are only speculative at this time.

The superlattice ordering of barium ions in the channels of $Ba_{0.62}Mo_4O_6$ is similar to that observed in hollandites (13) and related materials (e.g., $Ba_xTi_{8-x}Mg_xO_{16}$). The channels in these hollandite phases are essentially identical to those in the Mo_4O_6 compounds. Apparently, the barium ions in the $Ba_{0.62}Mo_4O_6$ supercell are ordered in a manner that minimizes the barium-barium electrostatic repulsion contribution to the lattice energy. Least-squares refinement of the superstructure was plagued with correlation problems which made a final comparison of Mo-O bond distances impossible. In spite of

these problems, the alternating Mo-Mo bond distances along the c axis of the supercell appear statistically significant, but there is no obvious connection between this pattern and that of the barium ion ordering. There is no doubt that the presence of barium in the channels influences the relative positions of its surrounding oxygen atoms. It is very possible that the molybdenum atoms associated with these oxygen atoms also 'feel' the presence of the barium ions and become positioned in the observed periodic manner. Further research into the Mo_4O_6 structure type will, hopefully, answer many of the questions raised by the present superstructure analysis.

REFERENCES

1. Torardi, C. C.; McCarley, R. E. J. Am. Chem. Soc. 1979, 101, 3963.
2. Torardi, C. C.; McCarley, R. E. J. Solid State Chem. 1981, 37, 393.
3. Rohrbaugh, W. J.; Jacobson, R. A. Inorg. Chem. 1974, 13, 2535.
4. Jacobson, R. A. J. Appl. Crystallogr. 1976, 9, 115.
5. Lawton, S. L.; Jacobson, R. A. Inorg. Chem. 1968, 7, 2124.
6. Lapp, R. L.; Jacobson, R. A. "ALLS, A Generalized Crystallographic Least Squares Program", 1979, US DOE Report IS-4708.
7. Powell, D. R.; Jacobson, R. A. "FOUR: A General Crystallographic Fourier Program", 1980, US DOE Report IS-4737.
8. Karcher, B. A. Ph.D. Dissertation, Iowa State University, Ames, Iowa, 1981.
9. Hanson, H. P.; Herman, F.; Lea, J. D.; Skillman, S. Acta Crystallogr. 1964, 17, 1040.
10. Templeton, D. H. In "International Tables for X-ray Crystallography", 1st ed.; Macgillavry, C. H. and Rieck, G. D., Eds.; Kynoch Press: Birmingham, England, 1962; Vol. III, page 215.
11. Torardi, C. C. Ph.D. Dissertation, Iowa State University, Ames, Iowa, 1981, Section III.
12. Shannon, R. D. Acta Crystallogr. 1976, A32, 751.
13. Bursill, L. A.; Grzinic, G. Acta Crystallogr. 1980, B36, 2902.

SECTION V. THE PREPARATION AND PARTIAL CHARACTERIZATION OF SOME REDUCED TERNARY OXIDES OF MOLYBDENUM CONTAINING Na, K, AND Ca

INTRODUCTION

The syntheses and characterizations of several new reduced molybdenum oxides have recently been reported (1,2). Some of these compounds incorporate discrete trimeric or tetrameric molybdenum atom clusters, while others contain infinite chains of bonded molybdenum atoms. In the course of this reduced molybdenum oxide research, three more new compounds have been synthesized. From analytical and x-ray powder diffraction data, the tentative formulas $K_{2+x}Mo_{12}O_{19}$, $Na_{2+x}Mo_{12}O_{19}$, and $CaMo_5O_8$ have been assigned to these compounds. This section reports the preparation and partial characterization of these new ternary molybdenum oxides.

EXPERIMENTAL

Materials

The starting materials used were Fisher Certified A.C.S. MoO_3 and KOH, 'Baker Analyzed' Reagent $(NH_4)_6Mo_7O_{24}\cdot 4H_2O$ (83.0% as MoO_3) and anhydrous $CaCl_2$ (97.8%), Aldrich molybdenum powder (99.99%), Thermo-Electron Corp. molybdenum tubing (99.97%), and Rembar Co. molybdenum sheet (99.95%). Potassium molybdate was prepared by the reaction of KOH with the stoichiometric quantity of MoO_3 in deionized water. The molybdate solution was filtered, its volume reduced by heating, and the precipitate collected on a glass frit. The product was finally dried at 120°C and stored over P_4O_{10}. Calcium molybdate was prepared by mixing a filtered aqueous solution of $CaCl_2$ with an aqueous solution containing the stoichiometric quantity of ammonium heptamolybdate tetrahydrate and ammonium hydroxide. The white precipitate was collected on a glass frit, washed several times with deionized water, dried at 110°C for one hour and at 500°C overnight, and stored over P_4O_{10}. Molybdenum dioxide was prepared by the hydrogen reduction of MoO_3 at 460°C for 40 hours. The reduced material was washed several times with alternate portions of 3M NH_4OH, deionized water, and 3M HCl until the washings were colorless, and finally dried *in vacuo* at 110°C. *Anal.* Calculated for MoO_2: Mo, 74.99. Found: Mo, 74.96.

Syntheses

$K_{2+x}Mo_{12}O_{19}$

In a typical reaction, MoO_2 (1.32 g, 10.3 mmol) and K_2MoO_4 (0.61 g, 2.6 mmole) were mixed by grinding in a mortar and sealed in an evacuated molybdenum reaction tube (3.5 cm long, 1.3 cm o.d.). This Mo tube was sealed in an evacuated inconel protection tube, and then held at 1100°C for 5-7 days. The contents of the tube were washed several times with deionized water to remove unreacted K_2MoO_4, rinsed with several portions of acetone, and air dried.

A range of product crystallinity was observed from one preparation to another. One of these reactions produced many small black crystals each consisting of three intergrown hexagonal platelets. Guinier x-ray powder diffraction patterns were always free of MoO_2 and Mo lines. Elemental analyses and oxidation state determinations on molybdenum were performed for the products of two separate reactions. For determination of the molybdenum oxidation state, weighed samples were dissolved in standardized ceric sulfate-3M H_2SO_4 solution. After complete oxidation of all molybdenum to Mo(VI), the excess Ce(IV) was titrated with standard Fe(II) solution. The analytical results for the two reaction products were:

1) K, 5.05; Mo, 74.0; Mo (+2.95)

2) K, 6.26; Mo, 74.0; Mo (+2.94).

The first set of results gave a Mo/K ratio of 6/1, and the stoichiometry $K_2Mo_{12}O_{19}$ was obtained. Calculated values for this composition were: K, 5.10; Mo, 75.1; Mo (+3.00). The second set of analytical

data, which gave a Mo/K ratio of 6/1.25, resulted in the formula $K_{2.5}Mo_{12}O_{19}$. Calculated values for this composition were: K, 6.29; Mo, 74.1; Mo (+2.96). Based on the combined analytical information given above, the tentative formula $K_{2+x}Mo_{12}O_{19}$ was assigned.

$Na_{2+x}Mo_{12}O_{19}$

This phase was first discovered as small crystals growing on the ends of a molybdenum reaction vessel used in the preparation of the compound $NaMo_4O_6$ (2,3). Only a few milligrams of this new phase were obtained. Electron microprobe analyses confirmed the presence of sodium and molybdenum as well as the absence of potassium in this phase. From Guinier x-ray powder diffraction data, the sodium compound appeared to be isomorphous with $K_{2+x}Mo_{12}O_{19}$; therefore, the formula $Na_{2+x}Mo_{12}O_{19}$ was assigned.

$CaMo_5O_8$

Calcium molybdate and molybdenum dioxide in mole ratio 1:1 were mixed by grinding in a mortar and sealed in an evacuated molybdenum reaction tube (3.5 cm long, 1.9 cm o.d.). This Mo tube was sealed in an evacuated fused quartz tube and the reaction mixture held at 1100°C for 7 days. One end of the molybdenum tube contained bundles of small, black, chunk-like crystals mixed with unreacted $CaMoO_4$. The other end of the tube contained thin whiskers of MoO_2 as evidenced from an x-ray powder diffraction pattern. The chunk-like crystals were isolated from the calcium molybdate by dissolving the latter in 0.5 M HCl. There was no apparent affect on the new compound by this treatment. A Guinier

x-ray powder diffraction pattern of powdered crystals did not show any lines for Mo, MoO_2, or $CaMoO_4$. The stoichiometry $CaMo_5O_8$ was obtained from elemental analyses and results of oxidation-reduction titrations (as described above for $K_{2+x}Mo_{12}O_{19}$). Anal. Calculated for $CaMo_5O_8$: Ca, 6.19; Mo, 74.1; Mo (+2.80). Found: Ca, 6.25; Mo, 72.0; Mo (+2.80).

The compound $CaMo_5O_8$ was also prepared from the stoichiometric quantities of $CaMoO_4$, MoO_2, and Mo in the presence of a Cs_2MoO_4 flux. Thus, $CaMoO_4$ (0.62 g, 3.1 mmole), MoO_2 (0.79 g, 6.2 mmole), Mo (0.59 g, 6.2 mmole), and Cs_2MoO_4 (0.30 g, 0.70 mmole) were mixed by grinding in a mortar, pelletized under 700 kg/cm^2, and sealed in an evacuated molybdenum reaction tube (3.5 cm long, 1.3 cm o.d.). After sealing this Mo tube in an evacuated inconel protection tube, the reaction mixture was held at 1100°C for 5 days. The product was washed several times with 1.5 M HCl until the washings were colorless, then rinsed with deionized water and dried in vacuo at 110°C. A Guinier x-ray powder diffraction pattern of this polycrystalline material was identical to that obtained from the powdered crystals; the lines of MoO_2 and Mo were absent. The composition of this preparation was also calculated as $CaMo_5O_8$ from elemental analyses and oxidation state determinations for molybdenum. The results were: Ca, 5.87; Mo, 74.8; Mo (+2.84).

X-Ray Powder Diffraction Data

An Enraf Nonius Delft triple focusing Guinier x-ray powder diffraction camera was used with Cu K α_1 radiation (λ = 1.54056 Å) to obtain d-spacings. National Bureau of Standards silicon powder was mixed with all samples as an internal standard. The lines and their

relative intensities for the compounds $K_{2+x}Mo_{12}O_{19}$, $Na_{2+x}Mo_{12}O_{19}$, and $CaMo_5O_8$ are listed in Tables V-1 through V-3, respectively.

Table V-1. Observed d-spacings for $K_{2+x}Mo_{12}O_{19}$

d-Spacing	Intensity[a]	d-Spacing	Intensity[a]
6.776	vs	2.203	m
6.136	w	2.045	m
4.559	vw	1.953	s
4.231	vw	1.948	s
4.051	vw	1.941	s
3.112	m	1.909	m
2.967	m	1.834	m
2.838	vw	1.826	m
2.508	m	1.708	m
2.483	m	1.701	m
2.420	m	1.497	w
2.415	m	1.493	m
2.399	m	1.449	m
2.335	m	1.439	m
2.280	m	1.435	m
2.265	w	1.379	vw
2.209	m	1.323	vw

[a] vs = very strong, s = strong, m = medium, w = weak, vw = very weak.

Table V-2. Observed d-spacings for $Na_{2+x}Mo_{12}O_{19}$

d-Spacing	Intensity[a]	d-Spacing	Intensity[a]
6.654	vs	2.198	vw
6.047	w	2.184	w
5.178	vw	2.059	w
4.401	vw	2.040	w
4.002	vw	2.026	vw
3.423	w	1.941	s
3.110	w	1.931	s
3.048	vw	1.894	m
3.030	vw	1.822	w
2.931	s	1.814	w
2.875	w	1.787	vw
2.811	w	1.743	vw
2.763	w	1.696	w
2.687	s	1.689	m
2.502	m	1.581	vw
2.486	s	1.505	vw
2.481	m	1.486	w
2.414	s	1.481	m
2.396	s	1.440	m
2.308	m	1.439	m
2.266	m	1.429	m
2.251	w	1.324	vw
2.208	w		

[a] vs = very strong, s = strong, m = medium, w = weak, vw = very weak.

Table V-3. Observed d-spacings for $CaMo_5O_8$

d-Spacing	Intensity[a]	d-Spacing	Intensity[a]
6.555	vs	1.976	w
5.513	w	1.943	w
4.322	vw	1.925	s
3.793	w	1.904	s
3.110	m	1.849	m
2.954	m	1.822	m
2.898	w	1.798	w
2.877	s	1.780	m
2.843	m	1.701	w
2.769	w	1.679	m
2.750	w	1.674	w
2.673	s	1.665	m
2.498	s	1.648	w
2.480	m	1.567	w
2.451	m	1.469	m
2.435	w	1.465	m
2.406	m	1.461	w
2.393	s	1.459	m
2.366	s	1.445	m
2.266	m	1.427	m
2.232	m	1.419	m
2.192	s	1.351	w
2.174	w	1.324	w
2.155	w	1.294	w
2.054	s		

[a]vs = very strong, s = strong, m = medium, w = weak, vw = very weak.

Crystal Indexing

Crystals of $K_{2+x}Mo_{12}O_{19}$, $Na_{2+x}Mo_{12}O_{19}$, and $CaMo_5O_8$ were placed on the tip of a glass fiber with epoxy adhesive, or in a 0.2 mm Lindemann glass capillary with a small amount of silicone grease. Each crystal was mounted on an automated four-circle x-ray diffractometer designed and built in the Ames Laboratory (4). Three or four ω-oscillation photographs were then taken at various χ and ϕ settings. Several reflections obtained from these photographs were input into an automatic indexing program (5). Lattice parameters calculated by this program were not refined.

Pressed Pellet Electrical Resistivity Measurement

A pellet of $K_{2+x}Mo_{12}O_{19}$ powder (0.32 cm diam, 0.2 cm thick) was pressed under 500 kg/cm^2 and sintered in an evacuated fused quartz ampoule at 900°C for 60 hours. Four platinum wire leads were attached to the pellet with silver adhesive. Electrical resistivity measurements were made using a standard four probe a.c. (27.5 Hz) method by recording the voltage across the pressed pellet as a function of temperature. The cooling rate was adjusted to 1-2 degrees/minute and temperature readings were provided by Pt and Ge resistance thermometers. Voltage readings were recorded approximately every two degrees in the interval 20-280 K and at least every degree from 1.5 - 20 K. The voltage across a standard calibrated resistor was measured periodically and showed no significant change during the course of the

experiment. The ratio of the measured resistivity to that measured at 288 K was graphed as a function of temperature.

Magnetic Susceptibility Measurement

The magnetic susceptibility of the solid compound $K_{2+x}Mo_{12}O_{19}$ was measured by the Gouy method in air at room temperature. The molar susceptibility was corrected for diamagnetic contributions from the constituent atoms. Assuming the average composition $K_{2.25}Mo_{12}O_{19}$, a value for the corrected molar susceptibility, χ'_m, of 1200 x 10^{-6} (cgs units)/formula unit or 100 x 10^{-6} (cgs)/gram atom of Mo was obtained. The corresponding effective magnetic moment values of 1.7 and 0.5 B.M., respectively, were calculated assuming the compound obeyed the Curie law, $\mu_{eff} = 2.84\ (\chi'_m\ T)^{1/2}$.

RESULTS AND DISCUSSION

The compound $K_{2+x}Mo_{12}O_{19}$ can be easily prepared from K_2MoO_4, MoO_2, and Mo (supplied by the molybdenum reaction vessel) at 1100°C as long as a two-fold excess of K_2MoO_4 is present. Reactions involving the stoichiometric quantities of K_2MoO_4, MoO_2, and Mo powder, including a ten percent excess of potassium molybdate, always gave mixtures of $K_{2+x}Mo_{12}O_{19}$ and unreacted starting materials. Slightly different analytical results were obtained on the products of two separate preparations (i.e., $K_2Mo_{12}O_{19}$ and $K_{2.5}Mo_{12}O_{19}$). These results may indicate a structure possessing a variable potassium ion level. Although crystals of $K_{2+x}Mo_{12}O_{19}$ were obtained in one reaction product, the conditions for crystal growth have not yet been established. A problem associated with these crystals, as well as those of $Na_{2+x}Mo_{12}O_{19}$, is that they are actually composed of two or more intergrown single crystals. Several of these multiple crystals were broken into smaller pieces with the hope of obtaining a segment of a single crystal. The segments were of dimensions on the order of 0.1 mm along each edge. The potassium and sodium compounds were indexed, and large unit cells were calculated for both. A hexagonal unit cell was obtained for each of several $K_{2+x}Mo_{12}O_{19}$ crystals with cell dimensions of a = 40.5 Å and c = 9.35 Å. Only one crystal of $Na_{2+x}Mo_{12}O_{19}$ was indexed, and it also appeared to be hexagonal with unit cell dimensions of a = 40.0 Å and c = 9.30 Å. The smaller unit cell volume for the sodium compound was consistent with x-ray powder diffraction data

(Tables V-1 and V-2). If the large axial lattice parameters are correct, an x-ray structure determination for either of the two compounds will be very difficult.

A pressed pellet electrical resistivity ratio vs. temperature curve was obtained for $K_{2+x}Mo_{12}O_{19}$ and is shown in Figure V-1. The value of the pressed pellet electrical resistivity at room temperature is ca. 5×10^{-2} ohm-cm. Initially, the resistivity increases slowly as the temperature is lowered and is almost linear to 120 K. At this point, the increase in resistivity becomes more rapid and reaches a maximum value at T = 8 K with roughly twelve times the room temperature electrical resistance. The resistivity then drops sharply in the temperature interval 7 - 1.5 K. However, a.c. susceptibility measurements in the temperature range 1.1 - 30 K showed no evidence for a magnetic phase transition. The pressed pellet electrical resistivity behavior of $K_{2+x}Mo_{12}O_{19}$ is essentially identical to that of the compound $NaMo_4O_6$ (3). A magnetic phase transition in the temperature interval 1.1 - 30 K is also absent for the latter compound.

The observed magnetic moment of approximately 1.7 B.M. for $K_{2+x}Mo_{12}O_{19}$ implies the presence of one unpaired electron per formula unit. However, this value could very well be due to a temperature-independent paramagnetic contribution. A TIP effect is suggested by the corrected molar susceptibility value of only 100×10^{-6} (cgs)/gram atom Mo. Furthermore, there was no change in the a.c. susceptibility of $K_{2+x}Mo_{12}O_{19}$ through the temperature interval 30 - 1.1 K.

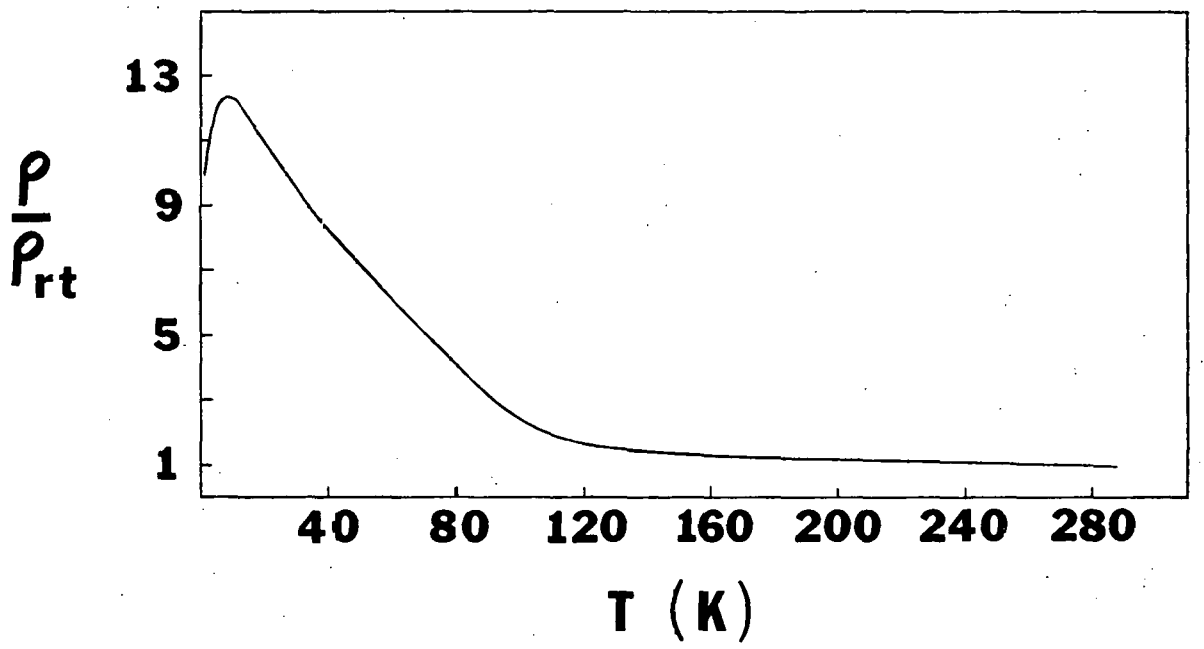

Figure V-1. Electrical resistivity ratio vs. temperature curve for a pressed pellet of the compound $K_{2+x}Mo_{12}O_{19}$. The resistivity at room temperature is approximately 5×10^{-2} ohm-cm

The compound $CaMo_5O_8$ can be prepared from the stoichiometric quantities of $CaMoO_4$, MoO_2, and Mo powder at 1100°C in the presence of a fluxing material such as cesium molybdate. Without the aid of a fluxing agent, significant levels of unreacted MoO_2 remained in the product. The largest crystals of $CaMo_5O_8$, however, were obtained from a reaction product which included long needles of MoO_2 as well as unreacted $CaMoO_4$. Oscillation photographs were taken on many of these $CaMo_5O_8$ crystals. The photographs revealed that most of the chunk-like specimens were actually twinned or multiple crystals. Three apparently single crystals were found, with average dimensions of 0.15 mm/edge, and indexed as orthorhombic with unit cell dimensions of a = 14.41 Å, b = 24.46 Å, and c = 9.06 Å. However, there were some weak low-angle reflections visible in the axial oscillation photographs that indicated the existence of a much larger unit cell than the one calculated by the indexing program.

CONCLUSIONS

Three new reduced ternary oxides of molybdenum have been synthesized. The compounds $K_{2+x}Mo_{12}O_{19}$, $Na_{2+x}Mo_{12}O_{19}$, and $CaMo_5O_8$ contain molybdenum in an average oxidation state of approximately +3. With an average of three electrons per molybdenum atom available for metal-metal bonding, these compounds would be expected to contain metal atom clusters of some sort. For example, the compound $NaMo_4O_6$ (3), with an average Mo oxidation state of +2.75, contains infinite chains of bonded molybdenum atoms. In the compound $Ba_{1.14}Mo_8O_{16}$ (6), containing molybdenum in a net oxidation state of +3.72, discrete tetrameric molybdenum atom clusters are found. Strong similarities in the electrical resistivity *vs.* temperature curves for $NaMo_4O_6$ and $K_{2+x}Mo_{12}O_{19}$ suggest a structural relationship between the two compounds. However, crystal morphology indicates otherwise; $NaMo_4O_6$ grows as long needles, while $K_{2+x}Mo_{12}O_{19}$ crystallizes as hexagonal plates. Single crystal x-ray diffraction data will be necessary to determine the structures of the three new reduced molybdenum oxides reported here.

REFERENCES

1. Torardi, C. C.; McCarley, R. E. J. Solid State Chem. 1981, 37, 393.

2. Torardi, C. C.; McCarley, R. E. J. Am. Chem. Soc. 1979, 101, 3963.

3. Torardi, C. C. Ph.D. Dissertation, Iowa State University, Ames, Iowa, 1981, Section III.

4. Rohrbaugh, W. J.; Jacobson, R. A. Inorg. Chem. 1974, 13, 2535.

5. Jacobson, R. A. J. Appl. Crystallogr. 1976, 9, 115.

6. Torardi, C. C. Ph.D. Dissertation, Iowa State University, Ames, Iowa, 1981, Section II.

SUMMARY

The original goal of this research project was to prepare reduced solid state molybdenum oxide compounds containing trinuclear metal atom clusters in which the number of electrons available for molybdenum-molybdenum bonding was varied. This was accomplished with the synthesis of $LiZn_2Mo_3O_8$, $ScZnMo_3O_8$, and $Zn_3Mo_3O_8$. Metal-centered molecular orbitals in Mo_3O_{13} clusters are now known to accommodate six, seven, and eight electrons as observed in the compounds $Zn_2Mo_3O_8$, $LiZn_2Mo_3O_8$, and $Zn_3Mo_3O_8$, respectively. Differences between these compounds regarding Mo-Mo and Mo-O bond lengths were rationalized in terms of molybdenum-oxygen pi bonding interactions and their affect on the cluster's molecular orbitals.

In the course of further research in reduced molybdenum oxide chemistry, the compound $Ba_{1.14}Mo_8O_{16}$ was synthesized. It is the first example of an oxide system containing tetrameric metal atom clusters, and is also the first example of a molybdenum hollandite. The structure of $Ba_{1.14}Mo_8O_{16}$ was found to contain infinite molybdenum-oxide cluster chains extended parallel with the c axis. Four of these metal-oxide cluster chains are interlinked via Mo-O-Mo bridge bonding to create tunnels in which the Ba^{2+} ions reside. There are two different types of infinite chains in this compound which contain $Mo_4O_8^{2-}$ and $Mo_4O_8^{0.28-}$ cluster units, respectively. The five Mo-Mo bonds in the $Mo_4O_8^{2}$ units were described as containing a total of ten electrons with two electrons per bond; whereas, the $Mo_4O_8^{0.28-}$ units contain

approximately eight electrons distributed in 3 two-electron bonds, and 2 one-electron bonds. The compound $Ba_{1.14}Mo_8O_{16}$ also exhibits a superlattice ordering of barium ions within the partially occupied channels.

The most interesting material to emerge from this molybdenum-oxide research was the compound $NaMo_4O_6$. The structure of $NaMo_4O_6$ consists of infinite chains of bonded molybdenum atom clusters. These chains are comprised of clusters of the type Mo_6O_{12} fused at opposite edges by removal of two edge-bridging oxygen atoms, and sharing of the metal and remaining oxygen atoms between cluster units. Crosslinking of the infinite chains by Mo-O-Mo bonds provides channels parallel with the c axis in which the Na^+ ions reside. The connectivity within and between molybdenum-oxide cluster chains can be represented by the formulation $(Mo_2Mo_{4/2}O_{8/2}O_{2/2})O_{2/2}^-$. There are thirteen electrons in thirteen Mo-Mo bonds in every Mo_4O_6 repeat unit; this results in an average metal-metal bond order of 0.5. Each sodium ion is coordinated to eight oxygen atoms at the corners of a compressed cube. The sodium ions can be partially ion exchanged with Li^+ and K^+ in molten LiCl and KCl salts, respectively.

A continuation of this research into highly reduced molybdenum oxide compounds led to the preparation of $Ba_{0.62}Mo_4O_6$. The structure of $Ba_{0.62}Mo_4O_6$ is essentially the same as that of $NaMo_4O_6$, but of lower symmetry. Cluster chains in the barium compound possess an additional 0.24 electrons per Mo_4O_6 repeat unit. Barium ion ordering within the channels creates a superlattice where the cations are positioned in a manner that minimizes Ba^{2+}-Ba^{2+} electrostatic repulsions.

The syntheses and partial characterizations of the compounds $K_{2+x}Mo_{12}O_{19}$, $Na_{2+x}Mo_{12}O_{19}$, and $CaMo_5O_8$ were also discussed. Unfortunately, crystal structures for these compounds have not yet been determined.

The research presented above has uncovered several new and interesting solid state compounds, and has opened the door to some exciting reduced molybdenum-oxide chemistry. There can be little doubt that the future holds many more surprising results as research in this area continues.

LITERATURE CITED

1. Yvon, K. Curr. Top. Materials Sci. 1978, 3, 55.
2. Lokken, D. A.; Corbett, J. D. Inorg. Chem. 1973, 12, 556.
3. Poeppelmeier, K. R.; Corbett, J. D. J. Am. Chem. Soc. 1978, 100, 5039.
4. Adolphson, D. G.; Corbett, J. D. Inorg. Chem. 1976, 15, 1820.
5. Rogers, D. B.; Shannon, R. D.; Sleight, A. W.; Gillson, J. L. Inorg. Chem. 1969, 8, 841.
6. Wilhelmi, K. A.; Lagervall, E.; Muller, O. Acta Chem. Scand. 1970, 24, 3406.
7. Waltersson, K. Acta Crystallogr. 1976, B32, 1485.
8. McCarroll, W. H.; Katz, L.; Ward, R. J. Am. Chem. Soc. 1957, 79, 5410.
9. Donohue, P. C.; Katz, L.; Ward, R. Inorg. Chem. 1965, 4, 306.
10. Magnéli, A. Acta Chem. Scand. 1957, 11, 28.
11. Muller, O.; Roy, R. J. Less-Common Metals 1968, 16, 129.
12. Chandrashekar, G. V.; Mayo, J.; Honig, J. M. J. Solid State Chem. 1970, 2, 528.
13. Tourne, G.; Czeskleba, H. C. R. Acad. Sci. Paris 1970, 271, 136.
14. McCarroll, W. H. Inorg. Chem. 1977, 16, 3351.
15. Marinder, B. O. Chemica Scripta 1977, 11, 97.
16. Torardi, C. C.; McCarley, R. E. J. Solid State Chem. 1981, 37, 393.
17. Torardi, C. C.; McCarley, R. E. J. Am. Chem. Soc. 1979, 101, 3963.

ACKNOWLEDGEMENTS

First of all, I wish to thank Professor R. E. McCarley for many interesting discussions as well as his guidance during my graduate years. Special thanks are due to Professor R. A. Jacobson and Dr. Douglas Powell for their valuable assistance during the x-ray structural determinations. Other members of the crystallographic group whose help was sincerely appreciated are Jim Benson, Barb Helland, Barb Karcher, Jim Richardson, and Brenda Smith. I wish to thank Professor R. N. Shelton and Ms. H.-E. Horng for their assistance in the electrical resistivity and a.c. susceptibility measurements. The discussions and suggestions provided by members of my research group were also much appreciated.

A large debt of gratitude goes to my parents, Josephine and Carmelo Torardi, who always encouraged my educational goals. I am sincerely grateful to my very close friends, Mary and Patty Montag, for their love and support, and for making my graduate days most enjoyable. Above all, however, I thank my dear friend, Alicia Faggella, for her love, friendship, and loyal support throughout my graduate years.